Twisted bilayer graphene. V. Exact analytic many-body excitations in Coulomb Hamiltonians: Charge gap, Goldstone modes, and absence of Cooper pairing

B. Andrei Bernevig,[1,*] Biao Lian,[1] Aditya Cowsik,[1] Fang Xie,[1] Nicolas Regnault,[1,2] and Zhi-Da Song[1,†]

[1]*Department of Physics, Princeton University, Princeton, New Jersey 08544, USA*

[2]*Laboratoire de Physique de l'Ecole normale superieure, ENS, Université PSL, CNRS, Sorbonne Université, Université Paris-Diderot, Sorbonne Paris Cité, Paris, France*

(Received 28 October 2020; revised 15 April 2021; accepted 16 April 2021; published 11 May 2021)

We find exact analytic expressions for the energies and wave functions of the charged and neutral excitations above the exact ground states (at rational filling per unit cell) of projected Coulomb Hamiltonians in twisted bilayer graphene. Our exact expressions are valid for any form of the Coulomb interaction and any form of *AA* and *AB*/*BA* tunneling. The single charge excitation energy is a convolution of the Coulomb potential with a quantum geometric tensor of the TBG bands. The neutral excitations are (high-symmetry group) magnons, and their dispersion is analytically calculated in terms of the form factors of the active bands in TBG. The two-charge excitation energy and wave functions are also obtained, and a sufficient condition on the graphene eigenstates for obtaining a Cooper pair from Coulomb interactions is obtained. For the actual TBG bands at the first magic angle, we can analytically show that the Cooper pair binding energy is zero in all such projected Coulomb models, implying that either phonons and/or nonzero kinetic energy are needed for superconductivity. Since Vafek and Kang [Phys. Rev. Lett. **125**, 257602 (2020)] showed that the kinetic energy bounds on the superexchange energy are less 10^{-3} in Coulomb units, the phonon mechanism becomes then very likely. If nonetheless the superconductivity is due to kinetic terms which render the bands nonflat, one prediction of our theory is that the highest T_c would *not* occur at the highest DOS.

DOI: 10.1103/PhysRevB.103.205415

I. INTRODUCTION

The rich physics of the experimentally observed insulating states in magic angle twisted bilayer graphene (TBG) at integer number of electrons per unit cell and the superconducting phase with finite doping above the insulating states has attracted considerable interest [1–111]. The single-particle picture predicts a gapless metallic state at electron number $\pm(3, 2, 1)$, and hence the insulating states have to follow from many-body interactions. The initial observations of the insulating states [2–5] were then followed by the experimental discovery by both scanning tunneling microscope [20,21] and transport [6,11,22–25] that these states might exhibit Chern numbers, even when the TBG substrate is not aligned with hBN, which would indicate a many-body origin of the Chern insulator.

These remarkable experimental advances have been followed by extensive theoretical efforts aimed at their explanation [51–104]. Using a strong-coupling approach where the interaction is projected into a Wannier basis, Kang and Vafek [71] constructed a special Coulomb Hamiltonian, of an enhanced symmetry, where the ground state (of Chern number 0) at ± 2 electrons per unit cell can be exactly obtained (with rather weak assumptions). In Ref. [110], we have showed that the type of Kang-Vafek type Hamiltonians [71] (hereby called positive semidefinite Hamiltonians - PSDH) are actually *generic* in projected Hamiltonians, and that the presence of extra symmetries [38,63,71] renders some Slater determinant states to be exact eigenstates of PSDH. We found at zero filling, these states are the ground states of PSDH. At nonzero integer filling, these states are the ground states of the PSDH under weak assumptions (first considered by Kang and Vafek [71]). With a unitary particle-hole (PH) symmetry first derived in Ref. [43], the PSDH projected to the active bands has enhanced U(4) (in all the parameter space) and U(4) × U(4) (in a certain, first chiral limit) symmetries first mentioned in Refs. [71–73]. We showed [109,110] that these symmetries are valid for PSDHs of TBG irrespective of the number of projected bands. We also found that, for two projected bands in the first chiral limit (a second chiral limit, of U(4) × U(4) defined in Ref. [109] was also found), ground states of different Chern numbers are exactly degenerate [110]. These ground states are all variants of U(4) ferromagnets (FM) in valley/spin. When kinetic energy is added or away from the chiral limit, the lowest/highest Chern number becomes the ground state in low/high magnetic field, which explains/is consistent with experimental findings [6,11,20–25].

In this paper, we show that the Kang-Vafek type of PSDH also allow, remarkably, for an exact expression of the charge ± 1 excitation (relevant for transport gaps) energy and eigenstate, neutral excitation (relevant for the Goldstone and thermal transport), and charge ± 2 excitation (relevant for possible Cooper pair binding energy). We show that the charge excitation dispersion is fully governed by a generalized "quantum geometric tensor" of the projected bands, convoluted with the Coulomb interaction. The smallest charge

*bernevig@princeton.edu

†zhidas@princeton.edu

1 excitation gap is at the Γ_M point. The neutral, and charge ± 2 excitation, on top of every FM ground state can also be obtained as a single-particle diagonalization problem, despite the state having a thermodynamic number of particles. The neutral excitation has an exact zero mode, which we identify with the FM U(4)-spin wave, and whose low-momentum dispersion (velocity) can be computed exactly. The charge ± 2 excitations allows for a simple check of the Richardson criterion [112–115] of superconductivity: we check if states appear below the noninteracting two-particle continuum. We find a sufficient criterion for the appearance/lack of Cooper binding energy in these type of PSDH Hamiltonian systems based on the eigenvalues of the generalized "quantum geometric tensor." We analytically show that, generically, the projected Coulomb Hamiltonians cannot exhibit Cooper pairing binding energy. As such, this implies that either phonons or nonzero kinetic energy are needed for superconductivity. Since the Ref. [103] showed that the kinetic energy bounds on the superexchange energy are less 10^{-3} in Coulomb units, the phonon mechanism becomes becomes likely. If however, experimentally, the kinetic energy is stronger, a Coulomb mechanism for superconductivity is still possible. Since we proved that flat bands cannot Cooper pair under Coulomb, a prediction of a Coulomb with nonflat bands mechanism for superconductivity would be that the highest superconducting temperature does *not* happen at the point of highest density of states DOS. This is in agreement with recent experimental data [25].

II. THE POSITIVE SEMIDEFINITE HAMILTONIAN AND ITS GROUND STATES

We generically consider the TBG system with a Coulomb interaction Hamiltonian projected to the active eight lowest bands (2 per spin-valley flavor) obtained by diagonalizing the single-particle Bistritzer-MacDonald (BM) [1] TBG Hamiltonian (see Appendix A 1 for a brief review, and more detail in Refs. [107,108]). The projected single-particle Hamiltonian reads

$$H_0 = \sum_{n=\pm 1} \sum_{\mathbf{k}\eta s} \epsilon_{n,\eta}(\mathbf{k}) c^\dagger_{\mathbf{k},n,\eta,s} c_{\mathbf{k},n,\eta,s}, \tag{1}$$

where we define $\eta = \pm$ for graphene valleys K and K', $s = \uparrow, \downarrow$ for electron spin, and $n = \pm 1$ for the lowest conduction/valence bands in each spin-valley flavor. $c^\dagger_{\mathbf{k},n,\eta,s}$ is the electron creation operator of energy band n, with the origin of $\mathbf{k}$ chosen at Γ point of the moiré Brillouin zone (MBZ).

The density-density Coulomb interaction, when projected into the active bands of Eq. (1), always takes the form of a positive semidefinite Hamiltonian (PSDH) (see proof in Ref. [109], see also brief review in Appendix A 2):

$$H_I = \frac{1}{2\Omega_{\text{tot}}} \sum_{\mathbf{G}} \sum_{\mathbf{q}\in \text{MBZ}} O_{\mathbf{q},\mathbf{G}} O_{-\mathbf{q},-\mathbf{G}}, \tag{2}$$

where Ω_{tot} is the sample area, and $\mathbf{G}$ runs over all vectors in the (triangular) moiré reciprocal lattice $\mathcal{Q}_0$. This Hamiltonian is of a same positive semidefinite form as that Kang and Vafek [71] obtained by projecting the Coulomb interaction into the Wannier basis of the active bands. In this work, we will omit the kinetic energy. Due Ref. [110], the energy splitting between the degenerate ground states of Eq. (2) is smaller than 0.1meV per electron. As shown in the rest of this work, the characteristic energy of charged and neutral excitations is about 10 meV. Thus it is safe to neglect the kinetic energy for most of the excitations. But some of the U(4) Goldstone modes might be opened a small gap due to the kinetic energy. We leave this effect of kinetic energy to future studies.

The $O_{\mathbf{q},\mathbf{G}}$ operator takes the form

$$O_{\mathbf{q},\mathbf{G}} = \sum_{\mathbf{k},m,n,\eta,s} \sqrt{V(\mathbf{G}+\mathbf{q})} M^{(\eta)}_{m,n}(\mathbf{k}, \mathbf{q}+\mathbf{G}) \times \left(\rho^{\eta}_{\mathbf{k},\mathbf{q},m,n,s} - \frac{1}{2}\delta_{\mathbf{q},\mathbf{0}}\delta_{m,n} \right), \tag{3}$$

where $V(\mathbf{q})$ is the Fourier transform of the Coulomb interaction, $\rho^{\eta}_{\mathbf{k},\mathbf{q},m,n,s} = c^\dagger_{\mathbf{k}+\mathbf{q},m,\eta,s} c_{\mathbf{k},n,\eta,s}$ is the density operator in band basis, and the $-\frac{1}{2}\delta_{\mathbf{q},\mathbf{0}}\delta_{m,n}$ factor is a chemical potential added to respect many-body charge conjugation symmetry (see Appendix A 2 a and Ref. [109]). For theoretical derivations, we shall keep $V(\mathbf{q})$ general except that we assume $V(\mathbf{q}) \geqslant 0$ and only depends on $q = |\mathbf{q}|$; although for numerical calculations we will take $V(\mathbf{q}) = 2\pi e^2 \xi \tanh(q\xi/2)/\epsilon q$ for dielectric constant $\epsilon(\sim 6)$ and screening length $\xi(\sim 10$ nm) (see Appendix A 2). In particular, $O_{-\mathbf{q},-\mathbf{G}} = O^\dagger_{\mathbf{q},\mathbf{G}}$, and thus H_I in Eq. (2) is a PSDH. An important quantity in Eq. (3) for our many-body Hamiltonian are the *form factors*, or the overlap matrices, of a set of bands m, n (Appendix A 2 a)

$$M^{(\eta)}_{m,n}(\mathbf{k}, \mathbf{q}+\mathbf{G}) = \sum_{\alpha\mathbf{Q}} u^*_{\mathbf{Q}-\mathbf{G},\alpha;m\eta}(\mathbf{k}+\mathbf{q}) u_{\mathbf{Q},\alpha;n\eta}(\mathbf{k}), \tag{4}$$

where $u_{\mathbf{Q}\alpha;n\eta}$ is the Bloch wave function of band n and valley η (here $\alpha = A, B$ denotes the microscopic graphene sublattices, and $\mathbf{Q}$ are sites of a honeycomb momentum lattice with definition in Appendix A 1, see also Ref. [107] for details). A nonzero Berry phase of the projected bands renders the spectra of the PSDH Eq. (2) not analytically solvable: the $O_{\mathbf{q},\mathbf{G}}$'s at different $\mathbf{q}, \mathbf{G}$ generically do not commute (unless in the stabilizer code limit discussed in Refs. [109,110]), and hence the PSDH is not solvable. The properties of the PSDH Eq. (2) depend on the quantitative and qualitative (symmetries) properties of the form factors in Eq. (4), which are detailed in Refs. [107–109] and briefly reviewed in Appendix A 2 a. First, in Ref. [107], we showed that $M^{(\eta)}_{m,n}(\mathbf{k}, \mathbf{q}+\mathbf{G})$ falls off exponentially with $|\mathbf{G}|$, and can be neglected for $|\mathbf{G}| > \sqrt{3}k_\theta$, where $k_\theta = 2|\mathbf{K}|\sin(\theta/2)$ is the distance between the K points of two graphene sheets. Furthermore, we showed in Refs. [108,109] that by gauge fixing the C_{2z}, T, and unitary particle-hole symmetry P [43], the form factors can be rewritten into a matrix form in the n, η basis as [see Eq. (A11)]

$$M^{(\eta)}_{mn}(\mathbf{k}, \mathbf{q}+\mathbf{G}) = \sum_{j=0}^{3} (M_j)_{m,\eta;n,\eta} \alpha_j(\mathbf{k}, \mathbf{q}+\mathbf{G}), \tag{5}$$

where $M_0 = \zeta^0\tau^0$, $M_1 = \zeta^x\tau^z$, $M_2 = i\zeta^y\tau^0$, and $M_3 = \zeta^z\tau^z$, and $\alpha_j(\mathbf{k}, \mathbf{q}+\mathbf{G})$ are real scalar functions satisfying [Eqs. (A12) and (A13) in Appendix A 3].

A further simplification [72] happens in a region of the parameter space where the AA interlayer coupling $w_0 = 0$

[72], which is called the (first) chiral limit [37] (a similar simplification occurs in a second chiral limit [109]). In this limit there is another chiral symmetry C anticommuting with the single-particle Hamiltonian, which further imposes the constraints $\alpha_1(\mathbf{k}, \mathbf{q}+\mathbf{G}) = \alpha_3(\mathbf{k}, \mathbf{q}+\mathbf{G}) = 0$ (see Ref. [110] and Appendix A 3). The first chiral limit also allows for the presence of a *Chern band basis* in which bands of Chern number $e_Y = \pm 1$ are created by the operators

$$d^\dagger_{\mathbf{k},e_Y,\eta,s} = \frac{1}{\sqrt{2}}(c^\dagger_{\mathbf{k},+,\eta,s} + ie_Y c^\dagger_{\mathbf{k},-,\eta,s}), \tag{6}$$

In Ref. [108], we detail the gauge-fixing for this basis. The Chern basis is also discussed in Refs. [72,74,108]. The form factors under the Chern basis take the simple diagonal form

$$M^{(\eta)}_{e_Y}(\mathbf{k}, \mathbf{q}+\mathbf{G}) = \alpha_0(\mathbf{k}, \mathbf{q}+\mathbf{G}) + ie_Y\alpha_2(\mathbf{k}, \mathbf{q}+\mathbf{G}). \tag{7}$$

The symmetries of the projected Hamiltonian in the nonchiral ($w_0, w_1 \neq 0$) and two chiral $w_0 = 0$ or $w_1 = 0$ limits are important. We will use the matrices ζ^a, τ^a, s^a with $a = 0, x, y, z$ as identity and x, y, z Pauli matrices in (particle-hole related) band, valley and spin-space respectively. In Ref. [109] (short review in Appendix A 2 c), we have showed that the PSDH has a U(4) symmetry in the nonchiral limit (with single-particle representations of generators $s^{ab} = \{\zeta^y\tau^y s^a, \zeta^y\tau^x s^a, \zeta^0\tau^0 s^a, \zeta^0\tau^z s^a\}$ with $a, b = 0, x, y, z$ in the energy band basis $c^\dagger_{\mathbf{k},+,\eta,s}$), and a U(4) × U(4) symmetry in the two chiral-flat limits (with single-particle representations of generators $s^{ab}_\pm = (1 \pm e_Y)\tau^a s^b/2$ in the Chern band basis $d^\dagger_{\mathbf{k},e_Y,\eta,s}$ [108], Appendix A 2 b), mirroring the results obtained by Refs. [42,71–73] for projection into the two active bands. We note that in Ref. [109] we showed these symmetries hold for any number of PH symmetric projected bands. In Appendixes A 2 c and A 2 e, we provide a summary of these detailed results. Adding the kinetic term in the first chiral limit breaks the U(4) × U(4) symmetry of the projected interaction to a U(4) subset(with generators $\tilde{s}^{ab} = \zeta^0\tau^a s^b$ in the energy band basis, $(a, b = 0, x, y, z)$). The symmetries we found in the first chiral and nonchiral limits agrees with that in Ref. [72], and the relation between our U(4) symmetry generators and those of Kang and Vafek [71] are given in Ref. [109]. We will restrict our study within the nonchiral-flat limit and first chiral-flat limit in this paper. Thus, without ambiguity, we will simply call the first chiral limit the "chiral limit."

With these symmetries, in the nonchiral-flat limit (where the projected kinetic Hamiltonian $H_0 = 0$), one can write down exact eigenstates of the PSDH Eq. (2), which we have analyzed in full detail in Ref. [110] and review in Appendix A 3 b. In the nonchiral limit, $O_{\mathbf{q},\mathbf{G}}$ is diagonal in η and s, and filling both $n = \pm$ bands of any valley/spin gives a Chern number 0 eigenstate for all even fillings $\nu = 0, \pm 2, \pm 4$ (along with any U(4) rotation) [110]:

$$|\Psi_\nu\rangle = \prod_{\mathbf{k}}\left(\prod_{j=1}^{(\nu+4)/2} c^\dagger_{\mathbf{k},+,\eta_j,s_j}c^\dagger_{\mathbf{k},-,\eta_j,s_j}\right)|0\rangle, \tag{8}$$

where $\{\eta_j, s_j\}$ are distinct valley-spin flavors which are fully occupied. They form the $[(2N_M)^{(\nu+4)/2}]_4$ irreducible representation (irrep) of the nonchiral-flat limit U(4) symmetry group, where $[\lambda^p]_4$ is short for the Young tableau notation $[\lambda, \lambda, \cdots]_4$ with $0 \leqslant p \leqslant 4$ identical rows of length λ (see Ref. [110] for a brief review). With $M^{(\eta)}_{m,n}(\mathbf{k}, \mathbf{q}+\mathbf{G})$ in Eq. (A11), we have that the state $|\Psi_\nu\rangle$ is an eigenstate of $O_{\mathbf{q},\mathbf{G}}$ satisfying $O_{\mathbf{q},\mathbf{G}}|\Psi_\nu\rangle = \delta_{\mathbf{q}0}N_M A_{\mathbf{G}}|\Psi_\nu\rangle$, where $A_{\mathbf{G}}$ is given by [Eq. (A34)]

$$A_{\mathbf{G}} = \nu\frac{\sqrt{V(\mathbf{G})}}{N_M}\sum_{\mathbf{k}}\alpha_0(\mathbf{k}, \mathbf{G}), \tag{9}$$

where N_M is the total number of moiré unit cells. For $\nu = 0$, the state Eq. (8) is always a ground state as it is annihilated by $O_{\mathbf{q},\mathbf{G}}$ [110].

In the first chiral-flat limit (where $H_0 = 0$ and $w_0 = 0$), the projected Hamiltonian Eq. (2) has as eigenstates, the *filled band* wave functions [110] (see Appendix A 3 a for brief review):

$$\left|\Psi^{\nu_+,\nu_-}_\nu\right\rangle = \prod_{\mathbf{k}}\left(\prod_{j_1=1}^{\nu_+} d^\dagger_{\mathbf{k},+1,\eta_{j_1},s_{j_1}}\prod_{j_2=1}^{\nu_-} d^\dagger_{\mathbf{k},-1,\eta_{j_2},s_{j_2}}\right)|0\rangle, \tag{10}$$

where $\nu_+ - \nu_- = \nu_C$ is the total Chern number of the state and $\nu_+ + \nu_- = \nu + 4$ $(0 \leqslant \nu_\pm \leqslant 4)$ is the total number of electrons per moiré unit cell in the projected bands, $\mathbf{k}$ runs over the entire MBZ and the occupied spin/valley indices $\{\eta_{j_1}, s_{j_1}\}$ and $\{\eta_{j_2}, s_{j_2}\}$ can be arbitrarily chosen. Moreover, these eigenstates of Eq. (2) are also eigenstates of $O_{\mathbf{q},\mathbf{G}}$ in Eq. (3), satisfying $O_{\mathbf{q},\mathbf{G}}|\Psi^{\nu_+,\nu_-}_\nu\rangle = \delta_{\mathbf{q}0}N_M A_{\mathbf{G}}|\Psi^{\nu_+,\nu_-}_\nu\rangle$, where $A_{\mathbf{G}}$ is still given by Eq. (9). They form the $([N_M^{\nu_+}]_4, [N_M^{\nu_-}]_4)$ irrep of U(4) × U(4) (Young tableaux notation, see Ref. [110]). For a fixed integer filling factor ν, we found that the states with different Chern numbers ν_C are all degenerate in the chiral-flat limit [110]. In particular, at charge neutrality $\nu = 0$, the U(4) × U(4) multiplet of $|\Psi^{\nu_+,\nu_-}_0\rangle$ with Chern number $\nu_C = \nu_+ - \nu_- = 0, \pm 2, \pm 4$ are exact degenerate ground states. At nonzero fillings ν, we cannot guarantee that the $\nu \neq 0$ eigenstates are the ground states.

In Ref. [110], we found that under a weak condition, the eigenstates Eqs. (8) and (10) become the ground states of H_I for all integer fillings $-4 \leqslant \nu \leqslant 4$ (ν even in Eq. 8). If the $\mathbf{q} = \mathbf{0}$ component of the form factor $M^{(\eta)}_{m,n}(\mathbf{k}, \mathbf{G})$ is independent of $\mathbf{k}$ for all $\mathbf{G}$'s, i.e.,

$$\text{flat metric condition: } M^{(\eta)}_{m,n}(\mathbf{k}, \mathbf{G}) = \xi(\mathbf{G})\delta_{m,n}, \tag{11}$$

then all the states in Eqs. (8) and (10) become ground states of H_I by an operator shift [Eq. (A29)] [71,109,110] (see Appendixes A 3 b and A 3 a). We noted in Ref. [107] that this flat metric condition is always true for $\mathbf{G} = \mathbf{0}$, for which $M^{(\eta)}_{m,n}(\mathbf{k}, 0) = \delta_{mn}$ from wave-function normalization. In Ref. [107] we have shown that, around the first magic angle, $M^{(\eta)}_{m,n}(\mathbf{k}, \mathbf{G}) \approx 0$ for $|\mathbf{G}| > \sqrt{3}k_\theta$ for $i = 1, 2$. Hence, the condition Eq. (11) is valid for all $\mathbf{G}$ with the exception of the 6 smallest nonzero $\mathbf{G}$ satisfying $|\mathbf{G}| = \sqrt{3}k_\theta$. Hence, the condition is largely valid, and our numerical analysis [107] confirms its validity for $\mathbf{k}$ in a large part of the MBZ. The idea to impose a similar condition as Eq. (11) first used by Kang and Vafek [71] to find the $\nu = \pm 2$ ground state for their PSDH. Due to a slightly different U(4) symmetry, our U(4) FM states are different, but overlap with the Kang and Vafek ones in the chiral limit, as discussed in detail in Refs. [109,110].

We note that for $\nu \neq 0$, the states in Eqs. (8) and (10) still remain the exact ground states if the flat metric condition Eq. (11) is not violated too much [110,111]. This is because they correspond to gapped insulator eigenstates [110,111] when condition Eq. (11) is satisfied, and the flat metric condition Eq. (11) has to be largely broken to bring down another state into the ground state. From now on, we "call" Eqs. (8) and (10) ground states of the system.

Remarkably, as we will show in the rest of our paper below, one can analytically find a large series of excitations above the ground states Eqs. (8) and (10).

Our excitations will be build out of acting with the band creation and annihilation operators on the ground states in Eqs. (8) and (10). We first need to compute the commutators in the nonchiral Hamiltonian (see Appendix B, in particular, Appendix B 1)

$$\begin{aligned}[O_{\mathbf{q},\mathbf{G}}, c^\dagger_{\mathbf{k},n,\eta,s}] &= \sum_m \sqrt{V(\mathbf{G}+\mathbf{q})} M^{(\eta)}_{m,n}(\mathbf{k}, \mathbf{q}+\mathbf{G}) c^\dagger_{\mathbf{k}+\mathbf{q},m,\eta,s},\\ [O_{\mathbf{q},\mathbf{G}}, c_{\mathbf{k},n,\eta,s}] &= -\sum_m \sqrt{V(\mathbf{G}+\mathbf{q})} M^{(\eta)*}_{m,n} \\ &\quad \times (\mathbf{k}, -\mathbf{q}-\mathbf{G}) c_{\mathbf{k}-\mathbf{q},m,\eta,s}, \end{aligned} \tag{12}$$

where we have used the property $M^{(\eta)*}_{m,n}(\mathbf{k}, -\mathbf{q}-\mathbf{G}) = M^{(\eta)}_{n,m}(\mathbf{k}-\mathbf{q}, \mathbf{q}+\mathbf{G})$ [109]. In the chiral limit, the same operators read in the Chern basis (see Appendix B 2)

$$\begin{aligned}[O_{\mathbf{q},\mathbf{G}}, d^\dagger_{\mathbf{k},e_Y,\eta,s}] &= \sqrt{V(\mathbf{G}+\mathbf{q})} M_{e_Y}(\mathbf{k}, \mathbf{q}+\mathbf{G}) d^\dagger_{\mathbf{k}+\mathbf{q},e_Y,\eta,s},\\ [O_{\mathbf{q},\mathbf{G}}, d_{\mathbf{k},e_Y,\eta,s}] &= -\sqrt{V(\mathbf{G}+\mathbf{q})} M^*_{e_Y}(\mathbf{k}, -\mathbf{q}-\mathbf{G}) d_{\mathbf{k}-\mathbf{q},e_Y,\eta,s}. \end{aligned} \tag{13}$$

From these equations, we can obtain the commutators of $O_{-\mathbf{q},-\mathbf{G}} O_{\mathbf{q},\mathbf{G}}$ with the band electron creation operators in the nonchiral case as

$$\begin{aligned}&[O_{-\mathbf{q},-\mathbf{G}} O_{\mathbf{q},\mathbf{G}}, c^\dagger_{\mathbf{k},n,\eta,s}] \\ &= \sum_m P^{(\eta)}_{mn}(\mathbf{k}, \mathbf{q}+\mathbf{G}) c^\dagger_{\mathbf{k},m,\eta,s} \\ &\quad + \sqrt{V(\mathbf{G}+\mathbf{q})} \sum_m \big(M^{(\eta)}_{m,n}(\mathbf{k}, \mathbf{q}+\mathbf{G}) c^\dagger_{\mathbf{k}+\mathbf{q},m,\eta,s} O_{-\mathbf{q},-\mathbf{G}} \\ &\quad + \sum_m M^{(\eta)}_{m,n}(\mathbf{k}, -\mathbf{q}-\mathbf{G}) c^\dagger_{\mathbf{k}-\mathbf{q},m,\eta,s} O_{\mathbf{q},\mathbf{G}} \big) \end{aligned} \tag{14}$$

and in the first chiral limit in Chern basis as

$$\begin{aligned}&[O_{-\mathbf{q},-\mathbf{G}} O_{\mathbf{q},\mathbf{G}}, d^\dagger_{\mathbf{k},e_Y,\eta,s}] \\ &= P(\mathbf{k}, \mathbf{q}+\mathbf{G}) d^\dagger_{\mathbf{k},e_Y,\eta,s} \\ &\quad + \sqrt{V(\mathbf{G}+\mathbf{q})} (M_{e_Y}(\mathbf{k}, \mathbf{q}+\mathbf{G}) d^\dagger_{\mathbf{k}+\mathbf{q},e_Y,\eta,s} O_{-\mathbf{q},-\mathbf{G}} \\ &\quad + M_{e_Y}(\mathbf{k}, -\mathbf{q}-\mathbf{G}) d^\dagger_{\mathbf{k}-\mathbf{q},e_Y,\eta,s} O_{\mathbf{q},\mathbf{G}}), \end{aligned} \tag{15}$$

respectively. Similar relations for $[O_{-\mathbf{q},-\mathbf{G}} O_{\mathbf{q},\mathbf{G}}, c_{\mathbf{k},n,\eta,s}]$ and $[O_{-\mathbf{q},-\mathbf{G}} O_{\mathbf{q},\mathbf{G}}, d_{\mathbf{k},e_Y,\eta,s}]$, where $M^{(\eta)}(\mathbf{k}, \mathbf{q}+\mathbf{G}) \to M^{(\eta)*}(\mathbf{k}, -\mathbf{q}-\mathbf{G})$, are derived in Appendix B. The matrix factor P is the convolution of the Coulomb potential and the form factor matrices. In the nonchiral case, P is a matrix given by

$$P^{(\eta)}_{mn}(\mathbf{k}, \mathbf{q}+\mathbf{G}) = V(\mathbf{G}+\mathbf{q}) (M^{(\eta)\dagger} M^{(\eta)})_{mn}(\mathbf{k}, \mathbf{q}+\mathbf{G}). \tag{16}$$

In the first chiral limit, it is a number independent on e_Y:

$$\begin{aligned} P(\mathbf{k}, \mathbf{q}+\mathbf{G})) &= V(\mathbf{G}+\mathbf{q}) |M_{e_Y}(\mathbf{k}, \mathbf{q}+\mathbf{G})|^2 \\ &= V(\mathbf{G}+\mathbf{q}) \big(\alpha_0^2(\mathbf{k}, \mathbf{q}+\mathbf{G}) + \alpha_2^2(\mathbf{k}, \mathbf{q}+\mathbf{G}) \big), \end{aligned} \tag{17}$$

where $\alpha_0(\mathbf{k}, \mathbf{q}+\mathbf{G})$ and $\alpha_2(\mathbf{k}, \mathbf{q}+\mathbf{G})$ are the decomposition of the form factors in Eq. (7). The above commutators and the existence of exact eigenstates Eqs. (10) and (8), which are ground states with the flat metric condition Eq. (11), allow for the computation of part of the low energy excitations with polynomial efficiency. We now show the summary of the computation for the bands of charge $+1$, $+2$ and neutral excitations. The charge -1, -2 excitations can be found in Appendixes C 3 and E 4, respectively.

III. CHARGE ±1 EXCITATIONS

A. Method to obtain the ±1 excitation spectrum

To find the charge one excitations (adding an electron into the system), we sum the commutators in Eq. (14) over $\mathbf{q}$, $\mathbf{G}$, and use the fact that the ground states in Eqs. (8) and (10) satisfy $(O_{\mathbf{q},\mathbf{G}} - A_{\mathbf{G}} N_M \delta_{\mathbf{q},0})|\Psi\rangle = 0$ for coefficient $A_{\mathbf{G}}$ in Eq. (9) in their corresponding limits. For any state $|\Psi\rangle$ in Eqs. (8) and (10), we find

$$[H_I - \mu N, c^\dagger_{\mathbf{k},n,\eta,s}]|\Psi\rangle = \frac{1}{2\Omega_{\text{tot}}} \sum_m R^\eta_{mn}(\mathbf{k}) c^\dagger_{\mathbf{k},m,\eta,s}|\Psi\rangle, \tag{18}$$

where N is the electron number operator, and the matrix

$$\begin{aligned} R^\eta_{mn}(\mathbf{k}) &= \sum_{\mathbf{G}\mathbf{q}m'} V(\mathbf{G}+\mathbf{q}) M^{(\eta)*}_{m'm}(\mathbf{k}, \mathbf{q}+\mathbf{G}) M^{(\eta)}_{m'n}(\mathbf{k}, \mathbf{q}+\mathbf{G}) \\ &\quad + \sum_{\mathbf{G}} 2N_M A_{-\mathbf{G}} \sqrt{V(\mathbf{G})} M^{(\eta)}_{m,n}(\mathbf{k}, \mathbf{G}) - \mu\delta_{mn}. \end{aligned} \tag{19}$$

We hence see that, if $|\Psi\rangle$ is one of the $|\Psi_\nu^{\nu_+,\nu_-}\rangle$ Eq. (10) or one of the $|\Psi_\nu\rangle$ Eq. (8) eigenstates of H_I, then $c^\dagger_{\mathbf{k},m,\eta,s}|\Psi\rangle$ can be recombined as eigenstates of H_I with eigenvalues obtained by diagonalizing the 2×2 matrix $R^\eta_{mn}(\mathbf{k})$.

In the nonchiral case, the eigenstates $|\Psi_\nu\rangle$ we found in Ref. [110] (and re-written in Eq. (8)) have both active bands $n = \pm 1$ in each valley η and spin s either fully occupied or fully empty.

In this case, we can consider two charge $+1$ states $c^\dagger_{\mathbf{k},n,\eta,s}|\Psi\rangle$ $(n = \pm)$ at a fixed $\mathbf{k}$ in a fully empty valley η and spin s. These two states then form a closed subspace with a 2×2 subspace Hamiltonian $R^\eta(\mathbf{k})$ defined by Eq. (19). Diagonalizing the matrix $R^\eta(\mathbf{k})$ then gives the excitation eigenstates and excitation energies. Furthermore, at $\nu = 0$, the state $|\Psi_{\nu=0}\rangle$ in Eq. (8) is the *ground state* of the interaction Hamiltonian H_I regardless of the flat metric condition Eq. (11), and hence $c^\dagger_{\mathbf{k},n,\eta,s}|\Psi_{\nu=0}\rangle$ always gives the charge excitation above the ground state.

If we further assume the flat band condition Eq. (11) (or its violation is small enough), all eigenstates $|\Psi_\nu\rangle$ become exact ground states and the second row of Eq. (19) vanishes (see Appendix C 1 a). Since the U(4) irrep of the ground state $|\Psi_\nu\rangle$ is $[(2N_M)^{(\nu+4)/2}]_4$, the U(4) irrep of the charge 1 excited state is given by $[(2N_M)^{(\nu+4)/2}, 1]_4$. A similar equation for the

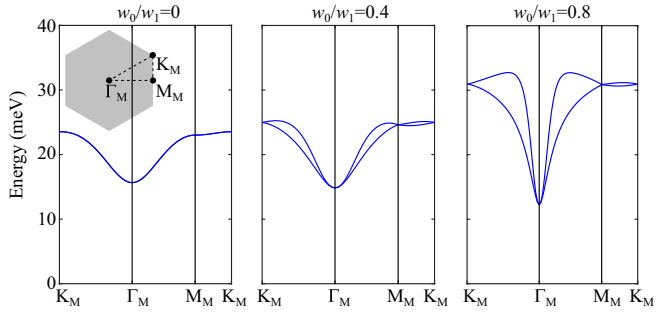

FIG. 1. Exact charge ±1 excitations given by the simplified excitation matrix [Eq. (20)] for three different w_0/w_1 at the twist angle $\theta = 1.05°$. Here we change w_0 while keeping $w_1 = 110$ meV fixed. Other parameters are given in Appendix A. These excitations are exact at the charge neutrality point ($\nu = 0$) for generic state and are exact at finite integer fillings if the flat metric condition is satisfied. The charge +1 and −1 excitations are degenerate. The exact charge ±1 excitations obtained using the full excitation matrix [Eq. (19)] without assuming the flat metric condition are given in Figs. 5 and 6 in Appendix C 4. The charge gap in those cases shrinks considerably.

charge −1 excitations is derived in in Appendix C 3, where we denote the excitation matrix as $\widetilde{R}$.

As explained in Appendix A 3, when the flat metric condition is satisfied, the second term in R^η [Eq. (19)] can be canceled by the chemical potential term (the third term), and thus we obtain a simplified expression for R^η *independent* of ν:

$$R^\eta_{mn}(\mathbf{k}) = \sum_{\mathbf{G}\mathbf{q}m'} V(\mathbf{G}+\mathbf{q}) M^{(\eta)*}_{m'm}(\mathbf{k}, \mathbf{q}+\mathbf{G}) M^{(\eta)}_{m'n}(\mathbf{k}, \mathbf{q}+\mathbf{G}). \tag{20}$$

It is worth noting that Eq. (20) is *exact* for $\nu = 0$ even without the flat metric condition Eq. (11), because the coefficient $A_{\mathbf{G}}$ [Eq. (9)] in the second term of R^η [Eq. (19)] and the chemical potential in the third term of R^η vanish at $\nu = 0$.

The simplified matrix $\widetilde{R}^\eta$ for charge −1 excitation with the flat metric condition Eq. (11) is the complex conjugation of R^η, i.e.,$\widetilde{R}^\eta_{mn}(\mathbf{k}) = R^{\eta*}_{mn}(\mathbf{k})$. This shows that, the charge −1 excitations are degenerate with the charge +1 excitations if either $\nu = 0$ or the flat metric condition Eq. (11) is satisfied. The charge +1 excitation dispersion determined by Eq. (20) (which does not depend on ν) is plotted in Fig. 1.

The parameters used in the calculation to obtain the spectrum are given in Appendix A. We find that, with the flat metric condition imposed, the charge ±1 excitation (Fig. 1) is gapped, and the minimum is at the Γ point, with a large dispersion velocity. The exact charge ±1 excitations at different fillings obtained using the full R^η matrix [Eq. (19)] of realistic parameters [which break the flat metric condition Eq. (11)] are given in Figs. 5 and 6 in Appendix C 4.

The degeneracy of the excitation spectrum depends on the filling ν of the ground state. In the nonchiral-flat U(4) limit, R^η does not depend on spin, and R^+, R^- have the same eigenvalues because they are related by the symmetry $C_{2z}P$, where P is a single-body unitary PH symmetry (App. A 2 a) [43,108,109]. Thus charge +1 excitations in different valley-spin flavors have the same energy. For the state $|\Psi_\nu\rangle$ [Eq. (8)], the +1 excitations in the empty $(4-\nu)/2$ spin-valley flavors are degenerate. Correspondingly, −1 excitations in the occupied $(4+\nu)/2$ spin-valley flavors are also degenerate.

In the (first) chiral-flat limit, and with the flat metric condition Eq. (11) [or at $\nu = 0$ without (11)], the expression for the charged excitations in the Chern basis $d^\dagger_{\mathbf{k},e_Y,\eta,s}|\Psi_\nu^{\nu_+,\nu_-}\rangle$ becomes diagonal and independent of e_Y [see Appendix C 2 for the chiral-flat limit without the flat metric condition Eq. (11)]:

$$\left[H_I - \mu N, d^\dagger_{\mathbf{k},e_Y,\eta,s}\right]|\Psi\rangle = \frac{1}{2\Omega_{\text{tot}}} R_0(\mathbf{k}) d^\dagger_{\mathbf{k},e_Y,\eta,s}|\Psi\rangle,$$
$$R_0(\mathbf{k}) = \sum_{\mathbf{G},\mathbf{q}} P(\mathbf{k}, \mathbf{q}+\mathbf{G}), \tag{21}$$

provided that the Chern band $e_Y(=\pm 1)$ in valley η and spin s is fully empty and $P(\mathbf{k}, \mathbf{q}+\mathbf{G})$ given in Eq. (17). We obtain

$$R_0(\mathbf{k}) = \sum_{\mathbf{G},\mathbf{q}} V(\mathbf{G}+\mathbf{q})[\alpha_0(\mathbf{k}, \mathbf{q}+\mathbf{G})^2 + \alpha_2(\mathbf{k}, \mathbf{q}+\mathbf{G})^2]. \tag{22}$$

The spectrum at the magic angle is shown in Fig. 1. The U(4) × U(4) irrep of the charge +1 excited states with $e_Y = 1$ and $e_Y = -1$ are given by $([N_M^{\nu_+}, 1]_4, [N_M^{\nu_-}]_4)$ and $([N_M^{\nu_+}]_4, [N_M^{\nu_-}, 1]_4)$, respectively. The charge −1 excitation details can be found in Appendix C 3.

Since in the chiral-flat limit the scattering matrix $R_0(\mathbf{k})$ is identity in the e_Y space, the excitation has degeneracy in addition to the valley-spin degeneracies. For a state in Eq. (10) with filling ν, the charge +1 and −1 excitations have degeneracies $4-\nu$ and $4+\nu$, respectively.

B. Bounds on the charge ±1 excitation gap

In this section, we will focus on the charge neutrality point ($\nu = 0$), where the second and third terms in $R^\eta(\mathbf{k})$ [Eq. (19)] vanish, and nonzero integer fillings $\nu = \pm 1, \pm 2, \pm 3$ with the flat metric condition Eq. (11) such that the second and third terms in $R^\eta(\mathbf{k})$ cancel each other. In these cases, $R^\eta(\mathbf{k})$ is a positive semidefinite matrix and hence has non-negative eigenvalues. We are able to obtain some analytical bounds for the gap of the ±1 excitation. Detail calculations are given in Appendix C 1 b. Since charge ±1 excitations in this case are degenerate, our conclusion below for charge +1 excitations also apply to charge −1 excitations.

We rewrite the $R^\eta(\mathbf{k})$ matrix as $R^\eta_{mn}(\mathbf{k}) = (M^{(\eta)\dagger}(\mathbf{k}) V M^{(\eta)}(\mathbf{k}))_{mn}$, where now $M^{(\eta)}(\mathbf{k})$ with given η and $\mathbf{k}$ is a matrix of the dimension $2N_M \cdot N_{\mathbf{G}} \times 2$ (with 2 because we are projecting into the two active TBG bands). N_M is number of moiré unit cells, $N_{\mathbf{G}}$ is the number of plane waves (MBZs) taken into consideration. By separating the $\{\mathbf{q}, \mathbf{G}\} = 0$ contribution, and using Weyl's inequalities we find in Appendix C 1 b that the energies of the excited states are $\geqslant \frac{1}{2}V(\mathbf{q}=0)/\Omega_{\text{tot}}$. The bound $\frac{1}{2}V(\mathbf{q}=0)/\Omega_{\text{tot}}$ is small but nonzero for large but finite Ω_{tot}. This shows that the states $c^\dagger_{\mathbf{k},n,\eta,s}|\Psi\rangle$ are not exactly degenerate to the ground state $|\Psi\rangle$ (note that we did not prove these are the unique ground states).

The excited states of the PSDH appears to give rise to finite gap charge 1 excitations. The largest gap happens in the atomic limit or a material, where $\langle u_m(\mathbf{k}+\mathbf{q})|u_n(\mathbf{k})\rangle = \delta_{mn}$, for which $R_{mn} = \delta_{mn}\sum_{\mathbf{q},\mathbf{G}} V(\mathbf{q}+\mathbf{G}) = \delta_{mn}\Omega_{\text{tot}} V(\mathbf{r}=0)$. Hence the gap is $\frac{1}{2}V(\mathbf{r}=0)$. Away from the atomic limit,

the gap is reduced, but will generically remain finite. We now give an argument for this. Since we know that TBG is far away from an atomic limit—the bands being topological, we expect a reduction in this gap. We perform a different decomposition of the matrix R^{η}_{mn}: we separate it into $\mathbf{G} = \mathbf{0}$ and $\mathbf{G} \neq 0$ sums (see Appendix C 1 c). The $\mathbf{G} \neq 0$ part, besides being negligible for $|\mathbf{G}| \geqslant \sqrt{3}k_\theta$ [107], is also positive semidefinite, and the eigenvalues of R^{η}_{mn} are bounded by (and close to) the $\mathbf{G} = 0$ part:

$$R^{\eta}_{mn}(\mathbf{k}) \geqslant \sum_{\mathbf{q}} V(\mathbf{q}) M^{(\eta)*}_{m',m}(\mathbf{k},\mathbf{q}) M^{(\eta)}_{m',n}(\mathbf{k},\mathbf{q}), \tag{23}$$

where $\mathbf{q}$ is summed over the MBZ, and the inequality means that the eigenvalues of the left-hand side are equal to or larger than the eigenvalues of the right-hand side. We then rewrite the right-hand side as $\sum_{\mathbf{q}} V(\mathbf{q})(\delta_{mn} - \mathfrak{G}^{mn}_{\eta}(\mathbf{k},\mathbf{q}))$, where we call the *positive semidefinite* matrix $\mathfrak{G}^{mn}(\mathbf{k},\mathbf{q})$ the generalized "quantum geometric," whose trace is the generalized Fubini-Study metric. For small momentum transfer $\mathbf{q}$, we can show that $\mathfrak{G}^{mn}(\mathbf{k},\mathbf{q}) = \sum_{ij} q_i q_j \mathfrak{G}^{mn}_{ij}(\mathbf{k}) + \mathcal{O}(q^3)$. where $\mathfrak{G}^{mn}_{ij}(\mathbf{k})$ is the conventional quantum geometric tensor (and the Fubini-Study metric) [77,116] defined by

$$\mathfrak{G}^{mn}_{ij}(\mathbf{k}) = \sum_{a,b=1}^{N} \partial_{k_i} u^{*}_{a,m}(\mathbf{k}) \left(\delta_{a,b} - \sum_{l\in\mathcal{B}} u_{a,l}(\mathbf{k}) u^{*}_{b,l}(\mathbf{k})\right) \times \partial_{k_j} u_{b,n}(\mathbf{k}), \tag{24}$$

in which $m, n \in \mathcal{B}$ are energy band indices and i, j are spatial direction indices of the orthonormal vectors $u_m(\mathbf{k})$ in a N dimensional Hilbert space, with $\mathbf{k}$ being the momentum (or other parameter). The $\mathfrak{G}^{mn}(\mathbf{k},\mathbf{q})$ tensor quantifies the distance between two eigenstates in momentum space.

Generically, we expect [77] that the inner product between two functions at $\mathbf{k}$ and $\mathbf{k}+\mathbf{q}$ to fall off as $\mathbf{q}$ increases, leaving a finite term in $R^{\eta}_{mn}(\mathbf{k})$, the electron gap, at every $\mathbf{k}$. In trivial bands in the atomic limit, the positive semidefinite matrix $\mathfrak{G}^{mn}(\mathbf{k},\mathbf{q})$ reaches its theoretical lower bound 0 and hence the charge 1 gap is maximal. In topological bands, such as TBG, the quantum metric has a lower bound and hence the charge 1 gap is reduced.

IV. CHARGE NEUTRAL EXCITATIONS

A. Method to obtain charge neutral excitations

To obtain the charge neutral excitations, we choose the natural basis $c^{\dagger}_{\mathbf{k}+\mathbf{p},m_2,\eta_2,s_2} c_{\mathbf{k},m_1,\eta_1,s_1}|\Psi\rangle$, where $|\Psi\rangle$ is any of the exact ground states and/or eigenstates in Eqs. (10) and (8) and $\mathbf{p}$ is the momentum of the excited state. The scattering matrix of these basis can be solved as easily as a one-body problem, despite the fact that Eqs. (10) and (8) hold a thermodynamic number of electrons. The details are given in Appendix D. For $|\Psi\rangle$ being a state in Eq. (8), the scattering of $c^{\dagger}_{\mathbf{k}+\mathbf{p},m_2,\eta_2,s_2} c_{\mathbf{k},m_1,\eta_1,s_1}|\Psi\rangle$ by the interaction is

$$\left[H_I - \mu N, c^{\dagger}_{\mathbf{k}+\mathbf{p},m_2,\eta_2,s_2} c_{\mathbf{k},m_1,\eta_1,s_1}\right]|\Psi_\nu\rangle = \frac{1}{2\Omega_{\text{tot}}} \sum_{m,m'} \sum_{\mathbf{q}} S^{(\eta_2,\eta_1)}_{m,m';m_2,m_1}(\mathbf{k}+\mathbf{q},\mathbf{k};\mathbf{p}) \times c^{\dagger}_{\mathbf{k}+\mathbf{p}+\mathbf{q},m,\eta_2,s_2} c_{\mathbf{k}+\mathbf{q},m',\eta_1,s_1}|\Psi_\nu\rangle, \tag{25}$$

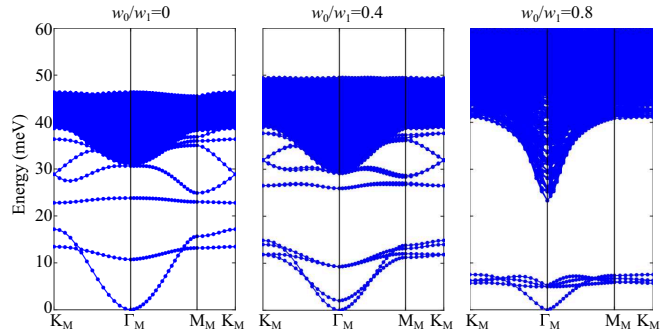

FIG. 2. Exact charge neutral excitations with the flat metric condition being imposed for three different w_0/w_1 at the twist angle $\theta = 1.05^\circ$. Here we change w_0 while keeping $w_1 = 110$meV fixed. Other parameters are given in Appendix A. These excitations are exact at the charge neutrality point ($\nu = 0$) for generic states and are exact at finite integer fillings if the flat metric condition is satisfied. The exact charge neutral excitations at different fillings without imposing flat metric condition are given in Figs. 7 and 8 in Appendix D 4. Note the softening of further Goldstone modes from finite to zero w_0, reflecting the symmetry enhancement of the first chiral limit. The continuum above the Goldstone modes is fundamentally made of independent particle-hole excitations

$$S^{(\eta_2,\eta_1)}_{m,m';m_2,m_1}(\mathbf{k}+\mathbf{q},\mathbf{k};\mathbf{p}) = \delta_{\mathbf{q},0}\left(\delta_{m,m_2}\widetilde{R}^{\eta_1}_{m'm_1}(\mathbf{k}) + \delta_{m',m_1} R^{\eta_2}_{mm_2}(\mathbf{k}+\mathbf{p})\right) - 2\sum_{\mathbf{G}} V(\mathbf{G}+\mathbf{q}) M^{(\eta_2)}_{m,m_2}(\mathbf{k}+\mathbf{p},\mathbf{q}+\mathbf{G}) M^{(\eta_1)*}_{m',m_1} \times (\mathbf{k},\mathbf{q}+\mathbf{G}), \tag{26}$$

where $R^{\eta}_{mn}(\mathbf{k})$ (Eq. (19)) and $\widetilde{R}^{\eta}_{mn}(\mathbf{k})$ are the charge ± 1 excitation matrices. A valley-spin flavor in $|\Psi_\nu\rangle$ (Eq. (8)) is either fully occupied or fully empty, thus $\{\eta_1, s_1\}$ belongs to the valley-spin flavors which are fully occupied, while $\{\eta_2, s_2\}$ belongs to the valley-spin flavors which are not occupied. Equation (26) shows that the neutral excitation scattering matrix is a sum of the two single-particle energies $(\delta_{m,m_2}\widetilde{R}^{\eta_1}_{mm_1}(\mathbf{k}_1) + \delta_{m,m_1} R^{\eta_2}_{mm_2}(\mathbf{k}_2))$ plus an interaction term. By translation invariance, the scattering preserves the total momentum $\mathbf{p}$. The spectrum of the charge neutral excitations at each $\mathbf{p}$ is a diagonalization problem of a matrix of the dimension $4N_M \times 4N_M$, where the left and right indices are $(\mathbf{k}+\mathbf{q}, m, m')$ and $(\mathbf{k}, m_2, m_2)$, respectively.

The excitation spectrum with the flat metric condition Eq. (11) being imposed, i.e.,with the R^{η} [Eq. (19)] being replaced by the simplified Eq. (20), is shown in Fig. 2. As explained in Appendix III A, the simplified charge ± 1 matrices R and $\widetilde{R}$ do not depend on the filling ν. Thus the obtained charge neutral excitation dispersion also do not depend on ν. Figure 2 is exact for $\nu = 0$ even when the flat metric condition is not satisfied since Eq. (20) is exact for $\nu = 0$. The exact charge neutral excitations at different fillings without imposing the flat metric condition Eq. (11) are given in Figs. 7 and 8 in Appendix D 4.

It is worth noting that, in the Figs. 2, 7, and 8 we just plot the eigenvalues of the scattering matrix Eq. (26), which does not assume any information of the occupied valley-spin flavors in the ground state. In practice, for a given ground state

TABLE I. The little groups (remaining symmetry subgroups) and the number of Goldstone modes (denoted by GMs in the table) of the ground states $|\Psi_\nu^{\nu_+,\nu_-}\rangle$ in the (first) chiral-flat U(4) × U(4) limit. Only $\nu \leqslant 0$ states are tabulated since the symmetry and Goldstone modes of $\nu > 0$ states are same as the $\nu < 0$ states since they are related by the many-body charge-conjugation operator (Appendix A 2 c) [109]. Only states with $\nu_+ \geqslant \nu_-$ are tabulated since $|\Psi_\nu^{\nu_+,\nu_-}\rangle$ and $|\Psi_\nu^{\nu_-,\nu_+}\rangle$ have the equivalent little groups upon interchanging of the two U(4)s, and thus have the same number of Goldstone modes.

Little group	Number of GMs	Ground states
U(4) × U(4)	0	$\|\Psi_0^{4,0}\rangle$
U(1) × U(3) × U(4)	3	$\|\Psi_{-3}^{1,0}\rangle$, $\|\Psi_{-1}^{3,0}\rangle$
U(2) × U(2) × U(4)	4	$\|\Psi_{-2}^{2,0}\rangle$
U(1) × U(3) × U(1) × U(3)	6	$\|\Psi_{-2}^{1,1}\rangle$, $\|\Psi_0^{3,1}\rangle$
U(2) × U(2) × U(1) × U(3)	7	$\|\Psi_{-1}^{2,1}\rangle$
U(2) × U(2) × U(2) × U(2)	8	$\|\Psi_0^{2,2}\rangle$

$|\Psi\rangle$, the spectrum branch annihilating (creating) electrons in empty (occupied) states does not exist.

B. Goldstone modes

Solving Eq. (26) provides us with the expression for the neutral excitations at momentum $\mathbf{p}$ on top of the TBG ground states, including the Goldstone mode, whose dispersion relation can be obtained in terms of the quantum geometry factors of the TBG. In general, the scattering matrix is not guaranteed to be positive semidefinite, and negative energy would imply instability of the ground states. However, in a large (physical) range of parameters (Appendix A) of TBG at the twist angle $\theta = 1.05°$, we find that, as shown in Figs. 2, 7, and 8, the energies of charge neutral excitations of the exact ground states $|\Psi_\nu\rangle$ in Eq. (8) in the nonchiral-flat limit and $|\Psi_\nu^{\nu_+,\nu_-}\rangle$ in Eq. (10) in the chiral-flat limit are non-negative, implying these are indeed stable ground states. As shown in Figs. 5 and 7 and discussed in Appendixes C 4 and D 4, strong (first) chiral symmetry breaking may lead to an instability to a metallic phase.

In Tables II and I, we have tabulated the little group (defined as the remaining symmetry subgroup of the state) and the number of Goldstone modes for each ground state in Eqs. (8) and (10). As examples, here we only derive the little groups and number of Goldstone modes for $|\Psi_{-2}^{1,1}\rangle$ (10) and $|\Psi_{-2}\rangle$ (8). The little groups and Goldstone modes for other states can be obtained by the same method. First we consider the ground state $|\Psi_{-2}^{1,1}\rangle$ in the (first) chiral-flat U(4) × U(4) limit, which has vanishing total Chern number. Recall that the U(4) × U(4) irrep of $|\Psi_{-2}^{1,1}\rangle$ is $([N_M^1]_4, [N_M^1]_4)$. In each of the $e_Y = \pm 1$ sectors, only one U(4) spin-valley flavor is occupied. Hence the little group of the state $|\Psi_{-2}^{1,1}\rangle$ in each e_Y sector is U(1) × U(3), where the U(1) is the phase rotation in the occupied flavor and the U(3) is the unitary rotations within the three empty flavors. Thus the total little group of the state $|\Psi_{-2}^{1,1}\rangle$ is U(1) × U(3) × U(1) × U(3), which has the rank (number of independent generators) 20. Since the Hamiltonian has a symmetry group U(4) × U(4) which has rank 32, we find the number of broken symmetry generators to be $32 - 20 = 12$. On the other hand, since all the Goldstone modes we derived are quadratic [similar to the SU(2) ferromagnets, see Eq. (30)], it is known that [117] the number of Goldstone modes is equal to 1/2 of the number of broken generators, namely, $12/2 = 6$. This is because a quadratic Goldstone mode is always a complex boson, which is equivalent to two real boson degrees of freedom corresponding to 2 broken generators.

TABLE II. The little groups (remaining symmetry subgroups) and the number of Goldstone modes (GMs) of the ground states $|\Psi_\nu\rangle$ in the nonchiral-flat U(4) limit.

Little group	Number of GMs	Ground states
U(1) × U(3)	3	$\|\Psi_{-2}\rangle$, $\|\Psi_2\rangle$
U(2) × U(2)	4	$\|\Psi_0\rangle$

Next, we consider the ground state $|\Psi_{-2}\rangle$ in the nonchiral-flat U(4) limit. Since the U(4) irrep of $|\Psi_{-2}\rangle$ is $[2N_M]_4$, only one U(4) spin-valley flavor is occupied. Thus the little group of $|\Psi_{-2}\rangle$ is U(1) × U(3), where the U(1) is within the occupied flavor and the U(3) is within the 3 empty flavors. Hence the number of broken generators is $16 - 10 = 6$, where 16 and 10 are the ranks of U(4) × U(4) and U(1) × U(3), and the number of (quadratic) Goldstone modes is $6/2 = 3$.

In the above paragraph, we have shown that state $|\Psi_{-2}^{1,1}\rangle$ in the chiral-flat limit has three more Goldstone modes than $|\Psi_{-2}\rangle$ in the nonchiral-flat limit, although their wave functions are identical. This is because, if we slightly go away from the (first) chiral-flat limit towards the nonchiral-flat limit, i.e.,take the parameter $0 < w_0 \ll w_1$, some branches of the Goldstone modes will be gapped by a finite w_0, as shown in Figs. 2, 7, and 8.

The number of Goldstone modes can also be obtained by examining the scattering matrix in Eq. (26). Here we take $|\Psi_{-2}^{1,1}\rangle$ as an example. As discussed in Appendix IV C, in the first chiral limit, the state $d^\dagger_{\mathbf{k}+\mathbf{p},e_{Y2},\eta_2,s_2} d_{\mathbf{k},e_{Y1},\eta_1,s_1} |\Psi_{-2}^{1,1}\rangle$ will be scattered to $d^\dagger_{\mathbf{k}'+\mathbf{p},e_{Y2},\eta_2,s_2} d_{\mathbf{k}',e_{Y1},\eta_1,s_1} |\Psi_{-2}^{1,1}\rangle$ through the scattering matrix $S_{e_{Y2},e_{Y1}}(\mathbf{k}', \mathbf{k}; \mathbf{p})$, which does not depend on η_1, s_1, η_2, s_2, and $S_{e_{Y2},e_{Y1}}(\mathbf{k}', \mathbf{k}; \mathbf{0})$ has an exact zero state for $e_{Y2} = e_{Y1}$ (Appendix D 3). Now we count the number of Goldstone modes on top of $|\Psi_{-2}^{1,1}\rangle$ using this property of scattering matrix.

Suppose the occupied flavors in $|\Psi_{-2}^{1,1}\rangle$ are $\{e_Y, \eta, s\} = \{+1, +, \uparrow\}, \{-1, +, \uparrow\}$. Then, for the state $d^\dagger_{\mathbf{k}+\mathbf{p},e_{Y1},\eta_2,s_2} d_{\mathbf{k},e_{Y1},\eta_1,s_1} |\Psi_{-2}^{1,1}\rangle$ to be nonvanishing, $\{e_{Y_1}, \eta_1, s_1\}$ can only take the values in the two e_Y-valley-spin flavors $\{+1, +, \uparrow\}, \{-1, +, \uparrow\}$, and $\{\eta_2, s_2\}$ can only take values in the other three valley-spin flavors in each e_Y sector. There are in total 6 nonvanishing channels. Since each channel has an zero mode given by the zero of $S_{e_{Y1},e_{Y1}}(\mathbf{k}', \mathbf{k}; \mathbf{0})$, there are 6 Goldstone modes, consistent with the group theory analysis in Table I.

C. Exact Goldstone mode and its stiffness in the (first) chiral-flat U(4) × U(4) limit

In the first chiral limit, we are able to obtain the Goldstone modes analytically. We pick the basis as

$d^\dagger_{\mathbf{k}+\mathbf{p},e_{Y2},\eta_2,s_2} d_{\mathbf{k},e_{Y1},\eta_1,s_1}|\Psi_\nu^{\nu_+,\nu_-}\rangle$, where the valley-spin flavor $\{\eta_1, s_1\}$ with Chern band basis e_{Y1} is fully occupied and the valley-spin flavor $\{\eta_2, s_2\}$ and Chern band basis e_{Y2} is fully empty. The PSDH scatters the basis to

$$\sum_{\mathbf{k}'} S_{e_{Y2},e_{Y1}}(\mathbf{k}', \mathbf{k}; \mathbf{p}) d^\dagger_{\mathbf{k}'+\mathbf{p},e_{Y2},\eta_2,s_2} d_{\mathbf{k}',e_{Y1},\eta_1,s_1} \left|\Psi_\nu^{\nu_+,\nu_-}\right\rangle, \quad (27)$$

where the scattering matrix S does not depend on η_1, η_2, s_1, s_2. The simple commutators between $O_{-\mathbf{q},-\mathbf{G}} O_{\mathbf{q},\mathbf{G}}$ and fermion creation and annihilation operators in the chiral limit [Eq. (15)] lead to a simple scattering matrix. We here focus on the $e_{Y1} = e_{Y2}$, $\mathbf{p} = 0$ channel. For generic $\nu = 0$ states and the $\nu = \pm 1, \pm 2, \pm 3$ states with flat metric condition [Eq. (11)], we have

$$\begin{aligned} &S_{e_Y;e_Y}(\mathbf{k}+\mathbf{q}, \mathbf{k}; 0) \\ &= 2\delta_{\mathbf{q},0} \sum_{\mathbf{G},\mathbf{q}'} V(\mathbf{G}+\mathbf{q}')[\alpha_0(\mathbf{k}, \mathbf{q}'+\mathbf{G})^2 + \alpha_2(\mathbf{k}, \mathbf{q}'+\mathbf{G})^2] \\ &\quad - 2\sum_{\mathbf{G}} V(\mathbf{G}+\mathbf{q})[\alpha_0(\mathbf{k}, \mathbf{q}+\mathbf{G})^2 + \alpha_2(\mathbf{k}, \mathbf{q}+\mathbf{G})^2]. \end{aligned} \quad (28)$$

The general expression of $S_{e_{Y2};e_{Y1}}(\mathbf{k}+\mathbf{q}, \mathbf{k}; \mathbf{p})$ for all channels without imposing the flat metric condition is given in Appendix D 2. We first show the presence of an exact zero eigenstate of Eq. (28) by remarking that the scattering matrix $S_{e_Y;e_Y}(\mathbf{k}+\mathbf{q}, \mathbf{k}; \mathbf{0})$ satisfies (irrespective of $\eta_{1,2}$, $s_{1,2}$):

$$\sum_{\mathbf{q}} S_{e_Y;e_Y}(\mathbf{k}+\mathbf{q}, \mathbf{k}; \mathbf{0}) = 0. \quad (29)$$

This guarantees that the rank of the scattering matrix is not maximal, and that there is at least one *exact* zero energy eigenstate, with equal amplitude on every state in the Hilbert space: $\sum_{\mathbf{k}} d^\dagger_{\mathbf{k},e_Y,\eta_2,s_2} d_{\mathbf{k},e_Y,\eta_1,s_1}|\Psi_\nu^{\nu_+,\nu_-}\rangle$. More details are given in Appendixes D 3 and D 3 a. The U(4)× U(4) multiplet of this state is also at zero energy. Moreover, the scattering matrix $S_{e_Y;e_Y}(\mathbf{k}+\mathbf{q}, \mathbf{k}; \mathbf{0})$ is positive semidefinite. The details of this proof can be found in App. D 3 a.

Since the $\mathbf{p} = \mathbf{0}$ state has zero energy, for small $\mathbf{p}$, by continuity, there will be low-energy states in the neutral continuum. By performing a k · p perturbation in the $\mathbf{p} = 0$ states in Eq. (D11), one can compute the dispersion of the low-lying states. Full details are given in Appendix D 3 b. In the chiral limit, and imposing the flat metric condition Eq. (11) we find, by using $\alpha_a(\mathbf{k}, \mathbf{q}+\mathbf{G}) = \alpha_a(-\mathbf{k}, -\mathbf{q}-\mathbf{G})$ for $a = 0, 2$ and as expected for the Goldstone of a FM, the linear term in $\mathbf{p}$ vanishes and

$$E_{\text{Goldstone}}(\mathbf{p}) = \frac{1}{2}\sum_{ij=x,y} m_{ij} p_i p_j, \quad (30)$$

to second order in $\mathbf{p}$. We find the Goldstone stiffness

$$\begin{aligned} m_{ij} = \frac{1}{2\Omega_{\text{tot}}} \sum_{\mathbf{k},\mathbf{q},\mathbf{G}} V(\mathbf{G}+\mathbf{q}) \big[&\alpha_0(\mathbf{k}, \mathbf{q}+\mathbf{G}) \partial_{k_i}\partial_{k_j} \alpha_0(\mathbf{k}, \mathbf{q}+\mathbf{G}) \\ &+ \alpha_2(\mathbf{k}, \mathbf{q}+\mathbf{G}) \partial_{k_i}\partial_{k_j} \alpha_2(\mathbf{k}, \mathbf{q}+\mathbf{G}) \\ &+ 2\partial_{k_i}\alpha_0(\mathbf{k}, \mathbf{q}+\mathbf{G}) \partial_{k_j}\alpha_0(\mathbf{k}, \mathbf{q}+\mathbf{G}) \\ &+ 2\partial_{k_i}\alpha_2(\mathbf{k}, \mathbf{q}+\mathbf{G}) \partial_{k_j}\alpha_2(\mathbf{k}, \mathbf{q}+\mathbf{G})\big]. \end{aligned} \quad (31)$$

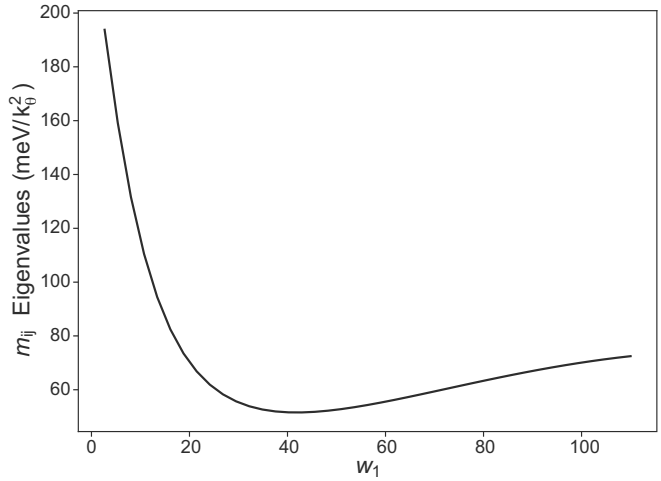

FIG. 3. The eigenvalues of the mass tensor of the Goldstone mode in the first chiral limit (31). Here w_1 is in units of meV.

Since C_{3z} symmetry is unbroken in the ground states in Eq. (10), an isotropic mass tensor $m_{ij} \propto \delta_{ij}$ is expected. The eigenvalues of m_{ij} with different values of w_1 are plotted in Fig. 3.

V. CHARGE ±2 EXCITATIONS

A. Method to obtain ±2 excitations

We now derive the charge ±2 excitations. We choose a basis for the charge +2 excitations as $c^\dagger_{\mathbf{k}+\mathbf{p},m_2,\eta_2,s_2} c^\dagger_{-\mathbf{k},m_1,\eta_1,s_1}|\Psi\rangle$, where $|\Psi\rangle$ is any of the exact ground states and or eigenstates in Eqs. (8) and (10) (for which $(O_{\mathbf{q},\mathbf{G}} - A_{\mathbf{G}} N_M \delta_{\mathbf{q},\mathbf{0}})|\Psi\rangle = 0$) and $\mathbf{p}$ is the momentum of the excited state. Hence $\{\eta_1, s_1\}$, $\{\eta_2, s_2\}$ belong to the valley-spin flavors which are not occupied. The details of the commutators of the Hamiltonian and the basis are given in Appendix E. We find

$$\begin{aligned} &\left[H_I - \mu N, c^\dagger_{\mathbf{k}+\mathbf{p},m_2,\eta_2,s_2} c^\dagger_{-\mathbf{k},m_1,\eta_1,s_1}\right]|\Psi\rangle \\ &= \frac{1}{2\Omega_{\text{tot}}} \sum_{m,m',\mathbf{q}} T^{(\eta_2,\eta_1)}_{m,m';m_2,m_1}(\mathbf{k}+\mathbf{q}, \mathbf{k}; \mathbf{p}) \\ &\quad \times c^\dagger_{\mathbf{k}+\mathbf{q}+\mathbf{p},m,\eta_2,s_2} c^\dagger_{-\mathbf{k}-\mathbf{q},m',\eta_1,s_1}|\Psi\rangle, \end{aligned} \quad (32)$$

$$\begin{aligned} &T^{(\eta_2,\eta_1)}_{m,m';m_2,m_1}(\mathbf{k}+\mathbf{q}, \mathbf{k}; \mathbf{p}) \\ &= \delta_{\mathbf{q},0}\left(\delta_{m,m_2} R^{\eta_1}_{mm_1}(-\mathbf{k}) + \delta_{m,m_1} R^{\eta_2}_{mm_2}(\mathbf{k}+\mathbf{p})\right) \\ &\quad + 2\sum_{\mathbf{G}} V(\mathbf{G}+\mathbf{q}) M^{(\eta_2)}_{mm_2}(\mathbf{k}+\mathbf{p}, \mathbf{q}+\mathbf{G}) \\ &\quad \times M^{(\eta_1)}_{m'm_1}(-\mathbf{k}, -\mathbf{q}-\mathbf{G}), \end{aligned} \quad (33)$$

where $R^\eta_{mn}(\mathbf{k})$ are the charge +1 excitation matrices in Eq. (19). We see that the charge +2 excitation energy is a sum of the two single-particle energies plus an interaction energy. By the translational invariance, scattering preserves the momentum ($\mathbf{p}$) of the excited state. The spectrum of the excitations at a given $\mathbf{p}$ is a diagonalization problem of a matrix of the dimension $4N_M \times 4N_M$. The scattering matrix $\widetilde{T}$ of the charge −2 excitations is derived in Appendix E 4. It has the same form as T here except that the charge +1 excitation

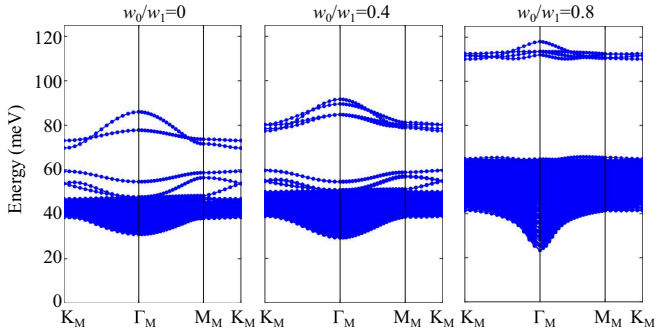

FIG. 4. Exact charge ± 2 excitations with the flat metric condition being imposed for three different w_0/w_1 at the twist angle $\theta = 1.05^\circ$. Here we change w_0 while keeping $w_1 = 110$ meV fixed. Other parameters are defined in Appendix A. These excitations are exact at charge neutrality point ($\nu = 0$) for generic states and are exact at finite integer fillings if the flat metric condition is satisfied. The charge $+2$ and -2 excitations are degenerate. The exact charge ± 2 excitations at different fillings without imposing the flat metric condition are given in Fig. 9 and 10 in Appendix E 5. Note bound states *above but not below* the two-particle continuum, confirming our analytic proof and showing the lack of Cooper pairing in TBG projected Coulomb Hamiltonians

matrix R^η is replaced by charge -1 excitation matrix $\widetilde{R}^\eta$ and the M matrix is replaced by the complex conjugation of M.

The spectrum of charge ± 2 excitations with the flat metric condition Eq. (11) imposed is shown in Fig. 4. By imposing the flat metric condition, we can replace the R^η matrix [Eq. (19)] in Eq. (33) by the simplified Eq. (20). Since Eq. (20) does not depend on ν, the obtained charge $+2$ excitation dispersion also do not depend on ν. Figure 4 is exact for $\nu = 0$ even when the flat metric condition is not satisfied since Eq. (20) is exact for $\nu = 0$. Due to the many-body charge-conjugation symmetry at $\nu = 0$ [109], the charge -2 excitations are degenerate with the charge $+2$ excitations. Exact charge ± 2 excitations without imposing the flat metric condition Eq. (11) at different fillings are given in Figs. 9 and 10 in Appendix E 5.

B. Absence of Cooper pairing in the projected Coulomb Hamiltonian

The exact expression of the three-particle excitation spectrum [Eq. (33)] allows for the determination of the Cooper pair binding energy (if any). We notice the scattering matrix Eq. (33), $T^{(\eta_2,\eta_1)}(\mathbf{k}+\mathbf{q},\mathbf{k};\mathbf{p})$, differs by a sign from the neutral charge energy Eq. (26). It is the sum of energies of two charge $+1$ excitations at momenta $\mathbf{k}+\mathbf{p}$, $-\mathbf{k}$ plus an interaction matrix, while Eq. (26) is the sum of charge $+1$ and -1 excitations minus an interaction matrix. This allows us to use the Richardson criterion [112–115] for the existence of Cooper pairing by examining the binding energy as follows:

$$\Delta(N+2) = E(N+2) + E(N) - 2E(N+1) < 0, \quad (34)$$

where $E(N)$ is the energy of the lowest state at N particles. We now assume that the lowest state of the charge $+2$ excitation continuum obtained by diagonalizing the matrices Eq. (33) is the lowest energy state at two particles above the ground state, which is confirmed by numerical calculations for a range of parameters [111]. We note that Eq. (19) is the charge $+1$ excitation. The lowest energy of the noninteracting two-particle spectrum is $2\min(R)$, where $\min(R)$ is the smallest eigenvalue of $R^\eta(\mathbf{k})$ over $\mathbf{k} \in$ MBZ and valley flavors $\eta = \pm$.

Hence we can write the binding energy as $\min(T) - 2\min(R)$, where $\min(T)$ represents the minimal eigenvalues of $T^{(\eta_2,\eta_1)}(\mathbf{k}+\mathbf{q},\mathbf{k};\mathbf{p})$ over momenta $\mathbf{p} \in$ MBZ and different valley flavors η_2, η_1. For later convenience, we denote the sum of the first two terms of Eq. (33) as Appendix

$$T'^{(\eta_2,\eta_1)}_{m,m';m_2,m_1}(\mathbf{k}+\mathbf{q},\mathbf{k};\mathbf{p}) = \delta_{\mathbf{q},0}\left(\delta_{m,m_2}R^{\eta_1}_{mm_1}(-\mathbf{k}) + \delta_{m,m_1}R^{\eta_2}_{mm_2}(\mathbf{k}+\mathbf{p})\right) \quad (35)$$

and the last term of Eq. (33) as

$$T''^{(\eta_2,\eta_1)}_{m,m';m_2,m_1}(\mathbf{k}+\mathbf{q},\mathbf{k};\mathbf{p}) = 2\sum_{\mathbf{G}} V(\mathbf{G}+\mathbf{q})M^{(\eta_2)}_{mm_2}(\mathbf{k}+\mathbf{p},\mathbf{q}+\mathbf{G})M^{(-\eta_1)*}_{m'm_1} \times (\mathbf{k},\mathbf{q}+\mathbf{G}). \quad (36)$$

We therefore have $T = T' + T''$ in short notations. Here we have used the time-reversal symmetry: $M^{(\eta_1)}_{m'm_1}(-\mathbf{k},-\mathbf{q}-\mathbf{G}) = M^{(-\eta_1)*}_{m'm_1}(\mathbf{k},\mathbf{q}+\mathbf{G})$, as explained in Appendix E 3. We use Weyl's inequalities to find sufficient conditions for the presence and absence of superconductivity. In particular, for given $\mathbf{p}$, η_2, η_1, the smallest eigenvalue of $T^{(\eta_2,\eta_1)}(\mathbf{k}+\mathbf{q},\mathbf{k};\mathbf{p})$ is smaller than the smallest eigenvalue of $T^{(\eta_2,\eta_1)'}(\mathbf{k}+\mathbf{q},\mathbf{k};\mathbf{p})$ plus the largest eigenvalue of $T^{(\eta_2,\eta_1)''}(\mathbf{k}+\mathbf{q},\mathbf{k};\mathbf{p})$. Hence we have $\min(T) \leqslant \min(T') + \max(T'') = 2\min(R) + \max(T'')$.

Therefore a sufficient criterion for the *presence* of Cooper pairing binding energy is that $T^{(\eta_2,\eta_1)''}(\mathbf{k}+\mathbf{q},\mathbf{k};\mathbf{p})$ has all eigenvalues negative:

$$\forall \eta_1, \eta_2, \mathbf{p}, \quad \mathrm{Eig}\left[T^{(\eta_2,\eta_1)''}_{mm';m_2m_1}(\mathbf{k}+\mathbf{q},\mathbf{k};\mathbf{p})\right] < 0. \quad (37)$$

On the other hand, for given $\mathbf{p}$, η_2, η_1, the smallest eigenvalue of $T^{(\eta_2,\eta_1)}(\mathbf{k}+\mathbf{q},\mathbf{k};\mathbf{p})$ is larger than the smallest eigenvalue of $T^{(\eta_2,\eta_1)'}(\mathbf{k}+\mathbf{q},\mathbf{k};\mathbf{p})$ plus the smallest eigenvalue of $T^{(\eta_2,\eta_1)''}(\mathbf{k}+\mathbf{q},\mathbf{k};\mathbf{p})$. Hence we have $\min(T) \geqslant \min(T') + \min(T'') = 2\min(R) + \min(T'')$. Therefore, a sufficient criterion for the *absence* of Cooper pairing binding energy is that $T^{(\eta_2,\eta_1)''}(\mathbf{k}+\mathbf{q},\mathbf{k};\mathbf{p})$ is positive semidefinite:

$$\forall \eta_1, \eta_2, \mathbf{p}, \quad \mathrm{Eig}\left[T^{(\eta_2,\eta_1)''}_{mm';m_2m_1}(\mathbf{k}+\mathbf{q},\mathbf{k};\mathbf{p})\right] \geqslant 0. \quad (38)$$

From the charge $+2$ excitation spectra in Figs. 4, 9, and 10 we can see that the spectrum of T consists of two parts: the two-particle continuum, which is given by the sums of two charge $+1$ excitations, and a set of charge $+2$ collective modes above the two-particle continuum. Thus it seems that T'' are always non-negative positive.

In Appendix E 3, we proved that, for the projected Coulomb Hamiltonian with the time-reversal symmetry, the matrix $T^{(\eta,-\eta)''}(\mathbf{k}+\mathbf{q},\mathbf{k};\mathbf{p})$, which corresponds to excitations of two particles from different valley, is positive semidefinite. Thus there is no inter-valley pairing superconductivity of the PSDH H_I at the integer fillings ν of the ground states in Eqs. (8) and (10). We expect this property to hold slightly away from integer fillings. Since TBG shows superconductivity at $\nu = 2$ or slightly away from integer fillings, our results

show that either kinetic energy or phonons are responsible for pairing.

Here we briefly sketch the proof. We consider the expectation value of $T^{(\eta,-\eta)\prime\prime}(\mathbf{k}+\mathbf{q},\mathbf{k};\mathbf{p})$ on an arbitrary complex function $\phi_{m_2,m_1}(\mathbf{k})$:

$$\langle T''\rangle^{\eta}_{\phi}(\mathbf{p}) = \sum_{\mathbf{k}_1,\mathbf{k}_2}\sum_{mm'm_2m_2} T^{(\eta,-\eta)\prime\prime}(\mathbf{k}_2,\mathbf{k}_1;\mathbf{p}) \times \phi^{*}_{mm'}(\mathbf{k}_2)\phi_{m_2,m_1}(\mathbf{k}_1). \tag{39}$$

As detailed in Appendix E 3, substituting the definition of the M matrix (Eq. (4) into Eq. (36), we can rewrite the expectation value as

$$\langle T''\rangle^{\eta}_{\phi}(\mathbf{p}) = \frac{2}{N_{\mathbf{G}}}\sum_{\mathbf{k}_1\mathbf{k}_2\mathbf{G}_1\mathbf{G}_2} \mathrm{Tr}[W^{\dagger}(\mathbf{k}_2+\mathbf{G}_2)W(\mathbf{k}_1+\mathbf{G}_1)] \times V(\mathbf{k}_2+\mathbf{G}_2-\mathbf{k}_1-\mathbf{G}_1), \tag{40}$$

where

$$W(\mathbf{k}+\mathbf{G}) = \sum_{m_2,m_1,\mathbf{G}} u_{m_2,\eta}(\mathbf{k}+\mathbf{p}+\mathbf{G})\phi_{m_2,m_1}(\mathbf{k})u^{\dagger}_{m_1,\eta}(\mathbf{k}+\mathbf{G}). \tag{41}$$

Here $u_{m_2,\eta}(\mathbf{k}+\mathbf{G})$ is the $2N_{\mathbf{Q}}\times 1$ vector $u_{\mathbf{Q}-\mathbf{G},\alpha;m_2,\eta}(\mathbf{k})$ and $W(\mathbf{k}+\mathbf{G})$ is a $2N_{\mathbf{Q}}\times 2N_{\mathbf{Q}}$ matrix, with $N_{\mathbf{Q}}$ being the $\mathbf{Q}$ lattice size (see Appendix A 1 for definition of the $\mathbf{Q}$ lattice). For simplicity, we use a and b to represent the composite indices $(\mathbf{Q},\alpha)$. Then $\langle T''\rangle^{\eta}_{\phi}(\mathbf{p})$ can be written as $\sum_{ab} W^{\dagger}_{ab}VW_{ab}$, where now W_{ab} is viewed as an $N_M\times 1$ vector and V an $N_M\times N_M$ matrix. Since V is positive semidefinite, for each pair of a, b, the summation over $\mathbf{k}_1,\mathbf{k}_2,\mathbf{G}_1,\mathbf{G}_2$ is non-negative. Thus T'' is positive semidefinite since $\langle T''\rangle^{\eta}_{\phi}(\mathbf{p})\geqslant 0$ for arbitrary ϕ.

In Appendix E 3, we also proved that, for $\eta_2=\eta_1=\eta$, $T^{(\eta,\eta)\prime\prime}(\mathbf{k}+\mathbf{q},\mathbf{k};\mathbf{p})$ is also positive semidefinite due to the symmetry $PC_{2z}T$, with P being the unitary single-body PH symmetry of TBG [43,108]. Therefore neither the intervalley pairing nor the intravalley Cooper pair has binding energy in the projected Coulomb Hamiltonian for any integer fillings ν in the chiral-flat limit, and for any even fillings $\nu=0,\pm2,\pm4$ in the nonchiral-flat limit.

VI. CONCLUSIONS

In this paper, we have calculated the excitation spectra of a series positive semidefinite Hamiltonians (PSDHs) initially introduced by Kang and Vafek [71] that generically appear [109] in projected Coulomb Hamiltonians to bands with nonzero Berry phases and which exhibit ferromagnetic states as ground states, under weak assumptions [109,110]. These assumptions were also used by Kang and Vafek [71] to find the $\nu=2$ ground states in TBG. In this paper, we show that not only the ground states, but a large number of low-energy excited states can be obtained in PSDHs. We obtain the general theory for the charge ±1, ±2 and neutral excitations energies and eigenstates and particularize it to the case of TBG insulating states. We find that charge $+1$ excitations are gapped, with the smallest gap at the Γ point. In both the (first) chiral-flat and nonchiral-flat limits, we find the Goldstone stiffness of the ferromagnetic state, as well as the Cooper pairing binding at integer fillings. In particular, we proved by the Richardson criterion [112–115] that Cooper pairing is not favored at integer fillings (even fillings when nonchiral) in the flat band limit. Since superconductivity has been observed in experiments with screened Coulomb potentials [7–9] (such as at $\nu=2$), we conjecture the origin of superconductivity in TBG is not Coulomb, but is contributed by other mechanisms, e.g.,the electron-phonon interaction [59,60,85], or due to kinetic terms. In particular, our theorem shows that the Luttinger-Kohn mechanism of creating attractive interactions out of repulsive Coulomb forces is ineffective for flat bands. A similar statement can be made for the superexchange interaction. A finite kinetic energy is hence required for these mechanisms.

In future work, the charge excitation energies of these Hamiltonians will be obtained in perturbation theory with the kinetic terms. A further question, of whether there are other further eigenstates of the PSDHs, remains unsolved.

ACKNOWLEDGMENTS

B.A.B thanks Oskar Vafek for fruitful discussions, and for sharing their similar results on this problem before publication [103], where they also compute the Goldstone and charge 1 excitation spectrum, which agrees with ours. B.A.B also thanks Pablo Jarillo-Herrero for discussions and for pointing out Ref. [25]. This work was supported by the DOE Grant No. DE-SC0016239, the Schmidt Fund for Innovative Research, Simons Investigator Grant No. 404513, the Packard Foundation, the Gordon and Betty Moore Foundation through Grant No. GBMF8685 towards the Princeton theory program, and a Guggenheim Fellowship from the John Simon Guggenheim Memorial Foundation. Further support was provided by the NSF-EAGER Grant No. DMR 1643312, NSF-MRSEC Grants No. DMR-1420541 and No. DMR-2011750, ONR No. N00014-20-1-2303, Gordon and Betty Moore Foundation through Grant GBMF8685 towards the Princeton theory program, BSF Israel US foundation No. 2018226, and the Princeton Global Network Funds. B.L. acknowledge the support of Princeton Center for Theoretical Science at Princeton University during the early stage of this work.

APPENDIX A: REVIEW OF NOTATION: SINGLE-PARTICLE AND INTERACTING HAMILTONIANS

For completeness, we here briefly review the notations used for the single-particle and interacting Hamiltonians. Their properties and (explicit and hidden) symmetries of both the single-particle and the interacting problems are detailed at length in our recent papers [107–110].

1. Single-particle Hamiltonian: short review of notation

The single-particle Hamiltonian, symmetries, and properties of the wave functions have been discussed at length in Refs. [43,107,108]. For completeness of notation, we give its expression here, for completeness, but we skip all details. The total single-particle Hamiltonian is

$$\hat{H}_0 = \sum_{\mathbf{k}\in\mathrm{MBZ}}\sum_{\eta\alpha\beta s}\sum_{\mathbf{Q}\mathbf{Q}'}\left[h^{(\eta)}_{\mathbf{Q}\mathbf{Q}'}(\mathbf{k})\right]_{\alpha\beta}c^{\dagger}_{\mathbf{k},\mathbf{Q},\eta,\alpha s}c_{\mathbf{k},\mathbf{Q}',\eta,\beta s}. \tag{A1}$$

where $c^\dagger_{\mathbf{k},\mathbf{Q},\eta,\alpha s}$ is the creation operator at momentum $\mathbf{k}$ (in the moiré BZ - MBZ) in valley η ($\pm$), sublattice α (1,2), spin s ($\uparrow\downarrow$), and moiré momentum lattice $\mathbf{Q}$. The Hamiltonians in the two valleys are

$$h^{(+)}_{\mathbf{Q}\mathbf{Q}'}(\mathbf{k}) = \delta_{\mathbf{Q},\mathbf{Q}'} v_F(\mathbf{k}-\mathbf{Q})\cdot\boldsymbol{\sigma} + \sum_{j=1}^{3}\left(\delta_{\mathbf{Q}-\mathbf{Q}',\mathbf{q}_j} + \delta_{\mathbf{Q}'-\mathbf{Q},\mathbf{q}_j}\right)T_j,$$

$$h^{(-)}_{\mathbf{Q}\mathbf{Q}'}(\mathbf{k}) = \delta_{\mathbf{Q},\mathbf{Q}'} v_F(\mathbf{k}-\mathbf{Q})\cdot\boldsymbol{\sigma}^* + \sum_{j=1}^{3}\left(\delta_{\mathbf{Q}-\mathbf{Q}',\mathbf{q}_j} + \delta_{\mathbf{Q}'-\mathbf{Q},\mathbf{q}_j}\right)\sigma_x T_j \sigma_x, \tag{A2}$$

where $\boldsymbol{\sigma} = (\sigma_x, \sigma_y)$, $\boldsymbol{\sigma}^* = (-\sigma_x, \sigma_y)$ are Pauli matrices, $T_j = w_0\sigma_0 + w_1(\cos\frac{2\pi}{3}(j-1)\sigma_x + \sin\frac{2\pi}{3}(j-1)\sigma_y)$, and $\mathbf{q}_j = k_\theta C_{3z}^{j-1}(0,1)^T$ $(j=1,2,3)$ with $k_\theta = 2|K|\sin\frac{\theta}{2}$ being the distance of the Graphene K momenta from the top layer and bottom layer, θ the twist angle, w_0 the interlayer AA hopping, and w_1 the interlayer AB hopping. $\mathbf{Q}$ belongs to a hexagonal momentum space lattice, $\mathbf{Q}\in\mathcal{Q}_\pm$, where $\mathcal{Q}_\pm = \mathcal{Q}_0 \pm \mathbf{q}_1$. The eigenstates of Eq. (A1) take the form

$$c^\dagger_{\mathbf{k}n\eta s} = \sum_{\mathbf{Q}\alpha} u_{\mathbf{Q}\alpha;n\eta}(\mathbf{k}) c^\dagger_{\mathbf{k},\mathbf{Q},\eta,\alpha s}. \tag{A3}$$

where $c^\dagger_{\mathbf{k}+\mathbf{G},\mathbf{Q},\eta\alpha s} = c^\dagger_{\mathbf{k},\mathbf{Q}-\mathbf{G},\eta\alpha s}$, for any moiré reciprocal wave vector $\mathbf{G}$, and hence

$$u_{\mathbf{Q}\alpha;n\eta}(\mathbf{k}+\mathbf{G}) = u_{\mathbf{Q}-\mathbf{G},\alpha;n\eta}(\mathbf{k}) \tag{A4}$$

such that $c^\dagger_{\mathbf{k}+\mathbf{G},n\eta s} = c^\dagger_{\mathbf{k}n\eta s}$. This is the MBZ periodic gauge.

In the numerical calculations, we take the parameters $\theta = 1.05^\circ$, $|K| = 1.703$ Å^{-1}, $v_F = 5.944$ eV Å, and $w_1 = 110$ meV. The projected kinetic Hamiltonian in the flat bands will be denoted by H_0 (without hat), which is given in Eq. (1).

2. Interaction Hamiltonian: short review of notation

The many-body Hamiltonian, symmetries, and properties of the wave functions, as well as the derivations, have been discussed at length in Refs. [109,110]. For completeness of notation, we give its expression here, for completeness, but we skip all details. The Hamiltonian before projection was derived to be (denoted by a hat) [109,110]:

$$\hat{H}_I = \frac{1}{2\Omega_{\rm tot}}\sum_{\mathbf{G}}\sum_{\mathbf{q}\in\rm MBZ} V(\mathbf{G}+\mathbf{q})\delta\rho_{-\mathbf{G}-\mathbf{q}}\delta\rho_{\mathbf{G}+\mathbf{q}};$$

$$V(\mathbf{r}) = \frac{1}{\Omega_{\rm tot}}\sum_{\mathbf{G}}\sum_{\mathbf{q}\in\rm MBZ} e^{-i(\mathbf{q}+\mathbf{G})\cdot\mathbf{r}} V(\mathbf{q}+\mathbf{G}), \tag{A5}$$

where

$$\delta\rho_{\mathbf{q}+\mathbf{G}} = \sum_{\eta,\alpha,s,\mathbf{k},\mathbf{Q}}\left(c^\dagger_{\mathbf{k}+\mathbf{q},\mathbf{Q}-\mathbf{G},\eta,\alpha,s}c_{\mathbf{k},\mathbf{Q},\eta,\alpha,s} - \frac{1}{2}\delta_{\mathbf{q},\mathbf{0}}\delta_{\mathbf{G},\mathbf{0}}\right) \tag{A6}$$

is the total electron density at momentum $\mathbf{q}+\mathbf{G}$ relative to the charge neutral point. $\Omega_{\rm tot}$ is the total area of the moiré lattice, $\mathbf{G}$ sums over the moiré reciprocal lattice, and $\mathbf{q}$ sums over momenta in MBZ zone.

For the analytic derivations in the current paper, we keep $V(\mathbf{r})$ generic. For the numerical plots of the energy dispersion and other properties, we use twisted bilayer graphene Coulomb interactions screened by the electrons in the two planar conducting gates [71,118]: $V(\mathbf{r}) = U_\xi\sum_{n=-\infty}^{\infty}(-1)^n/\sqrt{(\mathbf{r}/\xi)^2+n^2}$ with $\xi = 10$ nm being the distance between the two gates, $U_\xi = e^2/(\epsilon\xi) = 26$ meV (in Gauss units), $\epsilon\approx 6$ the dielectric constant of boron nitride. The derivation of this interaction was explained at length in Ref. [109,110]. It was also showed that the interaction has nonvanishing Fourier component only for intra-valley scattering to give

$$V(\mathbf{q}) = (\pi\xi^2 U_\xi)\frac{\tanh(\xi q/2)}{\xi q/2}. \tag{A7}$$

For the given values of the parameters, $V(\mathbf{q})$ was plotted in Ref. [108] and is a slowly decreasing function of $|\mathbf{q}|$ in the BZ, reaching (around the magic angle) about half of its maximal value as $|\mathbf{q}|$ spans the whole MBZ around.

a. Gauge fixing and the projected interaction

We define for our many-body Hamiltonian the form factors, also called the overlap matrix of a set of bands m, n as

$$M^{(\eta)}_{m,n}(\mathbf{k},\mathbf{q}+\mathbf{G}) = \sum_\alpha\sum_{\mathbf{Q}} u^*_{\mathbf{Q}-\mathbf{G},\alpha;m\eta}(\mathbf{k}+\mathbf{q})u_{\mathbf{Q},\alpha;n\eta}(\mathbf{k}), \tag{A8}$$

In terms of which the projected density operator interaction and Hamiltonian to a set of bands denoted by m, n can be written as

$$H_I = \frac{1}{2\Omega_{\rm tot}}\sum_{\mathbf{G}}\sum_{\mathbf{q}\in\rm MBZ} V(\mathbf{G}+\mathbf{q})\overline{\delta\rho}_{-\mathbf{G}-\mathbf{q}}\overline{\delta\rho}_{\mathbf{G}+\mathbf{q}},$$

$$\overline{\delta\rho}_{\mathbf{G}+\mathbf{q}} = \sum_{\eta s}\sum_{mn\in\rm proj}\sum_{\mathbf{k}} M^{\eta}_{m,n}(\mathbf{k},\mathbf{q}+\mathbf{G}) \times\left(c^\dagger_{\mathbf{k}+\mathbf{q},m,\eta,s}c_{\mathbf{k},n,\eta,s} - \frac{1}{2}\delta_{\mathbf{q},0}\delta_{mn}\right).$$

For our working convenience, we then define the operator

$$O_{\mathbf{q},\mathbf{G}} = \sqrt{V(\mathbf{q}+\mathbf{G})}\overline{\delta\rho}_{\mathbf{G}+\mathbf{q}}. \tag{A9}$$

This allows us to rewrite the projected interaction Hamiltonian H_I into the form of Eqs. (2) and (3). While most of the projected Hamiltonian properties are valid for any number of projected bands that respect the symmetries of the system (including PH), in TBG at the first magic angle we usually are interested in the projection of the Hamiltonian onto *the lowest two flat bands* per spin per valley of TBG (8 bands in total). An important step in any calculations—especially numerical—is the gauge-fixing procedure. Different gauges for the wave functions, that make different symmetries of the form factors Eq. (A8) more explicit, can be chosen. This is explained at length in our manuscript Ref. [109], but for completeness we briefly mention them here. We consider only two active bands, the general gauge-fixing mechanism for projection in more than two bands is found in Ref. [109]. To fix the gauge of the Bloch wave functions in Eq. (A3), $|\psi_{\mathbf{k},n,\eta,s}\rangle = \sum_{\mathbf{Q},\alpha} u_{\mathbf{Q},\alpha;m\eta}(\mathbf{k})c^\dagger_{\mathbf{k},\mathbf{Q},\eta,\alpha,s}|0\rangle$, where $u_{\mathbf{Q},\alpha;m\eta}(\mathbf{k})$ is the solution of the single-particle Hamiltonian $h^{(\eta)}_{\mathbf{Q}\mathbf{Q}'}(\mathbf{k})$, in each $\eta = \pm$, $s = \uparrow\downarrow$ sector, we label the higher energy band by $m = +$

and the lower band by $m = -$. Due to the spin-SU(2) symmetry, we set the real space wave functions for $s = \uparrow\downarrow$ to be identical and omit the index s for the single-particle states. For a symmetry operation g, the sewing matrices $B^g_{n'\eta',n\eta}(\mathbf{k}) = \langle\psi_{g\mathbf{k},n',\eta'}|g|\psi_{\mathbf{k},n,\eta}\rangle$, which relate states at momentum $\mathbf{k}$ with states at the transformed momentum $g\mathbf{k}$ can be consistently chosen to be

$$B^{C_{2z}T}(\mathbf{k}) = \zeta^0\tau^0, \quad B^{C_{2z}}(\mathbf{k}) = \zeta^0\tau^x,$$
$$B^{P}(\mathbf{k}) = i\zeta^y\tau^z, \quad B^{C_{2z}P}(\mathbf{k}) = \zeta^y\tau^y \tag{A10}$$

for the $C_{2z}T$, C_{2z}, P symmetries of TBG where ζ^a, τ^a ($a = 0, x, y, z$) are Pauli-matrices acting on the band and valley indices, respectively [109]. Here P is a unitary single-body PH symmetry that transforms $\mathbf{k}$ to $-\mathbf{k}$ [43,108]. We leave the other sewing matrices—for C_{3z}, C_{2x}—unfixed. With these sewing matrices, once we obtain, by diagonalizing the single-particle Hamiltonian, the wave functions in the valley $\eta = +$ for band $m = +$, then we first fix the $C_{2z}T$ (in TBG, this is done at the detriment of the wave function being continuous), then we use of the PH to generate the $m = -$ band, while finally, using C_{2z} symmetry to generate the wave functions in the valley $\eta = -$. In Ref. [109], we use the above gauge to determine the most generic form of the M matrix coefficient [Eq. (A8)]. We found that—away from the point $w_1 = 0$ in parameter space which we call "second chiral limit"—we can decompose the M matrix into four terms [108,109]

$$M(\mathbf{k}, \mathbf{q}+\mathbf{G}) = \zeta^0\tau^0\alpha_0(\mathbf{k}, \mathbf{q}+\mathbf{G}) + \zeta^x\tau^z\alpha_1(\mathbf{k}, \mathbf{q}+\mathbf{G}) + i\zeta^y\tau^0\alpha_2(\mathbf{k}, \mathbf{q}+\mathbf{G}) + \zeta^z\tau^z\alpha_3(\mathbf{k}, \mathbf{q}+\mathbf{G}), \tag{A11}$$

where $\alpha_{0,1,2,3}$ are real functions which satisfy the following symmetry conditions:

$$\alpha_a(\mathbf{k}, \mathbf{q}+\mathbf{G}) = \alpha_a(\mathbf{k}+\mathbf{q}, -\mathbf{q}-\mathbf{G}) \quad \text{for } a = 0, 1, 3, \quad \alpha_2(\mathbf{k}, \mathbf{q}+\mathbf{G}) = -\alpha_2(\mathbf{k}+\mathbf{q}, -\mathbf{q}-\mathbf{G}), \tag{A12}$$

$$\alpha_a(\mathbf{k}, \mathbf{q}+\mathbf{G}) = \alpha_a(-\mathbf{k}, -\mathbf{q}-\mathbf{G}) \quad \text{for } a = 0, 2, \quad \alpha_a(\mathbf{k}, \mathbf{q}+\mathbf{G}) = -\alpha_a(-\mathbf{k}, -\mathbf{q}-\mathbf{G}) \quad \text{for } a = 1, 3. \tag{A13}$$

In particular, the combination of Eqs. (A12) and (A13) implies that at $\mathbf{q} = \mathbf{0}$, we have

$$\alpha_0(\mathbf{k}, \mathbf{G}) = \alpha_0(-\mathbf{k}, \mathbf{G}), \quad \alpha_j(\mathbf{k}, \mathbf{G}) = -\alpha_j(-\mathbf{k}, \mathbf{G}), \quad (j = 1, 2, 3). \tag{A14}$$

Note that the same gauge fixing can be found with projection in a larger number of bands [109].

A further simplification occurs in the first chiral limit $w_0 = 0$ of the single-particle Hamiltonian due to the presence of an extra symmetry [72,108,109]. (A similar simplification takes place in the second chiral limit $w_1 = 0$, found in Refs. [108,109]). In this limit there is another (chiral) symmetry C of the one-body first-quantized Hamiltonian $h_{QQ'}(k)$, which in band space is defined by its sewing matrix:

$$B^C_{m\eta',n\eta}(\mathbf{k}) = \langle\psi_{\mathbf{k},m,\eta'}|C|\psi_{\mathbf{k},n,\eta}\rangle \propto \delta_{m,-n}\delta_{\eta',\eta}. \tag{A15}$$

A gauge choice in which $B^C_{m\eta',n\eta}(\mathbf{k})$ is $\mathbf{k}$ independent is possible

$$B^C(\mathbf{k}) = \zeta^y\tau^z. \tag{A16}$$

This allows us to find the wave function of the $-$ band at $\mathbf{k}$ from the $+$ band at $\mathbf{k}$, in the same valley. In Ref. [109], we prove that the M matrix in the interaction satisfies the chiral symmetry, $B^{C\dagger}M(\mathbf{k}, \mathbf{q}+\mathbf{G})B^C = M(\mathbf{k}, \mathbf{q}+\mathbf{G})$. Thus with the chiral symmetry, M takes the form

$$M(\mathbf{k}, \mathbf{q}+\mathbf{G}) = \zeta^0\tau^0\alpha_0(\mathbf{k}, \mathbf{q}+\mathbf{G}) + i\zeta^y\tau^0\alpha_2(\mathbf{k}, \mathbf{q}+\mathbf{G}). \tag{A17}$$

b. Chern band basis

In Ref. [108], we have shown that the two flat bands can be recombined as two Chern bands:

$$d^\dagger_{\mathbf{k},e_Y,\eta,s} = \frac{1}{\sqrt{2}}(c^\dagger_{\mathbf{k},+,\eta,s} + ie_Y c^\dagger_{\mathbf{k},-,\eta,s}). \tag{A18}$$

Their corresponding Berry curvatures are continuous in the MBZ and yield Chern numbers $e_Y = \pm 1$, respectively. We fixed the ambiguities by requiring that the Berry's curvature of each Chern band basis $d^\dagger_{\mathbf{k},e_Y,\eta,s}$ is continuous, or, equivalently,

$$\lim_{\mathbf{q}\to 0} |\langle u'_{\mathbf{k}+\mathbf{q},e_Y,\eta,s}|u'_{\mathbf{k},e'_Y,\eta,s}\rangle| = \delta_{e_Y,e'_Y}, \tag{A19}$$

where $|u'_{\mathbf{k},e_Y,\eta,s}\rangle$ is the periodic part of the Bloch wavefunction for the operator $d^\dagger_{\mathbf{k},e_Y,\eta,s}$. In this gauge the band $d^\dagger_{\mathbf{k},e_Y,\eta,s}$ has nonzero Chern number $C_{e_Y,\eta,s} = e_Y$ [74,108]. The Chern numbers of $d^\dagger_{\mathbf{k},e_Y,-,s}$ equals to the Chern numbers of $d^\dagger_{\mathbf{k},e_Y,+,s}$, because they are related by C_{2z} rotation.

The M matrix in the Chern band basis becomes

$$M^{(\eta)}_{e_Y,e_Y}(\mathbf{k}, \mathbf{q}+\mathbf{G}) = M_{e_Y}(\mathbf{k}, \mathbf{q}+\mathbf{G})$$
$$= \alpha_0(\mathbf{k}, \mathbf{q}+\mathbf{G}) + ie_Y\alpha_2(\mathbf{k}, \mathbf{q}+\mathbf{G}), \tag{A20}$$

$$M^{(\eta)}_{-e_Y,e_Y}(\mathbf{k}, \mathbf{q}+\mathbf{G}) = \eta F_{e_Y}(\mathbf{k}, \mathbf{q}+\mathbf{G}),$$
$$F_{e_Y}(\mathbf{k}, \mathbf{q}+\mathbf{G}) = \alpha_1(\mathbf{k}, \mathbf{q}+\mathbf{G}) + ie_Y\alpha_3(\mathbf{k}, \mathbf{q}+\mathbf{G}). \tag{A21}$$

For later convenience, we have introduced the factors $M_{e_Y}(\mathbf{k}, \mathbf{q}+\mathbf{G})$ and $F_{e_Y}(\mathbf{k}, \mathbf{q}+\mathbf{G})$ to represent the diagonal element and off-diagonal element in the Chern band basis, respectively. In the first chiral limit, where $\alpha_1 = \alpha_3 = 0$, we have $F_{e_Y} = 0$.

c. Many-body charge-conjugation symmetry of the projected interaction and kinetic Hamiltonian

In Ref. [109], we showed that the full projected Hamiltonian $H_0 + H_I$ has a many-body charge-conjugation symmetry, $\mathcal{P}_c$ defined as the single-particle transformation $C_{2z}TP$

followed by an interchange between electron annihilation operators c and creation operators $c^\dagger$: $\mathcal{P}_c c^\dagger_{\mathbf{k},n,\eta,s}\mathcal{P}_c^{-1} = c_{-\mathbf{k},m,\eta',s}B^{C_{2z}TP}_{m\eta',n\eta}(\mathbf{k})$:

$$\mathcal{P}_c H_0 \mathcal{P}_c^{-1} = H_0 + const. \quad \mathcal{P}_c \delta\rho_{\mathbf{G}+\mathbf{q}}\mathcal{P}_c^{-1} = -\delta\rho_{\mathbf{G}+\mathbf{q}}. \tag{A22}$$

The interaction has the charge-conjugation symmetry, and the many-body physics is PH symmetric in this limit.

d. The U(4) symmetry of the projected Hamiltonian in the flat-band limit

Using the unitary PH symmetry P introduced in Ref. [43], we demonstrated in Ref. [109] that the projected TBG Hamiltonian has a U(4) symmetry if the kinetic energy is set to zero (flat band limit), for *any* number of projected bands. This generalizes the U(4) symmetry introduced in Ref. [72] for the two active bands. Using the continuous symmetry operator notation

$$[e^{i\gamma_{ab}S^{ab}}, H_I] = 0, \quad \forall\gamma_{ab} \in \mathbb{R};$$
$$S^{ab} = \sum_{\mathbf{k},m,m',\eta,\eta',s,s'} c^\dagger_{\mathbf{k},m,\eta,s} s^{ab}_{m,\eta,s;m',\eta',s'} c_{\mathbf{k},m',\eta',s'}, \tag{A23}$$

we can generate a full set of U(4) generators given by [109]

$$s^{ab} = \{\zeta^0\tau^0 s^b,\ \zeta^y\tau^x s^b,\ \zeta^y\tau^y s^b,\ \zeta^0\tau^z s^b\} \quad (a, b = 0, x, y, z). \tag{A24}$$

where the Pauli matrices ζ^a, τ^a, s^a with $a = 0, x, y, z$ are identity and x, y, z Pauli matrices in band, valley, and spin space, respectively. For $2N_1$, $N_1 \in \mathbb{Z}$ projected bands, the generators would be identical, with the ζ representing the $+ = \{1, \ldots, N_1\}$ and $- = \{N_1 + 1, \ldots, 2N_1\}$ bands.

The kinetic plus the projected interaction term exhibit the Cartan symmetry $\mathrm{U}(2) \times U(2)$ subgroup of the U(4) symmetry group of the projected interaction, which can be most naturally chosen as the valley spin and charge: Cartan: $\zeta^0\tau^0 s^0$, $\zeta^0\tau^0 s^z$, $\zeta^0\tau^z s^0$, $\zeta^0\tau^z s^z$.

e. Enhanced U(4) × U(4) *symmetries in the first chiral limit* $w_0 = 0$

In Ref. [109], we demonstrated in detail the presence of two enhanced unitary U(4) × U(4) symmetry in two limits of the single-particle parameter space the first and second chiral limits $w_0 = 0 < w_1$ and $w_1 = 0 < w_0$. For the first chiral limit $w_0 = 0$, this symmetry was presented in Ref. [72] for the case of two projected bands, but we find that it is maintained, in both chiral limits, for a projection in any number of bands. For the matrix elements in Eq. (A17), the interaction commutes with the following matrices, which form the U(4) × U(4) generators [109]:

$$\zeta^0\tau^a s^b, \quad \zeta^y\tau^a s^b \quad (a, b = 0, x, y, z). \tag{A25}$$

The Cartan subalgebra of the chiral U(4) × U(4) is the Cartan subalgebra of the $\mathrm{U}(2)_{\mathrm{nonchiral}} \times \mathrm{U}(2)_{\mathrm{nonchiral}} \times \mathrm{U}(2)_{\mathrm{chiral}} \times \mathrm{U}(2)_{\mathrm{chiral}}$: $\zeta^0\tau^0 s^0$, $\zeta^0\tau^0 s^z$, $\zeta^0\tau^z s^0$, $\zeta^0\tau^z s^z$, $\zeta^y\tau^0 s^0$, $\zeta^y\tau^0 s^z$, $\zeta^y\tau^z s^0$, $\zeta^y\tau^z s^z$. The U(4) implied by $C_{2z}P$ [Eq. (A24)] is a subgroup of this U(4) × U(4), but not one of the U(4) factors [109].

In Ref. [108], we found that there exists a further more convenient gauge choice for the wave functions in the chiral limit $w_0 = 0$, called the Chern basis (an extension to many bands of the Chern basis in Ref. [72] to many bands), in which we choose the single-particle representations of U(4) × U(4) generators as

$$s^{ab}_+ = \tfrac{1}{2}(\zeta^0 + \zeta^y)\tau^a s^b,$$
$$s^{ab}_- = \tfrac{1}{2}(\zeta^0 - \zeta^y)\tau^a s^b, \quad (a, b = 0, x, y, z), \tag{A26}$$

which correspond to the first U(4) and second U(4), respectively. Adding the kinetic term in the chiral limit breaks the U(4) × U(4) symmetry of the projected interaction, to a U(4) subset $\zeta^0\tau^a s^b$, $(a, b = 0, x, y, z)$.

We note that the nonchiral-flat U(4) symmetry and the first chiral-flat U(4) × U(4) symmetry are first identified by Ref. [72]. A similar U(4) symmetry is proposed in Ref. [71], the difference and similarity between which and the symmetries reviewed here is studied in [109].

f. U(4) irrep of electrons in the nonchiral-flat case and the Chern basis in the U(4) × U(4) *chiral limit*

In Ref. [109], we showed that the eight single-particle basis of the nonchiral-flat U(4) symmetry generators given in Eq. (A24) can be decomposed into two four-dimensional fundamental irreps of the U(4) group, which have ζ_y eigenvalues $e_Y = \pm 1$, respectively, for each momentum $\mathbf{k}$ [Eq. (A18)]. The U(4) generators in the Chern band basis are $s^{ab}(e_Y) = e_Y\tau^x s^a,\ e_Y\tau^y s^a,\ \tau^0 s^a,\ \tau^z s^a$, respectively. We also showed [109] that the $e_Y = +1$ irrep and the $e_Y = -1$ irrep are the same—and not conjugate—irrep: the four-dimensional fundamental U(4) irrep represented by a one-box Young tableau labeled by $[1]_4$. We presented a detailed review of the U(4) representations related to TBG in Ref. [109], but for the purpose of the current paper, the notation adopted for irreps is the standard Young tableau, conveniently denoted by $[\lambda_1, \lambda_2, \cdots]_N$, where λ_i is the number of boxes in row i $(\lambda_i \geqslant \lambda_{i+1})$. The number of boxes in the i-th row is no smaller than that in the $(i + 1)$th row. The *Hook rule* then provides the dimensions of each of these irreps. In particular, $[1^N]_N$ is an $\mathrm{SU}(N)$ singlet state.

In the first chiral limit $w_0 = 0$, $d^\dagger_{\mathbf{k},e_Y,\eta,s}$ defined in Eq. (A18) gives the single-particle basis irrep U(4) × U(4) of Eq. (A26). We proved in Ref. [109] that $d^\dagger_{\mathbf{k},+1,\eta,s}$ generates the $([1]_4, [0]_4)$ irrep of U(4) × U(4), while $d^\dagger_{\mathbf{k},-1,\eta,s}$ generates the $([0]_4, [1]_4)$ irrep of U(4) × U(4) with generators $s^{ab}_\pm = \frac{1}{2}(1 \pm e_Y)\tau^a s^b$, respectively. A similar discussion is provided for the second chiral limit $w_1 = 0$ in Ref. [109].

In the chiral-nonflat case, the generators U(4) symmetry is given by generators $\zeta^0\tau^a s^b$ and either the original band basis $c^\dagger_{\mathbf{k},m,\eta,s}$ for a fixed band index $m(= \pm)$ or the Chern basis $d^\dagger_{\mathbf{k},e_Y,\eta,s}$ with a fixed $e_Y(= \pm 1)$ form a fundamental of U(4).

3. Exact ground states in different limits: review of notation

In Ref. [110], we have examined in detail the exact ground states in the nonchiral-flat U(4) symmetric limit and in the chiral-flat U(4) × U(4) symmetric limit. For completeness we briefly review the results. In Ref. [71], Kang and Vafek first

introduced a type of Hamiltonians which have, under some conditions, exact ground states. We have found [110] that *any* translationally invariant interaction Hamiltonian projected to some active bands can be written in a form of Ref. [71], and that, under some conditions, exact eigenstates and ground states can be found. The key idea of Kang and Vafek for obtaining exact ground states is to rewrite the interacting Hamiltonian into a non-negative form. A state with eigenvalue zero is then ensured to be the ground state.

In Ref. [109], we proved that the projected Coulomb Hamiltonian can be written as

$$H_I = \frac{1}{2\Omega_{\text{tot}}}\sum_{\mathbf{G}}\sum_{\mathbf{q}} O_{\mathbf{q},\mathbf{G}}O_{-\mathbf{q},-\mathbf{G}} = \frac{1}{2}\int_{\mathbf{r}\in\Omega_{\text{tot}}} d^2\mathbf{r}O(\mathbf{r})^2,$$
$$O(\mathbf{r}) = \frac{1}{\Omega_{\text{tot}}}\sum_{\mathbf{G}}\sum_{\mathbf{q}} O_{\mathbf{q},\mathbf{G}}e^{i(\mathbf{q}+\mathbf{G})\cdot\mathbf{r}}, \tag{A27}$$

which is non-negative, with

$$O_{\mathbf{q},\mathbf{G}} = \sum_{\mathbf{k},m,n,\eta,s}\sqrt{V(\mathbf{G}+\mathbf{q})}M^{(\eta)}_{m,n}(\mathbf{k},\mathbf{q}+\mathbf{G}) \times\left(\rho^{\eta}_{\mathbf{k},\mathbf{q},m,n,s} - \frac{1}{2}\delta_{\mathbf{q},\mathbf{0}}\delta_{m,n}\right),\quad O^{\dagger}_{\mathbf{q},\mathbf{G}} = O_{-\mathbf{q},-\mathbf{G}}, \tag{A28}$$

where $\rho^{\eta}_{\mathbf{k},\mathbf{q},m,n,s} = c^{\dagger}_{\mathbf{k}+\mathbf{q},m,\eta,s}c_{\mathbf{k},n,\eta,s}$ is the density operator in band basis. Note that $O(\mathbf{r})$ and $O(\mathbf{r}')$ generically do not commute and hence the Hamiltonian is not solvable. The interaction can in general be rewritten as

$$H_I = \frac{1}{2\Omega_{\text{tot}}}\sum_{\mathbf{G}}\left[\sum_{\mathbf{q}}(O_{\mathbf{q},\mathbf{G}} - A_{\mathbf{G}}N_M\delta_{\mathbf{q},0})(O_{-\mathbf{q},-\mathbf{G}} - A_{-\mathbf{G}}N_M\delta_{-\mathbf{q},0}) + 2A_{-\mathbf{G}}N_M O_{\mathbf{0},\mathbf{G}} - A_{-\mathbf{G}}A_{\mathbf{G}}N_M^2\right], \tag{A29}$$

where N_M is the number of moiré unit cells and $A_{\mathbf{G}}$ is some arbitrarily chosen $\mathbf{G}$ dependent coefficient satisfying $A_{\mathbf{G}} = A^*_{-\mathbf{G}}$. Note that the first term in Eq. (A29) is nonnegative.

In Ref. [110], we found an important condition which can show that eigenstates of H_I are in fact ground states of H_I. If the $\mathbf{q} = 0$ component of the matrix element in Eq. (A8) $M^{(\eta)}_{m,n}(\mathbf{k},\mathbf{G})$ is not dependent on k for all $\mathbf{G}$'s, i.e.,

$$\text{flat metric condition:}\quad M^{(\eta)}_{m,n}(\mathbf{k},\mathbf{G}) = \xi(\mathbf{G})\delta_{m,n} \tag{A30}$$

then much more information about Eq. (A27) can be obtained. This condition is always true for $\mathbf{G} = 0$, for which $M^{(\eta)}_{m,n}(\mathbf{k},0) = \delta_{mn}$ from wave-function normalization. In Ref. [107], we have showed that, around the first magic angle, $M^{(\eta)}_{m,n}(\mathbf{k},\mathbf{G}) \approx 0$ for, $|\mathbf{G}| > \sqrt{3}k_\theta$ for $i = 1, 2$. Hence, the condition Eq. (A30) is valid for all $\mathbf{G}$ with the exception of $\mathbf{G}$ for which $|\mathbf{G}| = \sqrt{3}k_\theta$. Hence, the condition is largely valid, and the numerical analysis [111] confirms its validity for a large part of the MBZ. In the below, we will always specify when the condition Eq. (A30) is used. If the Eq. (A30) is satisfied, one has $O_{\mathbf{0},\mathbf{G}}$ proportional to the total electron number N and the second term in Eq. (A29) is simply a chemical potential term

$$\mu = \frac{1}{N_M\Omega_M}\sum_{\mathbf{G}}A_{-\mathbf{G}}\sqrt{V(\mathbf{G})}\sum_{\mathbf{k}}M^{(\eta)}_{+1,+1}(\mathbf{k},\mathbf{G}) = \sum_{\mathbf{G}}A_{-\mathbf{G}}\sqrt{V(\mathbf{G})}\xi(\mathbf{G})/\Omega_M, \tag{A31}$$

where $\Omega_M = \Omega_{\text{tot}}/N_M$ is the area of moiré unit cell. For a fixed total number of electrons, $N = \sum_{\mathbf{k},m,\eta,s}c^{\dagger}_{\mathbf{k},m,\eta,s}c_{\mathbf{k},m,\eta,s} = (\nu+4)N_M$ is a constant, where ν is the filling fraction (number of doped electrons per moiré unit cell) relative to the charge neutrality point, thus the ground state at finite filling is solely determined by the first term which is non-negative.

a. Exact ground states in the first chiral-flat U(4) × U(4) *limit*

To build the excitations around a ground state, we review the ground states found in Ref. [110] of the projected Hamiltonian (A27). We proved that in the Chern basis of Eq. (A20) and Eq. (A18), diagonal in the valley index η, spin index s and Chern band index e_Y, the projected Hamiltonian (A27) has as eigenstates at integer filling ν the *filled band* wave functions [without assuming condition Eq. (A30)]:

$$\left|\Psi^{\nu_+,\nu_-}_{\nu}\right\rangle = \prod_{\mathbf{k}}\left(\prod_{j_1=1}^{\nu_+}d^{\dagger}_{\mathbf{k},+1,\eta_{j_1},s_{j_1}}\prod_{j_2=1}^{\nu_-}d^{\dagger}_{\mathbf{k},-1,\eta_{j_2},s_{j_2}}\right)|0\rangle, \tag{A32}$$

$$H_I\left|\Psi^{\nu_+,\nu_-}_{\nu}\right\rangle = \frac{1}{2\Omega_{\text{tot}}}\sum_{\mathbf{q},\mathbf{G}}O_{-\mathbf{q},-\mathbf{G}}O_{\mathbf{q},\mathbf{G}}\left|\Psi^{\nu_+,\nu_-}_{\nu}\right\rangle = \frac{\nu^2}{2\Omega_{\text{tot}}}\sum_{\mathbf{G}}V(\mathbf{G})\Big(\sum_{\mathbf{k}}\alpha_0(\mathbf{k},\mathbf{G})\Big)^2\left|\Psi^{\nu_+,\nu_-}_{\nu}\right\rangle, \tag{A33}$$

where $\nu_+ - \nu_- = \nu_C$ is the total Chern number of the state, and $\nu_+ + \nu_- = \nu + 4$ is the total number of electrons per moiré unit cell in the projected bands, with $0 \leqslant \nu_\pm \leqslant 4$, $\mathbf{k}$ running over the entire MBZ. The occupied spin/valley indices $\{\eta_{j_1}, s_{j_1}\}$ and $\{\eta_{j_2}, s_{j_2}\}$ can be arbitrarily chosen. These eigenstates of Eq. (A27) are moreover eigenstates of the $O_{\mathbf{q},\mathbf{G}}$ operator in Eq. (A28) [110]:

$$O_{\mathbf{q},\mathbf{G}}\left|\Psi^{\nu_+,\nu_-}_{\nu}\right\rangle = \delta_{\mathbf{q},\mathbf{0}}A_{\mathbf{G}}N_M\left|\Psi^{\nu_+,\nu_-}_{\nu}\right\rangle;\qquad A_{\mathbf{G}} = \frac{\sqrt{V(\mathbf{G})}}{N_M}\sum_{\mathbf{k}}\nu\alpha_0(\mathbf{k},\mathbf{G}). \tag{A34}$$

In Ref. [110], we found that the U(4) × U(4) irrep of this multiplet is labeled by $([N_M^{\nu_+}]_4, [N_M^{\nu_-}]_4)$. For a fixed filling factor ν, from Eq. (A33), we found [110] that the states with different Chern number ν_C are all degenerate.

At charge neutrality $\nu = 0$, the U(4) × U(4) multiplet of eigenstate state $|\Psi_0^{\nu_+,\nu_-}\rangle$ with Chern number $\nu_C = \nu_+ - \nu_- =$

$0, \pm 2, \pm 4$ has exactly zero energy and hence are exact degenerate ground states. At nonzero fillings ν, we cannot guarantee that the $\nu \neq 0$ eigenstates are ground states [without condition Eq. (A30)].

Assuming the flat metric condition Eq. (A30), we showed [110] that we can rewrite the interaction into the form of Eq. (A29), with the coefficient $A_{\mathbf{G}} = \nu\sqrt{V(\mathbf{G})}\xi(\mathbf{G})$ in Eq. (A34). By Eq. (A34), we showed that $(O_{\mathbf{q},\mathbf{G}} - A_{\mathbf{G}} N_M \delta_{\mathbf{q},0})$ annihilates $|\Psi_\nu^{\nu_+,\nu_-}\rangle$ for any $\nu_C = \nu_+ - \nu_-$ and thus all the eigenstates $|\Psi_\nu^{\nu_+,\nu_-}\rangle$ with any Chern number $\nu_C = \nu_+ - \nu_-$ are degenerate ground states at filling ν [110].

b. Exact ground states in the nonchiral-flat U(4) limit

Without chiral symmetry, with U(4) symmetry Eq. (A24), $O_{\mathbf{q},\mathbf{G}}$ is no longer diagonal in any band basis (such as the Chern basis). Nevertheless, $O_{\mathbf{q},\mathbf{G}}$ is still diagonal in η and s and hence filling both $m = \pm$ bands, of any valley/spin is still an exact, Chern number 0 eigenstates [110]:

$$|\Psi_\nu\rangle = \prod_{\mathbf{k}} \left(\prod_{j=1}^{(\nu+4)/2} c^\dagger_{\mathbf{k},+,\eta_j,s_j} c^\dagger_{\mathbf{k},-,\eta_j,s_j} \right) |0\rangle = \prod_{\mathbf{k}} \left(\prod_{j=1}^{(\nu+4)/2} d^\dagger_{\mathbf{k},+1,\eta_j,s_j} d^\dagger_{\mathbf{k},-1,\eta_j,s_j} \right) |0\rangle, \quad \text{(A35)}$$

for even fillings $\nu = 0, \pm 2, \pm 4$, where $\{\eta_j, s_j\}$ are distinct valley-spin flavors which are fully occupied. With $M^{(\eta)}_{m,n}(\mathbf{k}, \mathbf{q}+\mathbf{G})$ in Eq. (A11), we have the same eigenvalue expression as in Eq. (A34), $O_{\mathbf{q},\mathbf{G}}|\Psi_\nu\rangle = \nu\sqrt{V(\mathbf{G})}\delta_{\mathbf{q},\mathbf{0}} \sum_{\mathbf{k},m,\eta,s} \alpha_0(\mathbf{k},\mathbf{G})|\Psi_\nu\rangle$. Along with any U(4) rotation, it is an eigenstate of H_I, without using condition Eq. (A30). Moreover, for $\nu = 0$, the state (A35) is always a ground state with or without condition Eq. (A30) [110]. Furthermore if the condition Eq. (A30) is satisfied, by choosing $A_{\mathbf{G}} = \nu\sqrt{V(\mathbf{G})}\xi(\mathbf{G})$ we have showed in Ref. [110] that the states in Eq. (A35) are Chern number zero exact ground states. The multiplet of states forms a U(4) irrep $[(2N_M)^{(\nu+4)/2}]_4$ [110].

APPENDIX B: CHARGE COMMUTATION RELATIONS

In order to compute the charge $0, \pm 1, \pm 2$ excitations, a series of commutators are needed. We provide their expressions here.

1. The nonchiral case

In the nonchiral case of Eq. (A11), we have

$$\begin{aligned}
[O_{\mathbf{q},\mathbf{G}}, c^\dagger_{\mathbf{k},n,\eta,s}] &= \sum_{\mathbf{k}',m,n',\eta',s'} \sqrt{V(\mathbf{G}+\mathbf{q})} M^{(\eta)}_{m,n'}(\mathbf{k}', \mathbf{q}+\mathbf{G}) \left[\rho^{\eta'}_{\mathbf{k}',\mathbf{q},m,n',s'}, c^\dagger_{\mathbf{k},n,\eta,s}\right] \\
&= \sum_{\mathbf{k}',m,n',\eta',s'} \sqrt{V(\mathbf{G}+\mathbf{q})} M^{(\eta)}_{m,n'}(\mathbf{k}', \mathbf{q}+\mathbf{G}) c^\dagger_{\mathbf{k}'+\mathbf{q},m,\eta',s'} \{c_{\mathbf{k}',n',\eta',s'}, c^\dagger_{\mathbf{k},n,\eta,s}\} \\
&= \sum_{m} \sqrt{V(\mathbf{G}+\mathbf{q})} M^{(\eta)}_{m,n}(\mathbf{k}, \mathbf{q}+\mathbf{G}) c^\dagger_{\mathbf{k}+\mathbf{q},m,\eta,s}
\end{aligned} \quad \text{(B1)}$$

and

$$\begin{aligned}
[O_{\mathbf{q},\mathbf{G}}, c_{\mathbf{k},n,\eta,s}] &= \sum_{\mathbf{k}',m,n',\eta',s'} \sqrt{V(\mathbf{G}+\mathbf{q})} M^{(\eta)}_{m,n'}(\mathbf{k}', \mathbf{q}+\mathbf{G}) \left[\rho^{\eta'}_{\mathbf{k}',\mathbf{q},m,n',s'}, c_{\mathbf{k},n,\eta,s}\right] \\
&= -\sum_{\mathbf{k}',m,n',\eta',s'} \sqrt{V(\mathbf{G}+\mathbf{q})} M^{(\eta)}_{m,n'}(\mathbf{k}', \mathbf{q}+\mathbf{G}) \{c^\dagger_{\mathbf{k}'+\mathbf{q},m,\eta',s'}, c_{\mathbf{k},n,\eta,s}\} c_{\mathbf{k}',n',\eta',s'} \\
&= -\sum_{m} \sqrt{V(\mathbf{G}+\mathbf{q})} M^{(\eta)}_{n,m}(\mathbf{k}-\mathbf{q}, \mathbf{q}+\mathbf{G}) c_{\mathbf{k}-\mathbf{q},m,\eta,s} \\
&= -\sum_{m} \sqrt{V(\mathbf{G}+\mathbf{q})} M^{(\eta)*}_{m,n}(\mathbf{k}, -\mathbf{q}-\mathbf{G}) c_{\mathbf{k}-\mathbf{q},m,\eta,s},
\end{aligned} \quad \text{(B2)}$$

where we have used the property [109] $M^{(\eta)*}_{m,n}(\mathbf{k}, -\mathbf{q}-\mathbf{G}) = M^{(\eta)}_{n,m}(\mathbf{k}-\mathbf{q}, \mathbf{q}+\mathbf{G})$. From these basic equations, we further find

$$\begin{aligned}
[O_{-\mathbf{q},-\mathbf{G}} O_{\mathbf{q},\mathbf{G}}, c^\dagger_{\mathbf{k},n,\eta,s}] &= O_{-\mathbf{q},-\mathbf{G}} [O_{\mathbf{q},\mathbf{G}}, c^\dagger_{\mathbf{k},n,\eta,s}] + [O_{-\mathbf{q},-\mathbf{G}}, c^\dagger_{\mathbf{k},n,\eta,s}] O_{\mathbf{q},\mathbf{G}} \\
&= O_{-\mathbf{q},-\mathbf{G}} \sum_m \sqrt{V(\mathbf{G}+\mathbf{q})} M^{(\eta)}_{m,n}(\mathbf{k}, \mathbf{q}+\mathbf{G}) c^\dagger_{\mathbf{k}+\mathbf{q},m,\eta,s} + \sum_m \sqrt{V(\mathbf{G}+\mathbf{q})} M^{(\eta)}_{m,n}(\mathbf{k}, -\mathbf{q}-\mathbf{G}) c^\dagger_{\mathbf{k}-\mathbf{q},m,\eta,s} O_{\mathbf{q},\mathbf{G}} \\
&= \sum_{m',m} V(\mathbf{G}+\mathbf{q}) M^{(\eta)}_{m',m}(\mathbf{k}+\mathbf{q}, -\mathbf{q}-\mathbf{G}) M^{(\eta)}_{m,n}(\mathbf{k}, \mathbf{q}+\mathbf{G}) c^\dagger_{\mathbf{k},m',\eta,s} \\
&\quad + \sum_m \sqrt{V(\mathbf{G}+\mathbf{q})} M^{(\eta)}_{m,n}(\mathbf{k}, \mathbf{q}+\mathbf{G}) c^\dagger_{\mathbf{k}+\mathbf{q},m,\eta,s} O_{-\mathbf{q},-\mathbf{G}} \\
&\quad + \sum_m \sqrt{V(\mathbf{G}+\mathbf{q})} M^{(\eta)}_{m,n}(\mathbf{k}, -\mathbf{q}-\mathbf{G}) c^\dagger_{\mathbf{k}-\mathbf{q},m,\eta,s} O_{\mathbf{q},\mathbf{G}}
\end{aligned} \quad \text{(B3)}$$

and

$$\begin{aligned}
&[O_{-\mathbf{q},-\mathbf{G}}O_{\mathbf{q},\mathbf{G}}, c_{\mathbf{k},n,\eta,s}] \\
&= O_{-\mathbf{q},-\mathbf{G}}[O_{\mathbf{q},\mathbf{G}}, c_{\mathbf{k},n,\eta,s}] + [O_{-\mathbf{q},-\mathbf{G}}, c_{\mathbf{k},n,\eta,s}]O_{\mathbf{q},\mathbf{G}} \\
&= -O_{-\mathbf{q},-\mathbf{G}}\sum_m \sqrt{V(\mathbf{G}+\mathbf{q})}M^{(\eta)*}_{m,n}(\mathbf{k}, -\mathbf{q}+-\mathbf{G})c_{\mathbf{k}+\mathbf{q},m,\eta,s} - \sum_m \sqrt{V(\mathbf{G}+\mathbf{q})}M^{(\eta)}_{m,n}(\mathbf{k}, \mathbf{q}+\mathbf{G})c_{\mathbf{k}+\mathbf{q},m,\eta,s}O_{\mathbf{q},\mathbf{G}} \\
&= \sum_{m',m} V(\mathbf{G}+\mathbf{q})M^{(\eta)*}_{m',m}(\mathbf{k}-\mathbf{q}, \mathbf{q}+\mathbf{G})M^{(\eta)*}_{m,n}(\mathbf{k}, -\mathbf{q}-\mathbf{G})c_{\mathbf{k},m',\eta,s} \\
&\quad - \sum_m \sqrt{V(\mathbf{G}+\mathbf{q})}M^{(\eta)*}_{m,n}(\mathbf{k}, -\mathbf{q}-\mathbf{G})c_{\mathbf{k}-\mathbf{q},m,\eta,s}O_{-\mathbf{q},-\mathbf{G}} - \sum_m \sqrt{V(\mathbf{G}+\mathbf{q})}M^{(\eta)*}_{m,n}(\mathbf{k}, \mathbf{q}+\mathbf{G})c_{\mathbf{k}+\mathbf{q},m,\eta,s}O_{\mathbf{q},\mathbf{G}}. \qquad \text{(B4)}
\end{aligned}$$

Using $M^{(\eta)}_{m',m}(\mathbf{k}+\mathbf{q}, -\mathbf{q}-\mathbf{G}) = M^{(\eta)*}_{m,m'}(\mathbf{k}, \mathbf{q}+\mathbf{G})$ and $M^{(\eta)*}_{m',m}(\mathbf{k}-\mathbf{q}, +\mathbf{q}+\mathbf{G}) = M^{(\eta)}_{m,m'}(\mathbf{k}, -\mathbf{q}-\mathbf{G})$, we have

$$\begin{aligned}
[O_{-\mathbf{q},-\mathbf{G}}O_{\mathbf{q},\mathbf{G}}, c^\dagger_{\mathbf{k},n,\eta,s}] &= \sum_m P^{(\eta)}_{mn}(\mathbf{k}, \mathbf{q}+\mathbf{G})c^\dagger_{\mathbf{k},m,\eta,s} + \sum_m \sqrt{V(\mathbf{G}+\mathbf{q})}M^{(\eta)}_{m,n}(\mathbf{k}, \mathbf{q}+\mathbf{G})c^\dagger_{\mathbf{k}+\mathbf{q},m,\eta,s}O_{-\mathbf{q},-\mathbf{G}} \\
&\quad + \sum_m \sqrt{V(\mathbf{G}+\mathbf{q})}M^{(\eta)}_{m,n}(\mathbf{k}, -\mathbf{q}-\mathbf{G})c^\dagger_{\mathbf{k}-\mathbf{q},m,\eta,s}O_{\mathbf{q},\mathbf{G}}, \\
[O_{-\mathbf{q},-\mathbf{G}}O_{\mathbf{q},\mathbf{G}}, c_{\mathbf{k},n,\eta,s}] &= \sum_m P^{(\eta)*}_{mn}(\mathbf{k}, \mathbf{q}+\mathbf{G})c_{\mathbf{k},m,\eta,s} - \sum_m \sqrt{V(\mathbf{G}+\mathbf{q})}M^{(\eta)*}_{m,n}(\mathbf{k}, -\mathbf{q}-\mathbf{G})c_{\mathbf{k}-\mathbf{q},m,\eta,s}O_{-\mathbf{q},-\mathbf{G}} \\
&\quad - \sum_m \sqrt{V(\mathbf{G}+\mathbf{q})}M^{(\eta)*}_{m,n}(\mathbf{k}, +\mathbf{q}+\mathbf{G})c_{\mathbf{k}+\mathbf{q},m,\eta,s}O_{\mathbf{q},\mathbf{G}}, \qquad \text{(B5)}
\end{aligned}$$

where we define the new matrix element $P = VM^\dagger M$, the convolution of the Coulomb potential and the form factor matrices

$$P^{(\eta)}_{mn}(\mathbf{k}, \mathbf{q}+\mathbf{G}) = \sum_{m'} V(\mathbf{G}+\mathbf{q})M^{(\eta)*}_{m',m}(\mathbf{k}, \mathbf{q}+\mathbf{G})M^{(\eta)}_{m',n}(\mathbf{k}, \mathbf{q}+\mathbf{G}) = V(\mathbf{G}+\mathbf{q})(M^{(\eta)\dagger}M^{(\eta)})_{mn}(\mathbf{k}, \mathbf{q}+\mathbf{G}). \qquad \text{(B6)}$$

These are the commutators needed to obtain the wave functions and energies of the excitations in the nonchiral limit.

2. The first chiral limit

In the first chiral limit, we can use the Chern band basis Eq. (A20), where the $O_{\mathbf{q},\mathbf{G}}$ is diagonal in the Chern basis. Its form factors do not depend on the valley η and spin s:

$$O_{\mathbf{q},\mathbf{G}} = \sum_k \sum_{e_Y=\pm} \sqrt{V(\mathbf{G}+\mathbf{q})}M_{e_Y}(\mathbf{k}, \mathbf{q}+\mathbf{G}) \sum_{\eta,s}\left(d^\dagger_{\mathbf{k}+\mathbf{q},e_Y,\eta,s}d_{\mathbf{k},e_Y,\eta,s} - \frac{1}{2}\delta_{\mathbf{q},\mathbf{0}}\right). \qquad \text{(B7)}$$

In this limit, the commutators between $O_{\mathbf{q},\mathbf{G}}$ and the Chern number $e_Y = \pm 1$ band creation operators become simpler

$$[O_{\mathbf{q},\mathbf{G}}, d^\dagger_{\mathbf{k},e_Y,\eta,s}] = \sqrt{V(\mathbf{G}+\mathbf{q})}M_{e_Y}(\mathbf{k}, \mathbf{q}+\mathbf{G})d^\dagger_{\mathbf{k}+\mathbf{q},e_Y,\eta,s} \qquad \text{(B8)}$$

and

$$[O_{\mathbf{q},\mathbf{G}}, d_{\mathbf{k},e_Y,\eta,s}] = -\sqrt{V(\mathbf{G}+\mathbf{q})}M^*_{e_Y}(\mathbf{k}, -\mathbf{q}-\mathbf{G})d_{\mathbf{k}-\mathbf{q},e_Y,\eta,s} \qquad \text{(B9)}$$

leading to the commutators

$$\begin{aligned}
[O_{-\mathbf{q},-\mathbf{G}}O_{\mathbf{q},\mathbf{G}}, d^\dagger_{\mathbf{k},e_Y,\eta,s}] &= P_{e_Y}(\mathbf{k}, \mathbf{q}+\mathbf{G})d^\dagger_{\mathbf{k},m,\eta,s} + \sqrt{V(\mathbf{G}+\mathbf{q})}(M_{e_Y}(\mathbf{k}, \mathbf{q}+\mathbf{G})d^\dagger_{\mathbf{k}+\mathbf{q},e_Y,\eta,s}O_{-\mathbf{q},-\mathbf{G}} \\
&\quad + M_{e_Y}(\mathbf{k}, -\mathbf{q}-\mathbf{G})d^\dagger_{\mathbf{k}-\mathbf{q},e_Y,\eta,s}O_{\mathbf{q},\mathbf{G}}), \\
[O_{-\mathbf{q},-\mathbf{G}}O_{\mathbf{q},\mathbf{G}}, d_{\mathbf{k},e_Y,\eta,s}] &= P^*_{e_Y}(\mathbf{k}, \mathbf{q}+\mathbf{G})d_{\mathbf{k},e_Y,\eta,s} - \sqrt{V(\mathbf{G}+\mathbf{q})}(M^*_{e_Y}(\mathbf{k}, -\mathbf{q}-\mathbf{G})d_{\mathbf{k}-\mathbf{q},e_Y,\eta,s}O_{-\mathbf{q},-\mathbf{G}} \\
&\quad + M^*_{e_Y}(\mathbf{k}, \mathbf{q}+\mathbf{G})d_{\mathbf{k}+\mathbf{q},e_Y,\eta,s}O_{\mathbf{q},\mathbf{G}}), \qquad \text{(B10)}
\end{aligned}$$

where $P = VM^\dagger M$, the convolution of the Coulomb potential and the form factor matrices, takes the chiral limit form

$$P_{e_Y}(\mathbf{k}, \mathbf{q}+\mathbf{G}) = V(\mathbf{G}+\mathbf{q})|M_{e_Y}(\mathbf{k}, \mathbf{q}+\mathbf{G})|^2 = V(\mathbf{G}+\mathbf{q})(\alpha_0^2(\mathbf{k}, \mathbf{q}+\mathbf{G}) + \alpha_2^2(\mathbf{k}, \mathbf{q}+\mathbf{G}) = P(\mathbf{k}, \mathbf{q}+\mathbf{G})), \qquad \text{(B11)}$$

where $\alpha_0(\mathbf{k}, \mathbf{q}+\mathbf{G})$, $\alpha_2(\mathbf{k}, \mathbf{q}+\mathbf{G})$ are the decomposition of the form factors in Eq. (A20). Notice in the Chern basis, $P_{e_Y}(\mathbf{k}, \mathbf{q}+\mathbf{G})$ does not depend on e_Y, so we just denote it as $P(\mathbf{k}, \mathbf{q}+\mathbf{G})$. These are the commutators needed to obtain the wave functions and energies of the excitations in the first chiral limit.

APPENDIX C: CHARGE ±1 EXCITATIONS OF THE EXACT GROUND STATES

Remarkably, the existence of exact ground states and/or eigenstates Eqs. (A32) and (A35) allows for the presence of more eigenstates. In fact, a part of the low energy spectrum can be computed with polynomial efficiency. In this Appendix, we give the exact charge ±1 excitations on top of the exact (ground) states given in Ref. [110] and reviewed in Appendix A 3.

1. Exact charge +1 excitations in the nonchiral-flat U(4) limit

To look for the charge one excitations (adding an electron into the system), we sum the commutators in Eqs. (B3) and (B10) over $\mathbf{q}, \mathbf{G}$ and use the shifted Hamiltonian in Eq. (A29). For a generic exact eigenstate $|\Psi\rangle$ at chemical potential μ satisfying $(O_{\mathbf{q},\mathbf{G}} - A_{\mathbf{G}} N_M \delta_{\mathbf{q},0})|\Psi\rangle = 0$ for some coefficient $A_{\mathbf{G}}$, we find

$$[H_I - \mu N, c^\dagger_{\mathbf{k},n,\eta,s}]|\Psi\rangle = \frac{1}{2\Omega_{\text{tot}}} \sum_m R^\eta_{mn}(\mathbf{k}) c^\dagger_{\mathbf{k},m,\eta,s}|\Psi\rangle, \tag{C1}$$

where N is the electron number operator, and the matrix

$$\begin{aligned} R^\eta_{mn}(\mathbf{k}) &= \sum_{\mathbf{G}} \left[\left(\sum_{\mathbf{q},m'} V(\mathbf{G}+\mathbf{q}) M^{(\eta)*}_{m',m}(\mathbf{k}, \mathbf{q}+\mathbf{G}) M^{(\eta)}_{m',n}(\mathbf{k}, \mathbf{q}+\mathbf{G}) \right) + 2N_M A_{-\mathbf{G}} \sqrt{V(\mathbf{G})} M^{(\eta)}_{m,n}(\mathbf{k}, \mathbf{G}) \right] - \mu \delta_{mn} \\ &= \frac{1}{2\Omega_{\text{tot}}} \sum_{\mathbf{G}} \left[\left(\sum_{\mathbf{q}} P^{(\eta)}_{mn}(\mathbf{k}, \mathbf{q}+\mathbf{G}) \right) + 2N_M A_{-\mathbf{G}} \sqrt{V(\mathbf{G})} M^{(\eta)}_{m,n}(\mathbf{k}, \mathbf{G}) \right] - \mu \delta_{mn}. \end{aligned} \tag{C2}$$

We hence see that, if $|\Psi\rangle$ is one of the $|\Psi^{\nu_+,\nu_-}_\nu\rangle$ [Eq. (A32)] or $|\Psi_\nu\rangle$ (Eq. (A35)) eigenstates of H_I, then $c^\dagger_{\mathbf{k},m,\eta,s}|\Psi\rangle$ is also an eigenstate of H_I with eigenvalues obtained by diagonalizing the 2×2 matrix $R^\eta_{mn}(\mathbf{k})$. In the case of TBG, this is a 2×2 matrix, hence the diagonalization can be done by hand, providing a band of excitations. We note that, the expression $c^\dagger_{\mathbf{k},n,\eta,s}|\Psi\rangle = 0$ may vanish and give no charge excitation, for instance, if valley η and spin s is fully occupied. We now delve more into the energies and eigenstates $c^\dagger_{\mathbf{k},m,\eta,s}|\Psi\rangle$.

Due to the symmetry $C_{2z}P$ [Eq. (A10)], the M matrix [Eq. (A11)] satisfies $M^{(\eta)}_{m,n}(\mathbf{k}, \mathbf{q}+\mathbf{G}) = mnM^{(-\eta)}_{-m,-n}(\mathbf{k}, \mathbf{q}+\mathbf{G})$. Correspondingly, the R matrix satisfies

$$R^\eta_{m,n}(\mathbf{k}) = mnR^{-\eta}_{-m,-n}(\mathbf{k}). \tag{C3}$$

Since $R^+(\mathbf{k})$ and $R^-(\mathbf{k})$ are related by a unitary transformation, they must have the same spectrum.

a. Band of charge 1 excitation in the nonchiral-flat U(4) limit

In the nonchiral limit, the eigenstates $|\Psi_\nu\rangle$ we found in Ref. [110] (and re-written in Eq. (A35)) have only fully occupied or fully empty valley η and spin s flavors. For TBG, this means that both active bands $m = \pm$ are either full or empty for each valley η and spin s. In this case we can only obtain exact charge +1 excitation at even fillings, i.e.,$\nu = 0, \pm 2$. We can consider two charge +1 states $c^\dagger_{\mathbf{k},n,\eta,s}|\Psi\rangle$ $(n = \pm)$ at a fixed $\mathbf{k}$ in a fully empty valley η and spin s. These two states then form a closed subspace with a 2×2 subspace Hamiltonian $R^\eta(\mathbf{k})$ defined by Eq. (C2). Diagonalizing the matrix $R^\eta(\mathbf{k})$ then gives the excitation eigenstates and excitation energies. It is worth noting that, due to Eq. (C3), the spectrum of $R^\eta(\mathbf{k})$ does *not* depend on η. Since the U(4) irrep of the ground state is $|\Psi_\nu\rangle$ is $[(2N_M)^{(\nu+4)/2}]_4$, the U(4) irrep of the charge 1 excited state is given by $[(2N_M)^{(\nu+4)/2}, 1]_4$. Furthermore, at $\nu = 0$, the state $|\Psi_{\nu=0}\rangle$ in Eq. (A35) is the *ground state* of the interaction Hamiltonian H_I and hence $c^\dagger_{\mathbf{k},n,\eta,s}|\Psi_{\nu=0}\rangle$ is the charge excitation above the ground state. Note that this does not assume the "flat metric condition" (A30) and is hence fully generic.

If we further assume the flat band condition Eq. (A30), the eigenstates $|\Psi_\nu\rangle$ become exact ground states, and the chemical potential is given by Eq. (A31). In this case, the 2×2 excitation sub-Hamiltonian $R^\eta(\mathbf{k})$ takes a simpler form:

$$\begin{aligned} R^\eta_{mn}(\mathbf{k}) &= \sum_{q,G} P^{(\eta)}_{mn}(\mathbf{k}, \mathbf{q}+\mathbf{G}) \\ &= \sum_{\mathbf{G},\mathbf{q},m'} V(\mathbf{G}+\mathbf{q}) M^{(\eta)*}_{m',m}(\mathbf{k}, \mathbf{q}+\mathbf{G}) M^{(\eta)}_{m',n}(\mathbf{k}, \mathbf{q}+\mathbf{G}), \end{aligned} \tag{C4}$$

which can be diagonalized to give the band excitation eigenstates and energies above the ground state at each momentum $\mathbf{k}$.

b. Spectrum properties of a generic charge 1 excitation in the nonchiral-flat U(4) limit

The spectrum at every $\mathbf{k}$ is obtained from diagonalizing the matrix $R^\eta(\mathbf{k}) = \sum_{\mathbf{G},\mathbf{q}} V(\mathbf{G}+\mathbf{q}) M^{(\eta)\dagger}(\mathbf{k}, \mathbf{q}+\mathbf{G}) M^{(\eta)}(\mathbf{k}, \mathbf{q}+\mathbf{G})$, which depends (up to a convolution with the Coulomb potential), only on the projected band wave functions. This is clearly a sum (over $\mathbf{q}, \mathbf{G}$) of positive semidefinite matrices [remember that $V(\mathbf{G}+\mathbf{q}) > 0$]. Hence $R^\eta(\mathbf{k})$ is a positive semidefinite matrix, whose eigenvalues are non-negative (expected, since we proved that these are excitations *above* the ground state). We now find conditions that these excitations are gapped, i.e.,that the matrix $R^\eta(\mathbf{k})$ is positive *definite* at each $\mathbf{k}$. We now show this by re-writing the $R^\eta(\mathbf{k})$ as

$$R^\eta_{mn}(\mathbf{k}) = (M^{(\eta)\dagger}(\mathbf{k}) V M^{(\eta)}(\mathbf{k}))_{mn}, \tag{C5}$$

where now $M^{(\eta)}(k)$ is a matrix of $(2N_M \cdot N_{\mathbf{G}}) \times 2$ matrix (with 2 because we are projecting into the two active TBG bands), where N_M is number of moiré unit cells,

$N_{\mathbf{G}}$ is the number of plane waves (MBZs) taken into consideration. In Ref. [107], we have showed that the number of plane waves needed is very small: the matrix elements fall off exponentially with $|\mathbf{G}|$ and any contribution above $|\mathbf{G}| = \sqrt{3}k_\theta$ is negligible. The matrix elements read $M^{(\eta)}_{\{m\mathbf{q}\mathbf{G}\},n}(\mathbf{k}) = M^{(\eta)}_{m,n}(\mathbf{k}, \mathbf{q}+\mathbf{G})$. V is a $2N_M \cdot N_{\mathbf{G}} \times 2N_M \cdot N_{\mathbf{G}}$ diagonal matrix with elements $V_{\{m\mathbf{q}\mathbf{G}\},\{m'\mathbf{q}'\mathbf{G}'\}} = \delta_{m,m'}\delta_{\mathbf{q},\mathbf{q}'}\delta_{\mathbf{G},\mathbf{G}'}V(\mathbf{q}+\mathbf{G})$. Since $V(\mathbf{q}+\mathbf{G}) \geqslant 0$ and diagonal, we can re-write $R^\eta(\mathbf{k}) = (\sqrt{V}M^\eta(\mathbf{k}))^\dagger\sqrt{V}M^\eta(\mathbf{k})$, and its rank is equal to $\mathrm{Rank}(\sqrt{V}M^\eta(\mathbf{k})) \leqslant 2$. We show the rank has to be 2 (or in general the number of occupied bands), by the simple argument

$$\begin{aligned} R^\eta_{mn}(\mathbf{k}) &= \sum_m V(0)M^{(\eta)}_{m',m}(\mathbf{k},0)M^{(\eta)}_{m,n}(\mathbf{k},0) + \sum_{\{\mathbf{q},\mathbf{G}\}\neq\{0,0\}}\sum_{p,p'=1,2} M^{(\eta)\dagger}_{\{p\mathbf{q}\mathbf{G}\},m}(\mathbf{k})V_{\{p\mathbf{q}\mathbf{G}\},\{p'\mathbf{q}'\mathbf{G}'\}}M^{(\eta)}_{\{p'\mathbf{q}'\mathbf{G}'\},n}(\mathbf{k}) \\ &= V(0)\delta_{mn} + \sum_{\{\mathbf{q},\mathbf{G}\}\neq\{0,0\}}\sum_{p,p'=1,2} M^{(\eta)\dagger}_{\{p\mathbf{q}\mathbf{G}\},m}(\mathbf{k})V_{\{p\mathbf{q}\mathbf{G}\},\{p'\mathbf{q}'\mathbf{G}'\}}M^{(\eta)}_{\{p'\mathbf{q}'\mathbf{G}'\},n}(\mathbf{k}). \end{aligned} \tag{C6}$$

The second term is still a positive semidefinite matrix, while the first term is diagonal and has eigenvalues $V(0)/2\Omega_{\mathrm{tot}}$. Hence by Weyl's theorem, the energies of the excited states are $\geqslant V(0)/2\Omega_{\mathrm{tot}}$. In general, our discussion shows that the states $c^\dagger_{\mathbf{k},n,\eta,s}|\Psi\rangle$ are not degenerate to the ground state $|\Psi\rangle$ (note that we did not prove these are the unique ground states). However, we cannot exclude a gapless excitation.

c. Spectrum relation to the quantum distance and generic argument for the existence of a charge gap

In general, however, it seems that this method gives rise to finite gap charge 1 excitations. The largest gap happens in the atomic limit or a material, where $\langle u^m_{\mathbf{k}+\mathbf{q}}|u^n_{\mathbf{k}}\rangle = \delta_{mn}$, for which $R_{mn} = \delta_{mn}\sum_{\mathbf{q},\mathbf{G}}V(\mathbf{q}+\mathbf{G}) = \delta_{mn}\Omega_{\mathrm{tot}}V(\mathbf{r}=0)$. Since we know that TBG is far away from an atomic limit—the bands being topological, we expect a reduction in this gap. However, we argue that this type of charge excitation is always gapped. We perform a different decomposition of the matrix R^η_{mn}:

$$R^\eta_{mn}(\mathbf{k}) = \sum_{\mathbf{q}}\sum_{p,p'=1,2} M^{(\eta)\dagger}_{\{p\mathbf{q}0\},m}(\mathbf{k})V_{\{p\mathbf{q}0\},\{p'\mathbf{q}'0\}}M^{(\eta)}_{\{p'\mathbf{q}'0\},n}(\mathbf{k}) + \sum_{\{\mathbf{q},\mathbf{G}\}\neq\{0,0\}}\sum_{p,p'=1,2} M^{(\eta)\dagger}_{\{p\mathbf{q}\mathbf{G}\},m}(\mathbf{k})V_{\{p\mathbf{q}\mathbf{G}\},\{p'\mathbf{q}'\mathbf{G}'\}}M^{(\eta)}_{\{p'\mathbf{q}'\mathbf{G}'\},n}(\mathbf{k}). \tag{C7}$$

Since the second term is still a semi positive definite matrix by construction, the eigenvalues of $R^\eta(\mathbf{k})$ will be greater or larger than the eigenvalues of the first term. In fact, due to Ref. [107], we know that the eigenvalues of the second term are negligible for $|\mathbf{G}| \geqslant 2|\mathbf{b}_{M1}|$. Hence, using the math notation of $A \geqslant B$ for $A - B$ positive semidefinite, we have

$$\begin{aligned} R^\eta_{mn}(\mathbf{k}) &\geqslant \sum_{\mathbf{q}}\sum_{p,p'=1,2} M^{(\eta)\dagger}_{\{p\mathbf{q}0\},m}(\mathbf{k})V_{\{p\mathbf{q}0\},\{p'\mathbf{q}'0\}}M^{(\eta)}_{\{p'\mathbf{q}'0\},n}(\mathbf{k}) \\ &= \sum_{\mathbf{q}} V(\mathbf{q})M^{(\eta)*}_{m',m}(\mathbf{k},\mathbf{q})M^{(\eta)}_{m',n}(\mathbf{k},\mathbf{q}) = \sum_{\mathbf{q}} V(\mathbf{q})\big(\delta_{mn} - \mathfrak{G}^{mn}_\eta(\mathbf{k},\mathbf{q})\big). \end{aligned} \tag{C8}$$

We call $\mathfrak{G}^{mn}(\mathbf{k},\mathbf{q})$ the generalized "quantum geometric tensor," whose trace is the generalized Fubini-Study metric. The property of the generalized quantum geometric tensor/Fubini study metric is that they become the conventional quantum geometric tensor/Fubini study metric for small transfer momentum $\mathbf{q}$. The tensor quantifies the distance between two eigenstates in momentum space. The conventional quantum geometric tensor is defined as

$$\mathfrak{G}^{mn}_{ij}(\mathbf{k}) = \sum_{a,b=1}^{N} \partial_{k_i}u^*_{a,m}(\mathbf{k})\left(\delta_{a,b} - \sum_{l}^{n_{\mathrm{occupied}}} u_{a,l}(\mathbf{k})u^*_{b,l}(\mathbf{k})\right)\partial_{k_j}u_{b,n}(\mathbf{k}), \tag{C9}$$

in which m, n are energy band indices and i, j are spatial direction indices of n_{occupied} orthonormal vectors $u_m(\mathbf{k})$ in a N dimensional Hilbert space, where $\mathbf{k}$ is some parameter. We can show that

$$M^{(\eta)*}_{m',m}(\mathbf{k},\mathbf{q}) = \delta_{mn} - \mathfrak{G}^{mn}_\eta(\mathbf{k},\mathbf{q}) = M^{(\eta)}_{m',n}(\mathbf{k},\mathbf{q}) = \delta_{mn} - q_iq_j\mathfrak{G}^{mn}_{ij}(\mathbf{k}) + \mathcal{O}(q^2). \tag{C10}$$

Generically, we expect [77] that the overlap between two functions at $\mathbf{k}$ and $\mathbf{k}+\mathbf{q}$ to fall off as $\mathbf{q}$ increases, leaving a finite term in $R^\eta_{mn}(\mathbf{k})$, the electron gap, at every $\mathbf{k}$.

2. Exact charge +1 excitations in the (first) chiral-flat U(4) × U(4) limit

For an eigenstate $|\Psi^{\nu_+,\nu_-}_\nu\rangle$ defined by Eq. (A32) in the (first) chiral-flat U(4) × U(4) limit, one has the coefficients $M(\mathbf{k},\mathbf{q}+\mathbf{G}) = \zeta^0\tau^0\alpha_0(\mathbf{k},\mathbf{q}+\mathbf{G}) + i\zeta^y\tau^0\alpha_2(\mathbf{k},\mathbf{q}+\mathbf{G})$. Without condition Eq. (A30), the eigenstate $|\Psi^{\nu_+,\nu_-}_\nu\rangle$ (which is not necessarily the ground state) satisfies Eq. (A34), which is equivalent to choosing $N_M A_{\mathbf{G}} = \nu\sqrt{V(\mathbf{G})}\sum_{\mathbf{k}}\alpha_0(\mathbf{k},\mathbf{G})$ for Eq. (C2). Using the relation (A12), we can simplify the matrix $R^\eta_{mn}(\mathbf{k})$ defined in Eq. (C2) as

$$R^\eta(\mathbf{k}) = R_0(\mathbf{k})\zeta^0, \tag{C11}$$

where

$$R_0(\mathbf{k}) = \sum_{\mathbf{G}} \left[\left(\sum_{\mathbf{q}} V(\mathbf{G}+\mathbf{q})[\alpha_0(\mathbf{k},\mathbf{q}+\mathbf{G})^2 + \alpha_2(\mathbf{k},\mathbf{q}+\mathbf{G})^2] \right) + 2N_M A_{-\mathbf{G}} \sqrt{V(\mathbf{G})}\alpha_0(\mathbf{k},\mathbf{G}) \right] - \mu. \tag{C12}$$

Therefore $R^\eta(\mathbf{k})$ is proportional to the identity matrix. Since the state $|\Psi_\nu^{\nu_+,\nu_-}\rangle$ is written in the Chern band basis defined in Eq. (A18), it is more convenient to work in the Chern band basis. We then find the charge excitation eigenstates with the corresponding excitation energy $R_0^\eta(\mathbf{k})$ given by

$$d^\dagger_{\mathbf{k},e_Y,\eta,s}\left|\Psi_\nu^{\nu_+,\nu_-}\right\rangle, \quad \left[H_I - \mu N, d^\dagger_{\mathbf{k},e_Y,\eta,s}\right]|\Psi\rangle = \frac{1}{2\Omega_{\text{tot}}} R_0(\mathbf{k}) d^\dagger_{\mathbf{k},e_Y,\eta,s}|\Psi\rangle, \tag{C13}$$

provided the Chern band $e_Y(=\pm 1)$ at valley η and spin s is fully empty. With condition Eq. (A30) assumed, the states $|\Psi_\nu^{\nu_+,\nu_-}\rangle$ become ground states. At the same time, with the chemical potential is given by Eq. (A31), we can simplify the excitation energy $R_0(\mathbf{k})$ into

$$R_0(\mathbf{k}) = \sum_{\mathbf{G},\mathbf{q}} V(\mathbf{G}+\mathbf{q})[\alpha_0(\mathbf{k},\mathbf{q}+\mathbf{G})^2 + \alpha_2(\mathbf{k},\mathbf{q}+\mathbf{G})^2] = \sum_{\mathbf{G},\mathbf{q}} P(\mathbf{k},\mathbf{q}+\mathbf{G}) \tag{C14}$$

independent on η, and with $P(\mathbf{k},\mathbf{q}+\mathbf{G})$ defined in Eq. (B11). Since the U(4) × U(4) irrep of the ground state is $([N_M^{\nu_+}]_4, [N_M^{\nu_-}]_4)$, the U(4) × U(4) irrep of the charge 1 excited states with $e_Y = 1$ and $e_Y = -1$ are given by $([N_M^{\nu_+}, 1]_4, [N_M^{\nu_-}]_4)$ and $([N_M^{\nu_+}]_4, [N_M^{\nu_-}, 1]_4)$, respectively.

3. Charge −1 excitations

The charge −1 excitations are obtained in a similar manner as the charge +1 excitations. Charge −1 excitations can be obtained by considering states $c_{\mathbf{k},n,\eta,s}|\Psi\rangle$ $(n = \pm)$ at a fixed $\mathbf{k}$ in a fully filled valley η and spin s. By the Hermitian conjugate of Eq. (B3), we find similar to the charge 1 excitation,

$$[H_I - \mu N, c_{\mathbf{k},n,\eta,s}]|\Psi\rangle = \frac{1}{2\Omega_{\text{tot}}} \sum_m \widetilde{R}^\eta_{mn}(\mathbf{k}) c_{\mathbf{k},m,\eta,s}|\Psi\rangle, \tag{C15}$$

where N is the electron number operator, and the matrix

$$\begin{aligned}\widetilde{R}^\eta_{mn}(\mathbf{k}) &= \sum_{\mathbf{G}} \left[\left(\sum_{\mathbf{q},m'} V(\mathbf{G}+\mathbf{q}) M^{(\eta)*}_{m',m}(\mathbf{k},\mathbf{q}+\mathbf{G}) M^{(\eta)}_{m',n}(\mathbf{k},\mathbf{q}+\mathbf{G}) \right)^* - 2N_M A_{-\mathbf{G}} \sqrt{V(\mathbf{G})} M^{(\eta)*}_{m,n}(\mathbf{k},\mathbf{G}) \right] + \mu\delta_{mn} \\ &= \sum_{\mathbf{G}} \left[\left(\sum_{\mathbf{q}} P^{(\eta)}_{nm}(\mathbf{k},\mathbf{q}+\mathbf{G}) \right) - 2N_M A_{-\mathbf{G}} \sqrt{V(\mathbf{G})} M^{(\eta)*}_{m,n}(\mathbf{k},\mathbf{G}) \right] + \mu\delta_{mn}. \end{aligned} \tag{C16}$$

Note that $\widetilde{R}^\eta_{mn}(\mathbf{k})$ differs from Eq. (C2) by a sign in the last two terms as well as by the complex conjugation of the first term. Diagonalizing $\widetilde{R}^\eta_{mn}(\mathbf{k})$ gives the charge −1 (hole) excitations. The chemical potential is the one given in Eq. (A31). In the (first) chiral limit, $\widetilde{R}_m n^\eta$ becomes a two-by-two identity at each $\mathbf{k}$ and independent with η, i.e.,$\widetilde{R}^\eta_{mn} = \widetilde{R}_0(\mathbf{k})\delta_{mn}$. The $R_0(\mathbf{k})$ function is given by

$$\widetilde{R}_0(\mathbf{k}) = \sum_{\mathbf{G}} \left[\left(\sum_{\mathbf{q}} V(\mathbf{G}+\mathbf{q})[\alpha_0(\mathbf{k},\mathbf{q}+\mathbf{G})^2 + \alpha_2(\mathbf{k},\mathbf{q}+\mathbf{G})^2] \right) - 2N_M A_{-\mathbf{G}} \sqrt{V(\mathbf{G})}\alpha_0(\mathbf{k},\mathbf{G}) \right] + \mu. \tag{C17}$$

If condition Eq. (A30) is satisfied, and μ is given in Eq. (A31), the charge −1 excitations have identical dispersion as that of the charge +1 excitations [Eq. (C2)]. If condition Eq. (A30) is not satisfied and $\nu \neq 0$, the charge +1 and −1 excitations will have different dispersions. The dispersions will also depend on filling ν, since $A_{\mathbf{G}}$ defined in Eq. (A34) depends on ν.

Since U(4) irrep of the ground state $|\Psi_\nu\rangle$ is $[(2N_M)^{(\nu+4)/2}]_4$, in the nonchiral limit, the U(4) irrep of the charge −1 excited state is given by $[(2N_M)^{(\nu+2)/2}, 2N_M - 1]_4$. Since the U(4)× U(4) irrep of the ground state is $([N_M^{\nu_+}]_4, [N_M^{\nu_-}]_4)$, the U(4) × U(4) irrep of the charge -1 excited states with $e_Y = 1$ and $e_Y = -1$ are given by $([N_M^{\nu_+ - 1}, N_M - 1]_4, [N_M^{\nu_-}]_4)$ and $([N_M^{\nu_+}]_4, [N_M^{\nu_- - 1}, N_M - 1]_4)$, respectively. The computed charge gaps for the TBG Hamiltonian are of order 10 meV.

4. Charge ±1 excitation spectra for different parameters

Before we present the numerical results, let us first explain how we choose the chemical potential in the cases without assuming flat-metric condition. First, the sum of the lowest charge +1 (Δ_+) and charge −1 (Δ_-) gaps do not depend on the chemical potential since upon adding a $-\delta\mu N$ term the two gaps change by $-\delta\mu$ and $\delta\mu$, respectively. Then we choose the chemical potential such that $\Delta_+ = \Delta_-$. In a band structure picture, Δ_+ is the lowest conduction band energy and $-\Delta_-$ is the highest valence band energy. The condition

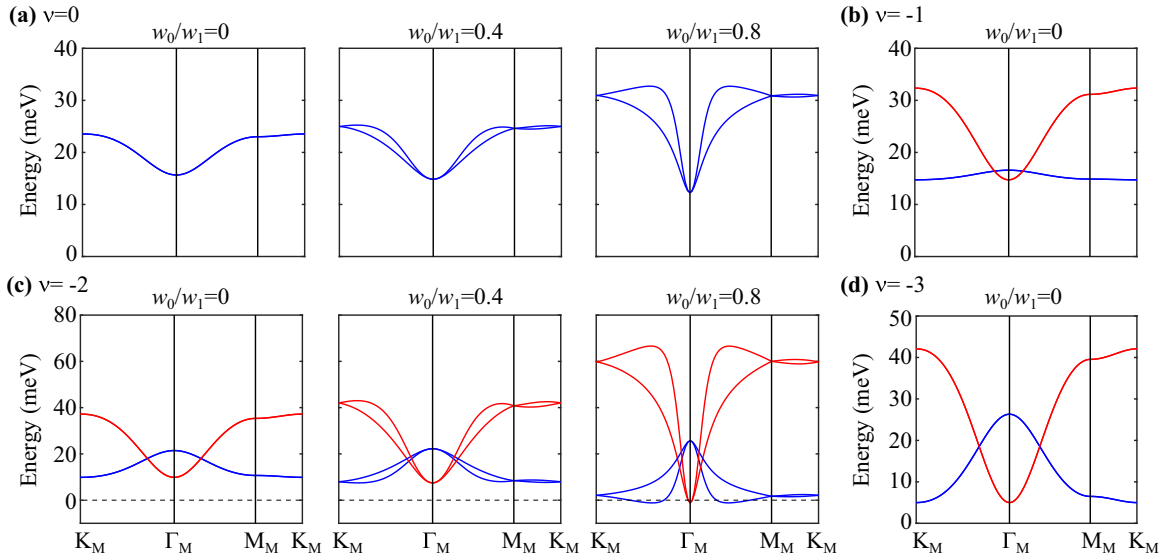

FIG. 5. Exact charge $+1$ (blue) and -1 (red) excitations at $\theta = 1.05^\circ$. The flat metric condition is *not* imposed. In this plot we have used the parameters defined in Appendix A: $v_F = 5.944$ eV Å, $|K| = 1.703$ Å^{-1}, $w_1 = 110$ meV, $U_\xi = 26$ meV, and $\xi = 10$ nm. Note that the excitation gap is largely reduced from the flat-condition limit.

$\Delta_+ = \Delta_-$ simply means that the chemical potential locates at the middle of conduction and valence bands.

In Figs. 5 and 6, the charge ± 1 excitations are plotted at different fillings and w_0/w_1's for two different screening lengths of the Coulomb interaction [Eq. (A7)], i.e.,$\xi = 10$ and 20 nm, respectively. The corresponding interaction strengths are $U_{10\,\mathrm{nm}} = 26$ meV and $U_{20\,\mathrm{nm}} = 13$ meV. We have used $w_1 = 110$ meV in all the calculations and $w_0/w_1 = 0$, 0.4, 0.8 for $\nu = 0, -2$ and $w_0/w_1 = 0$ for $\nu = -1, -3$.

For $\nu = 0$ and $\xi = 10$, 20 nm, the charge ± 1 gaps are at the Γ_M momentum and are always larger than 10 meV for different w_0/w_1's. For $\nu = -2$ and $\xi = 20$ nm, the charge ± 1 gaps are always larger than 5 meV for different w_0/w_1's. For $\nu = -2$ and $\xi = 10$ nm, the charge ± 1 gaps are finite for $w_0/w_1 = 0$, 0.4 but become negative at $w_0/w_1 = 0.8$ [Fig. 5(c)]. We find that the gaps close around $w_0/w_1 \approx 0.75$, implying that, with $\xi = 10$ nm and the other parameters we have used, the ground states in Eq. (8) become unstable for $w_0/w_1 \approx 0.75$.

The instability shown in Fig. 5(c) will lead to a metallic phase at $\nu = -2$ in the nonchiral-flat limit with strong chiral symmetry breaking ($w_0/w_1 = 0.8$). In the band structure picture, we can understand the charge $+1$ excitation as the conduction band and the charge -1 excitation as the reverted valence band. The negativities of both imply that the energy of conduction band overlaps with the energy of valence band.

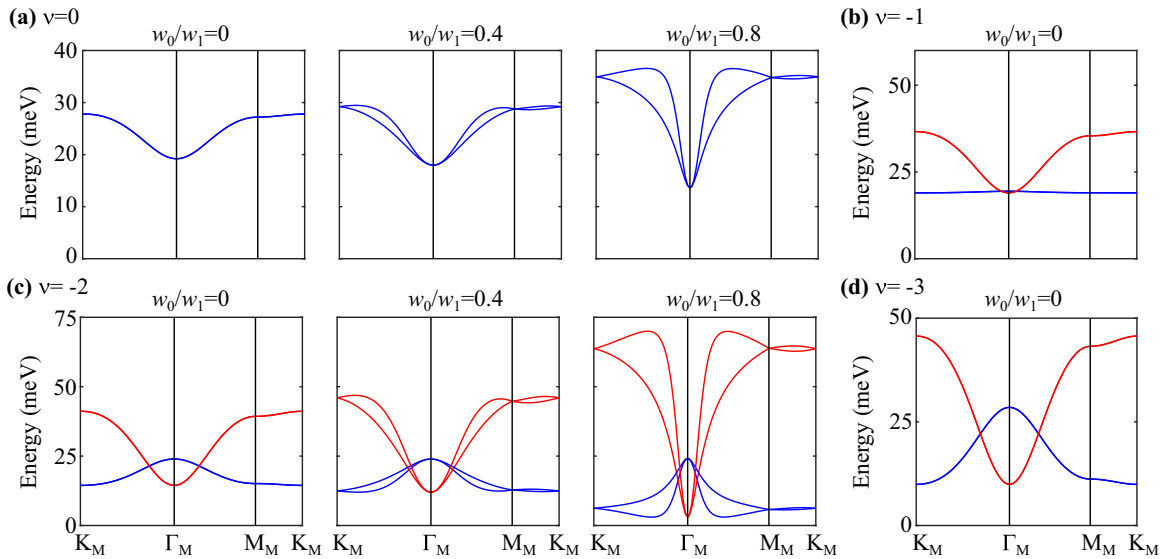

FIG. 6. Exact charge $+1$ (blue) and -1 (red) excitations at $\theta = 1.05^\circ$. The flat metric condition is *not* imposed. In this plot we set the screening length as $\xi = 20$nm and accordingly the interaction strength as $U_\xi = 13$meV. The other parameters are same as in Appendix A: $v_F = 5.944$ eV Å, $|K| = 1.703$ Å^{-1}, and $w_1 = 110$ meV.

Since we have chosen to fully occupy the valence bands, the ground state energy is not minimized in this case: One can move one particle from the top of valence band to bottom of conduction band to lower the energy. The ground state energy will be minimized by redistributing electrons to occupy the bands below the chemical potential. Due to the overlap between conduction and valence bands, the redistributed band structure will have electron and hole pockets and hence is a metallic state. In the resulted metallic phase at $\nu = -2$, there are two fully empty valley-spin sectors and two partially filled valley-spin sectors. The partially filled sectors contribute to the electron and hole pockets. This state is still invariant under a U(2) subgroup within the fully empty valley-spin sectors. Since U(4) and U(2) have 16 and 4 parameters, there will be $\frac{16-4}{2} = 6$ Goldstone modes.

APPENDIX D: CHARGE NEUTRAL EXCITATIONS AND THE GOLDSTONE STIFFNESS

While the charge ± 1 excitations can be obtained by diagonalizing a 2×2 matrix, we can obtain the charge neutral, two-body excitations above the ground state. These can be obtained by diagonalizing a $2N_M \times 2N_M$ matrix, or a *one-body* problem, despite the state having a thermodynamic number of particles. Due to the fact that we know the exact eigenstates (or ground states) of the system, building excitations of the Hamiltonian on top of these eigenstates (or ground states) becomes a problem of diagonalizing a basis formed only from the excitations. We now obtain the charge neutral excitations, show that they exhibit Goldstone modes with quadratic dispersion—as required by U(4) [or U(4) × U(4)] ferromagnetism, and obtain the stiffness of the Goldstone dispersion in the first chiral limit.

1. Exact charge neutral excitations in the nonchiral-flat U(4) limit

We choose a basis for the neutral excitations

$$c^\dagger_{\mathbf{k}_2,m_2,\eta_2,s_2} c_{\mathbf{k}_1,m_1,\eta_1,s_1} |\Psi\rangle, \tag{D1}$$

where $|\Psi\rangle$ is any of the exact ground states and/or eigenstates in Eqs. (A32) and (A35). The scattering matrix of this basis can be solved as easily as a one-body problem, despite the fact that Eqs. (A32) and (A35) hold a thermodynamic number of particles. We first have to compute the commutators:

$$\left[O_{-\mathbf{q},-\mathbf{G}} O_{\mathbf{q},\mathbf{G}}, c^\dagger_{\mathbf{k}_2,m_2,\eta_2,s_2} c_{\mathbf{k}_1,m_1,\eta_1,s_1}\right] = \left[O_{-\mathbf{q},-\mathbf{G}} O_{\mathbf{q},\mathbf{G}}, c^\dagger_{\mathbf{k}_2,m_2,\eta_2,s_2}\right] c_{\mathbf{k}_1,m_1,\eta_1,s_1} + c^\dagger_{\mathbf{k}_2,m_2,\eta_2,s_2}\left[O_{-\mathbf{q},-\mathbf{G}} O_{\mathbf{q},\mathbf{G}}, c_{\mathbf{k}_1,m_1,\eta_1,s_1}\right], \tag{D2}$$

which, in detail reads

$$\begin{aligned}
&\left[O_{-\mathbf{q},-\mathbf{G}} O_{\mathbf{q},\mathbf{G}}, c^\dagger_{\mathbf{k}_2,m_2,\eta_2,s_2} c_{\mathbf{k}_1,m_1,\eta_1,s_1}\right] \\
&= \sum_m P^{(\eta_2)}_{m m_2}(\mathbf{k}_2, \mathbf{q}+\mathbf{G}) c^\dagger_{\mathbf{k}_2,m,\eta_2,s_2} c_{\mathbf{k}_1,m_1,\eta_1,s_1} + \sum_m P^{(\eta_1)}_{m_1 m}(\mathbf{k}_1, -\mathbf{q}-\mathbf{G}) c^\dagger_{\mathbf{k}_2,m_2,\eta_2,s_2} c_{\mathbf{k}_1,m,\eta_1,s_1} \\
&\quad + \sqrt{V(\mathbf{G}+\mathbf{q})} \sum_m \left(M^{(\eta_2)}_{m,m_2}(\mathbf{k}_2, \mathbf{q}+\mathbf{G}) c^\dagger_{\mathbf{k}_2+\mathbf{q},m,\eta_2,s_2} c_{\mathbf{k}_1,m_1,\eta_1,s_1} O_{-\mathbf{q},-\mathbf{G}} + (\mathbf{q},\mathbf{G} \leftrightarrow -\mathbf{q},-\mathbf{G})\right) \\
&\quad - \sqrt{V(\mathbf{G}+\mathbf{q})} \sum_m \left(M^{(\eta_1)*}_{m,m_1}(\mathbf{k}_1, -\mathbf{q}-\mathbf{G}) c^\dagger_{\mathbf{k}_2,m_2,\eta_2,s_2} c_{\mathbf{k}_1-\mathbf{q},m,\eta_1,s_1} O_{-\mathbf{q},-\mathbf{G}} + (\mathbf{q},\mathbf{G} \leftrightarrow -\mathbf{q},-\mathbf{G})\right) \\
&\quad - V(\mathbf{G}+\mathbf{q}) \sum_{m,m'} \left(M^{(\eta_2)}_{m,m_2}(\mathbf{k}_2, \mathbf{q}+\mathbf{G}) M^{(\eta_1)*}_{m',m_1}(\mathbf{k}_1, \mathbf{q}+\mathbf{G}) c^\dagger_{\mathbf{k}_2+\mathbf{q},m,\eta_2,s_2} c_{\mathbf{k}_1+\mathbf{q},m',\eta_1,s_1} + (\mathbf{q},\mathbf{G} \leftrightarrow -\mathbf{q},-\mathbf{G})\right)
\end{aligned} \tag{D3}$$

By rewriting $\mathbf{k}_2 = \mathbf{k} + \mathbf{p}$ and $\mathbf{k}_1 = \mathbf{k}$, we can write the scattering equation as

$$\left[H_I - \mu N, c^\dagger_{\mathbf{k}+\mathbf{p},m_2,\eta_2,s_2} c_{\mathbf{k},m_1,\eta_1,s_1}\right]|\Psi\rangle = \frac{1}{2\Omega_{\text{tot}}} \sum_{m,m'} \sum_{\mathbf{q}} S^{(\eta_2,\eta_1)}_{mm';m_2m_1}(\mathbf{k}+\mathbf{q}, \mathbf{k}; \mathbf{p}) c^\dagger_{\mathbf{k}+\mathbf{p}+\mathbf{q},m,\eta_2,s_2} c_{\mathbf{k}+\mathbf{q},m',\eta_1,s_1} |\Psi\rangle. \tag{D4}$$

The $|\Psi\rangle$ are the states $|\Psi_\nu\rangle$ in Eq. (A35), and hence η_1, s_1 belong to the valley-spin flavor/s which are fully occupied, while η_2, s_2 belong to the valley/spin flavor which are not occupied.

For a generic exact eigenstate $|\Psi\rangle$ at chemical potential μ satisfying $(O_{\mathbf{q},\mathbf{G}} - A_{\mathbf{G}} N_M \delta_{\mathbf{q},0})|\Psi\rangle = 0$ for some coefficient $A_{\mathbf{G}}$, we find that the scattering matrix reads

$$\begin{aligned}
S^{(\eta_2,\eta_1)}_{m,m';m_2,m_1}(\mathbf{k}+\mathbf{q}, \mathbf{k}; \mathbf{p}) &= \delta_{\mathbf{q},\mathbf{0}}\left(\delta_{m,m_2} \widetilde{R}^{\eta_1}_{m'm_1}(\mathbf{k}) + \delta_{m',m_1} R^{\eta_2}_{mm_2}(\mathbf{k}+\mathbf{p})\right) \\
&\quad - 2 \sum_{\mathbf{G}} V(\mathbf{G}+\mathbf{q}) M^{(\eta_2)}_{m,m_2}(\mathbf{k}+\mathbf{p}, \mathbf{q}+\mathbf{G}) M^{(\eta_1)*}_{m',m_1}(\mathbf{k}, \mathbf{q}+\mathbf{G}),
\end{aligned}$$

where $R^\eta_{mn}(\mathbf{k})$, $\widetilde{R}^\eta_{mn}(\mathbf{k})$ are the ± 1-excitation matrices in Eqs. (C2) and (C16). We see that the neutral energy is a sum of the two single-particle energies [first row of Eq. (D5)] plus an interaction energy [second row of Eq. (D5)].

The exact expression of the PH excitation spectrum allows for the determination of the Goldstone stiffness. The Goldstone of the U(4) and U(4) × U(4) ferromagnetic ground states is part of the spectrum of the neutral excitation Eq. (D4), and is the state at small momentum $\mathbf{p} = \mathbf{k}_1 - \mathbf{k}_2$. We will solve this in the simpler, chiral limit, but it can be obtained in the general, nonchiral limit Eq. (D4).

2. Exact charge neutral excitations in the (first) chiral-flat U(4) × U(4) limit

We now consider the charge neutral excited states reachable by creating one electron-hole pair with total momentum $\mathbf{p}$ on the chiral-flat limit eigenstate $|\Psi_\nu^{\nu_+,\nu_-}\rangle$. Assume the valley-spin flavor $\{\eta_1, s_1\}$ has Chern band basis e_{Y1} fully occupied and the valley-spin flavor $\{\eta_2, s_2\}$ Chern band basis e_{Y2} fully empty. We consider the Hilbert space of the following sets of states of momentum quantum number $\mathbf{p}$

$$\left|\mathbf{k}+\mathbf{p}, \mathbf{k}, e_{Y1}, e_{Y2}, \eta_2, \eta_1, s_2, s_1, \Psi_\nu^{\nu_+,\nu_-}\right\rangle = d^\dagger_{\mathbf{k}+\mathbf{p},e_{Y2},\eta_2,s_2} d_{\mathbf{k},e_{Y1},\eta_1,s_1}\left|\Psi_\nu^{\nu_+,\nu_-}\right\rangle, \tag{D5}$$

The $O_{\mathbf{q},\mathbf{G}}$ operators in the chiral limit have the simple, diagonal expression of Eq. (B7), which leads to the scattering equation.

$$\left[H_I - \mu N, d^\dagger_{\mathbf{k}+\mathbf{p},e_{Y2},\eta_2,s_2} d_{\mathbf{k},e_{Y1},\eta_1,s_1}\right]|\Psi\rangle = \frac{1}{2\Omega_{\text{tot}}}\sum_{\mathbf{q}} S_{e_{Y2};e_{Y1}}(\mathbf{k}+\mathbf{q},\mathbf{k};\mathbf{p}) d^\dagger_{\mathbf{k}+\mathbf{p}+\mathbf{q},e_{Y2},\eta_2,s_2} d_{\mathbf{k}+\mathbf{q},e_{Y1},\eta_1,s_1}|\Psi\rangle. \tag{D6}$$

The $|\Psi\rangle$ are the states $|\Psi_\nu^{\nu_+,\nu_-}\rangle$ in Eq. (A32), and hence e_{Y1}, η_1, and s_1 belong to the valley-spin flavor/s which are fully occupied, while e_{Y2}, η_2, and s_2 belong to the valley/spin flavor which are not occupied. The scattering matrix in the chiral limit does not depend on η_1, η_2:

$$S_{e_{Y2};e_{Y1}}(\mathbf{k}+\mathbf{q},\mathbf{k};\mathbf{p}) = \delta_{\mathbf{q},\mathbf{0}}(R_0(\mathbf{k}+\mathbf{p}) + \widetilde{R}_0(\mathbf{k})) - 2\sum_{\mathbf{G}} V(\mathbf{G}+\mathbf{q}) M_{e_{Y2}}(\mathbf{k}+\mathbf{p},\mathbf{q}+\mathbf{G}) M^*_{e_{Y1}}(\mathbf{k},\mathbf{q}+\mathbf{G}), \tag{D7}$$

where $M_{e_Y}(\mathbf{k},\mathbf{q}+\mathbf{G})$ is given in Eq. (A20) and $R_0^\eta(\mathbf{k})$ is given in Eq. (C12).

If condition Eq. (A30) is satisfied, the eigenstates $|\Psi_\nu^{\nu_+,\nu_-}\rangle$ are the ground states, and hence the states Eq. (D6) are the neutral excitations on top of the ground states. Without the condition Eq. (A30), only $\nu = 0$ states are guaranteed to be the ground states, although the others are still eigenstates. With condition Eq. (A30), we have

$$\begin{aligned} S_{e_{Y2};e_{Y1}}(\mathbf{k}+\mathbf{q},\mathbf{k};\mathbf{p}) = {} & \delta_{\mathbf{q},\mathbf{0}}\sum_{\mathbf{G},\mathbf{q}'} V(\mathbf{G}+\mathbf{q}')[\alpha_0(\mathbf{k},\mathbf{q}'+\mathbf{G})^2 + \alpha_2(\mathbf{k},\mathbf{q}'+\mathbf{G})^2 + \alpha_0(\mathbf{k}+\mathbf{p},\mathbf{q}'+\mathbf{G})^2 + \alpha_2(\mathbf{k}+\mathbf{p},\mathbf{q}'+\mathbf{G})^2] \\ & - 2\sum_{\mathbf{G}} V(\mathbf{G}+\mathbf{q})(\alpha_0(\mathbf{k}+\mathbf{p},\mathbf{q}+\mathbf{G}) + ie_{Y2}\alpha_2(\mathbf{k}+\mathbf{p},\mathbf{q}+\mathbf{G}))(\alpha_0(\mathbf{k},\mathbf{q}+\mathbf{G}) - ie_{Y1}\alpha_2(\mathbf{k},\mathbf{q}+\mathbf{G})). \end{aligned} \tag{D8}$$

Solving Eq. (D6) provides us with the expression for the neutral excitations at momentum $\mathbf{p}$ on top of the TBG ground states.

3. Goldstone mode in the first chiral limit and the Goldstone stiffness

We show that the Goldstone mode of the ferromagnetic ground states are included in the neutral excitations of Eq. (D6) and we obtain their dispersion relation, in terms of the quantum geometry factors of the TBG. We are able to analytically obtain the Goldstone mode if the condition Eq. (A30) holds. We first show the presence of an exact zero eigenstate of Eq. (D6).

a. Exact zero energy neutral mode eigenstate

We now show that Eq. (D6) has an exact zero energy eigenstate. In order to see this, we remark that the $\mathbf{p} = 0, e_{Y1} = e_{Y2}$ state Eq. (D8) has a scattering matrix

$$\begin{aligned} S_{e_Y;e_Y}(\mathbf{k}+\mathbf{q},\mathbf{k};\mathbf{0}) = {} & 2\delta_{\mathbf{q},\mathbf{0}}\sum_{\mathbf{G},\mathbf{q}'} V(\mathbf{G}+\mathbf{q}')[\alpha_0(\mathbf{k},\mathbf{q}'+\mathbf{G})^2 + \alpha_2(\mathbf{k},\mathbf{q}'+\mathbf{G})^2] \\ & - 2\sum_{\mathbf{G}} V(\mathbf{G}+\mathbf{q})(\alpha_0(\mathbf{k},\mathbf{q}+\mathbf{G})^2 + \alpha_2(\mathbf{k},\mathbf{q}+\mathbf{G})^2), \end{aligned} \tag{D9}$$

whose elements in every row sums to zero (irrespective of $\eta_{1,2}, s_{1,2}$):

$$\sum_{\mathbf{q}} S_{e_Y;e_Y}(\mathbf{k}+\mathbf{q},\mathbf{k};\mathbf{0}) = 0. \tag{D10}$$

This guarantees that the rank of the scattering matrix is not maximal, and that there is at least one zero energy eigenstate, with equal amplitude on every $|\mathbf{k}, e_Y, e_Y, \eta_2, \eta_1, s_2, s_1, \Psi_\nu^{\nu_+,\nu_-}\rangle$

$$|e_Y, e_Y, \eta_2, \eta_1, s_2, s_1\rangle = \sum_{\mathbf{q}} d^\dagger_{\mathbf{k}+\mathbf{q},e_Y,\eta_2,s_2} d_{\mathbf{k}+\mathbf{q},e_Y,\eta_1,s_1}\left|\Psi_\nu^{\nu_+,\nu_-}\right\rangle, \quad (H_I - \mu N)|e_Y, e_Y, \eta_2, \eta_1, s_2, s_1\rangle = 0. \tag{D11}$$

A U(4) × U(4) multiplet of this state is also at zero energy. Moreover, the scattering matrix $S_{e_Y;e_Y}(\mathbf{k}+\mathbf{q},\mathbf{k};0)$ is positive semidefinite (as it should, since these eigenvalues are energies of excitations on top of the ground states). For the matrix $S_{e_Y;e_Y}(\mathbf{k}+\mathbf{q},\mathbf{k};0)$, we prove that its negative, $-S_{e_Y;e_Y}(\mathbf{k}+\mathbf{q},\mathbf{k};0)$, has only nonpositive eigenvalues, and hence $S_{e_Y;e_Y}(\mathbf{k}+\mathbf{q},\mathbf{k};0)$ has only non-negative eigenvalues. For $-S_{e_Y;e_Y}(\mathbf{k}+\mathbf{q},\mathbf{k};0)$, the diagonal elements $-S_{e_Y;e_Y}(\mathbf{k},\mathbf{k};0)$ are nonpositive, while the off-diagonal elements $-S_{e_Y;e_Y}(\mathbf{k}+\mathbf{q},\mathbf{k};0)$ ($\mathbf{q} \neq 0$) are non-negative. Hence by the Gershgorin circle

theorem, all eigenvalues lie in at least one of the Gershgorin disks (which, due to the fact that the matrix is Hermitian, are intervals) centered at $-S_{e_Y;e_Y}(\mathbf{k},\mathbf{k};0)$ and with radius $-\sum_{\mathbf{q}\neq 0} S_{e_Y;e_Y}(\mathbf{k}+\mathbf{q},\mathbf{k};0)$. These intervals are

$$\left[-S_{e_Y;e_Y}(\mathbf{k},\mathbf{k};0)+\sum_{\mathbf{q}\neq 0} S_{e_Y;e_Y}(\mathbf{k}+\mathbf{q},\mathbf{k};0), -S_{e_Y;e_Y}(\mathbf{k},\mathbf{k};0)-\sum_{\mathbf{q}\neq 0} S_{e_Y;e_Y}(\mathbf{k}+\mathbf{q},\mathbf{k};0)\right]=\left[2\sum_{\mathbf{q}\neq 0} S_{e_Y;e_Y}(\mathbf{k}+\mathbf{q},\mathbf{k};0),0\right]. \tag{D12}$$

Since $\sum_{\mathbf{q}\neq 0} S_{e_Y;e_Y}(\mathbf{k}+\mathbf{q},\mathbf{k};0)\leqslant 0,\ \ \forall\mathbf{k}$, all eigenvalues of $-S_{e_Y;e_Y}(\mathbf{k}+\mathbf{q},\mathbf{k};0)$ are nonpositive, and hence all eigenvalues of $S_{e_Y;e_Y}(\mathbf{k}+\mathbf{q},\mathbf{k};0)$ are non-negative.

b. Goldstone stiffness

Since the $\mathbf{p}=0$ state has zero energy, for small $\mathbf{p}$, there will be low-energy states in the neutral continuum. By using the $\mathbf{p}=0$ states in Eq. (D11), one can compute their dispersion. First, we write the Hamiltonian matrix elements acting on the two particle states

$$\begin{aligned}&\left\langle \mathbf{k}'+\mathbf{p},\mathbf{k}',e'_{Y1},e'_{Y2},\eta'_2,\eta'_1,s'_2,s'_1,\Psi_\nu^{\nu_+,\nu_-}\middle|H_I\middle|\mathbf{k}+\mathbf{p},\mathbf{k},e_{Y1},e_{Y2},\eta_2,\eta_1,s_2,s_1,\Psi_\nu^{\nu_+,\nu_-}\right\rangle\\&=\delta_{e'_{Y1},e'_{Y2},\eta'_2,\eta'_1,s'_2,s_1;e_{Y1},e_{Y2},\eta_2,\eta_1,s_2,s_1}\frac{1}{2\Omega_{\rm tot}}(\delta_{\mathbf{k}',\mathbf{k}}S_{e_{Y2};e_{Y1}}(\mathbf{k},\mathbf{k};\mathbf{p}))-S_{e_{Y2};e_{Y1}}(\mathbf{k}',\mathbf{k};\mathbf{p})).\end{aligned} \tag{D13}$$

Hence, for small $\mathbf{p}$, the energy of the Goldstone mode is given by the expectation value

$$\begin{aligned}E_{\rm Goldstone}(\mathbf{p})&=\sum_{\mathbf{k},\mathbf{k}'}\left\langle \mathbf{k}'+\mathbf{p},\mathbf{k}',e_Y,e_Y,\eta_2,\eta_1,s_2,s_1,\Psi_\nu^{\nu_+,\nu_-}\middle|H_I\middle|\mathbf{k}+\mathbf{p},\mathbf{k},e_Y,e_Y,\eta_1,\eta_1,s_2,s_1,\Psi_\nu^{\nu_+,\nu_-}\right\rangle\\&=\frac{1}{2\Omega_{\rm tot}}\sum_k\left(S_{e_Y;e_Y}(\mathbf{k},\mathbf{k};\mathbf{p})-\sum_{\mathbf{q}}S_{e_Y;e_Y}(\mathbf{k}+\mathbf{q},\mathbf{k};\mathbf{p})\right).\end{aligned} \tag{D14}$$

As expected for the Goldstone of a ferromagnet, the linear term in $\mathbf{p}$ vanishes; by using $\alpha_a(\mathbf{k},\mathbf{q}+\mathbf{G})=\alpha_a(-\mathbf{k},-\mathbf{q}-\mathbf{G})$ for $a=0,2$ of Eq. (A13), we find can prove that the linear terms vanish exactly. To second order in $\mathbf{p}$, we find the Goldstone stiffness

$$E_{\rm Goldstone}(\mathbf{p})=\frac{1}{2}m_{ij}p_ip_j, \tag{D15}$$

$$\begin{aligned}m_{ij}=\frac{1}{2\Omega_{\rm tot}}\sum_{\mathbf{k},\mathbf{q},\mathbf{G}}V(\mathbf{G}+\mathbf{q})\big[&\alpha_0(\mathbf{k},\mathbf{q}+\mathbf{G})\partial_{k_i}\partial_{k_j}\alpha_0(\mathbf{k},\mathbf{q}+\mathbf{G})+\alpha_2(\mathbf{k},\mathbf{q}+\mathbf{G})\partial_{k_i}\partial_{k_j}\alpha_2(\mathbf{k},\mathbf{q}+\mathbf{G})\\&+2\partial_{k_i}\alpha_0(\mathbf{k},\mathbf{q}+\mathbf{G})\partial_{k_j}\alpha_0(\mathbf{k},\mathbf{q}+\mathbf{G})+2\partial_{k_i}\alpha_2(\mathbf{k},\mathbf{q}+\mathbf{G})\partial_{k_j}\alpha_2(\mathbf{k},\mathbf{q}+\mathbf{G})\big].\end{aligned} \tag{D16}$$

4. Charge neutral excitation spectra for different parameters

In Figs. 7 and 8, the charge neutral excitations are plotted at different fillings and w_0/w_1's for two different screening lengths of the Coulomb interaction [Eq. (A7)], i.e.,$\xi=10$ and 20 nm, respectively. The corresponding interaction strengths are $U_{10\,\rm nm}=26$ meV and $U_{20\,\rm nm}=13$ meV. We have used $w_1=110$ meV in all the calculations and $w_0/w_1=0$, 0.4, and 0.8 for $\nu=0,\ -2$ and $w_0/w_1=0$ for $\nu=-1,\ -3$.

For the parameters we used, the $\nu=0$ states with $w_0/w_1=0,\ 0.4,\ 0.8$ and $\nu=-1,\ -3$ states with $w_0=0$ have non-negative excitations and hence are stable. The $\nu=-2$ states with $w_0/w_1=0,\ 0.4,$ and 0.8 are also stable for $\xi=20$ nm. However, the $\nu=-2$ states for $\xi=10$ nm become unstable at $w_0/w_1=0.8$ [Fig. 7(c)]. The instability can be understood from the instability of the charge ±1 excitations shown in Fig. 5(c). From Fig. 5(c), we can see that the charge $+1$ excitation is negative at some momenta between Γ_M and K_M and the charge -1 excitation is negative at Γ_M. Combining a pair of these negative particle and hole one obtains a negative charge neutral excitation. As discussed in the end of Appendix C 4, this instability will lead to a metallic phase.

For the stable ground states, where the spectrum is non-negative, the charge neutral spectrum consists of a particle-hole continuum (the blue area in Figs. 7 and 8) and a set of gapped collective modes. In Figs. 7 and 8, we only plot the eigenvalues of the scattering matrix. In practice, the existence and degeneracy of an excitation mode also depend on the occupied U(4) flavors [and U(4) × U(4) flavors in the first chiral limit] of the ground state, as discussed in Appendix III A. In particular, the number of Goldstone modes for different ground states are given in Tables II and I. In general, the states $|\Psi_\nu^{\nu_+,\nu_-}\rangle$ [Eq. (10)] in the (first) chiral-flat U(4) × U(4) limit with $\nu=0,\pm2$ and $\nu_+=\nu_-=\frac{\nu+4}{2}$ (such that it has vanishing Chern number) has more Goldstone modes than the state $|\Psi_\nu\rangle$ [Eq. (8)] with the same filling ν. From $w_0/w_1=0.4$ to $w_0/w_1=0$ for the states at $\nu=0,\ -2$, we can clearly see in Figs. 7 and 8 that a collective mode is soften and become Goldstone mode, consistent with the theoretical analysis.

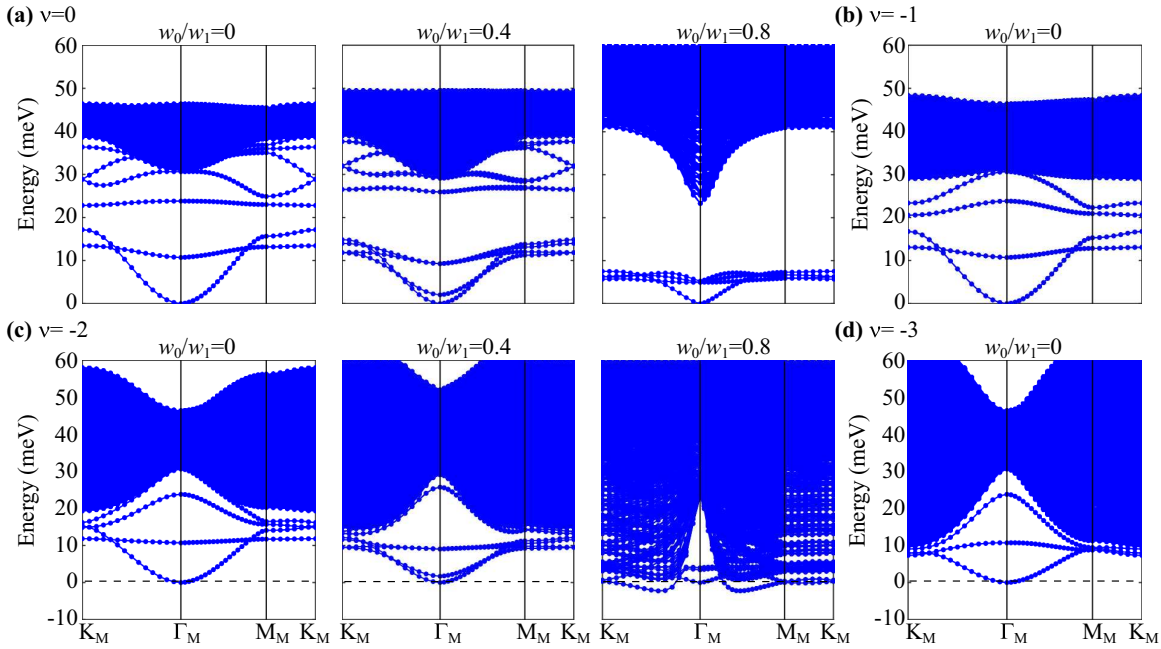

FIG. 7. Exact charge neutral excitations with $\theta = 1.05^\circ$. The flat metric condition is *not* imposed. In this plot we have used the parameters defined in Appendix A: $v_F = 5.944$ eV Å, $|K| = 1.703$ Å^{-1}, $w_1 = 110$ meV, $U_\xi = 26$ meV, and $\xi = 10$ nm.

APPENDIX E: CHARGE ±2 EXCITATIONS AND CONDITIONS ON COOPER PAIR INSTABILITY

The charge ± 1 excitations can be obtained by diagonalizing a 2×2 matrix; the charge neutral above the ground state can be obtained by diagonalizing a $2N_M \times 2N_M$ matrix, or a *one-body* problem, despite the state having a thermodynamic number of particles, due to the fact that we know the exact eigenstates (or ground states) of the system. We now show that the charge $+2$ excitations can also be obtained by diagonalizing a $2N_M \times 2N_M$ matrix. The conditions for which Cooper pairing occurs are also obtained.

1. Charge +2 excitations in the nonchiral-flat U(4) limit

We choose a basis for the neutral excitations

$$c^\dagger_{\mathbf{k}_2,m_2,\eta_2,s_2} c^\dagger_{\mathbf{k}_1,m_1,\eta_1,s_1} |\Psi\rangle \tag{E1}$$

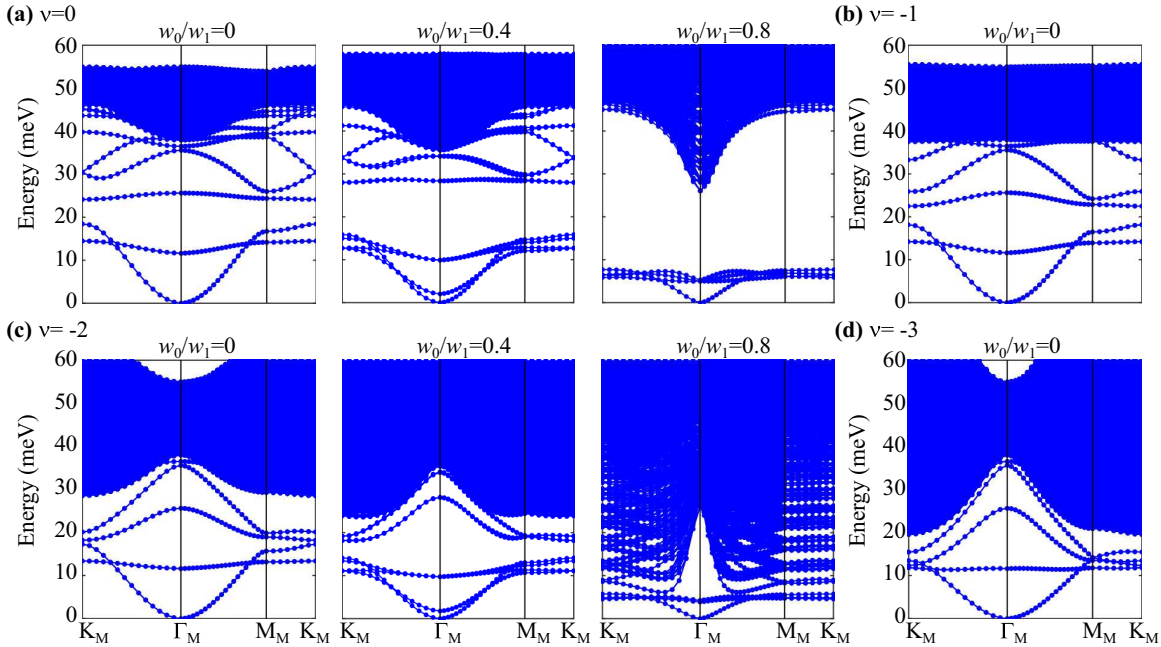

FIG. 8. Exact charge neutral excitations with $\theta = 1.05^\circ$. The flat metric condition is *not* imposed. In this plot, we use the screening length $\xi = 20$ nm and $U_\xi = 13$ meV accordingly. The other parameters are same as in Appendix A, i.e.,$v_F = 5.944$ eV Å, $|K| = 1.703$ Å^{-1}, and $w_1 = 110$ meV.

where $|\psi\rangle$ is any of the exact ground states/eigenstates Eqs. (A32) and (A35). The scattering matrix of these basis can be solved as easily as a one-body problem. We first have to compute the commutators:

$$\left[O_{-\mathbf{q},-\mathbf{G}}O_{\mathbf{q},\mathbf{G}}, c^\dagger_{\mathbf{k}_2,m_2,\eta_2,s_2}c^\dagger_{\mathbf{k}_1,m_1,\eta_1,s_1}\right] = \left[O_{-\mathbf{q},-\mathbf{G}}O_{\mathbf{q},\mathbf{G}}, c^\dagger_{\mathbf{k}_2,m_2,\eta_2,s_2}\right]c^\dagger_{\mathbf{k}_1,m_1,\eta_1,s_1} + c^\dagger_{\mathbf{k}_2,m_2,\eta_2,s_2}\left[O_{-\mathbf{q},-\mathbf{G}}O_{\mathbf{q},\mathbf{G}}, c^\dagger_{\mathbf{k}_1,m_1,\eta_1,s_1}\right], \tag{E2}$$

which in detail reads

$$\begin{aligned}
&\left[O_{-\mathbf{q},-\mathbf{G}}O_{\mathbf{q},\mathbf{G}}, c^\dagger_{\mathbf{k}_2,m_2,\eta_2,s_2}c^\dagger_{\mathbf{k}_1,m_1,\eta_1,s_1}\right]\\
&= \sum_m P^{(\eta_2)}_{mm_2}(\mathbf{k}_2, \mathbf{q}+\mathbf{G})c^\dagger_{\mathbf{k}_2,m,\eta_2,s_2}c^\dagger_{\mathbf{k}_1,m_1,\eta_1,s_1} + \sum_m P^{(\eta_1)}_{mm_1}(\mathbf{k}_1, \mathbf{q}+\mathbf{G})c^\dagger_{\mathbf{k}_2,m_2,\eta_2,s_2}c^\dagger_{\mathbf{k}_1,m,\eta_1,s_1}\\
&+ \sqrt{V(\mathbf{G}+\mathbf{q})}\sum_m \left(M^{(\eta_2)}_{m,m_2}(\mathbf{k}_2, \mathbf{q}+\mathbf{G})c^\dagger_{\mathbf{k}_2+\mathbf{q},m,\eta_2,s_2}c^\dagger_{\mathbf{k}_1,m_1,\eta_1,s_1}O_{-\mathbf{q},-\mathbf{G}} + (\mathbf{q},\mathbf{G}\leftrightarrow -\mathbf{q},-\mathbf{G})\right)\\
&+ \sqrt{V(\mathbf{G}+\mathbf{q})}\sum_m \left(M^{(\eta_1)}_{m,m_1}(\mathbf{k}_1, \mathbf{q}+\mathbf{G})c^\dagger_{\mathbf{k}_2,m_2,\eta_2,s_2}c^\dagger_{\mathbf{k}_1+\mathbf{q},m,\eta_1,s_1}O_{-\mathbf{q},-\mathbf{G}} + (\mathbf{q},\mathbf{G}\leftrightarrow -\mathbf{q},-\mathbf{G})\right)\\
&+ V(\mathbf{G}+\mathbf{q})\sum_{m,m'}\left(M^{(\eta_2)}_{m,m_2}(\mathbf{k}_2, \mathbf{q}+\mathbf{G})M^{(\eta_1)}_{m',m_1}(\mathbf{k}_1, -\mathbf{q}-\mathbf{G})c^\dagger_{\mathbf{k}_2+\mathbf{q},m,\eta_2,s_2}c^\dagger_{\mathbf{k}_1-\mathbf{q},m',\eta_1,s_1} + (\mathbf{q},\mathbf{G}\leftrightarrow -\mathbf{q},-\mathbf{G})\right).
\end{aligned} \tag{E3}$$

By rewriting $\mathbf{k}_2 = \mathbf{k}+\mathbf{p}$ and $\mathbf{k}_1 = -\mathbf{k}$, we can write the scattering equation as

$$\left[H_I - \mu N, c^\dagger_{\mathbf{k}+\mathbf{p},m_2,\eta_2,s_2}c^\dagger_{-\mathbf{k},m_1,\eta_1,s_1}\right]|\Psi\rangle = \frac{1}{2\Omega_{\text{tot}}}\sum_{m,m'}\sum_{\mathbf{q}} T^{(\eta_2,\eta_1)}_{mm';m_2m_1}(\mathbf{k}+\mathbf{q},\mathbf{k};\mathbf{p})c^\dagger_{\mathbf{k}+\mathbf{p}+\mathbf{q},m,\eta_2,s_2}c^\dagger_{-\mathbf{k}-\mathbf{q},m',\eta_1,s_1}|\Psi\rangle, \tag{E4}$$

The $|\Psi\rangle$ are the states $|\Psi_\nu\rangle$ in Eq. (A35), and hence η_1, s_1, η_2, and s_2 belong to the valley/spin flavor which are not occupied. For a generic exact eigenstate $|\Psi\rangle$ at chemical potential μ satisfying $(O_{\mathbf{q},\mathbf{G}} - A_{\mathbf{G}}N_M\delta_{\mathbf{q},0})|\Psi\rangle = 0$ for some coefficient $A_{\mathbf{G}}$, we find that the $T^{(\eta_2,\eta_1)}_{m_2,m;m_1m'}(\mathbf{k}_1,\mathbf{k}_2;\mathbf{q})$ matrix reads

$$\begin{aligned}
T^{(\eta_2,\eta_1)}_{mm';m_2m_1}(\mathbf{k}+\mathbf{q},\mathbf{k};\mathbf{p}) &= \delta_{\mathbf{q},\mathbf{0}}\left(\delta_{m,m_2}R^{\eta_1}_{m'm_1}(-\mathbf{k}) + \delta_{m',m_1}R^{\eta_2}_{mm_2}(\mathbf{k}+\mathbf{p})\right)\\
&\quad + 2\sum_{\mathbf{G}} V(\mathbf{G}+\mathbf{q})M^{(\eta_2)}_{m,m_2}(\mathbf{k}+\mathbf{p},\mathbf{q}+\mathbf{G})M^{(\eta_1)}_{m',m_1}(-\mathbf{k},-\mathbf{q}-\mathbf{G}),
\end{aligned} \tag{E5}$$

where $R^\eta_{mn}(\mathbf{k})$, $R^\eta_{mn}(\mathbf{k})$ are the $+1$ excitation matrices in Eqs. (C2) and (C16). We see that the charge $+2$ energy is a sum of the two single-particle energies [first row of Eq. (D5)] plus an interaction energy [second row of Eq. (D5)]. The exact expression of the charge $+2$ excitation spectrum allows for the determination of the Cooper pair binding energy (if any).

2. Charge +2 excitations in the (first) chiral-flat U(4) × U(4) limit

We now consider the charge $+2$ excited states reachable by creating two electron pair with total momentum $\mathbf{p}$ on the chiral-flat limit eigenstate $|\Psi^{\nu_+,\nu_-}_\nu\rangle$. Assume the valley-spin flavor $\{\eta_{1,2}, s_{1,2}\}$ has Chern band basis e_{Y1}, e_{Y2} fully empty. We consider the Hilbert space of the following sets of states of momentum quantum number $\mathbf{p}$ ($\mathbf{k}_2 = -\mathbf{k}_1+\mathbf{p}$, $\mathbf{k}_1 = \mathbf{k}$):

$$\left|\mathbf{k}+\mathbf{p}, -\mathbf{k}, e_{Y1}, e_{Y2}, \eta_2, \eta_1, s_2, s_1, \Psi^{\nu_+,\nu_-}_\nu\right\rangle = d^\dagger_{\mathbf{k}+\mathbf{p},e_{Y2},\eta_2,s_2}d^\dagger_{-\mathbf{k},e_{Y1},\eta_1,s_1}\left|\Psi^{\nu_+,\nu_-}_\nu\right\rangle, \tag{E6}$$

The $O_{\mathbf{q},\mathbf{G}}$ operators in the chiral limit have the simple, diagonal expression of Eq. (B7), which leads to the scattering equation

$$\left[H_I - \mu N, d^\dagger_{\mathbf{k}+\mathbf{p},e_{Y2},\eta_2,s_2}d^\dagger_{-\mathbf{k},e_{Y1},\eta_1,s_1}\right]|\Psi\rangle = \frac{1}{2\Omega_{\text{tot}}}\sum_{\mathbf{q}} T_{e_{Y2};e_{Y1}}(\mathbf{k}+\mathbf{q},\mathbf{k};\mathbf{p})d^\dagger_{\mathbf{k}+\mathbf{p}+\mathbf{q},e_{Y2},\eta_2,s_2}d^\dagger_{-\mathbf{k}-\mathbf{q},e_{Y1},\eta_1,s_1}|\Psi\rangle. \tag{E7}$$

The $|\Psi\rangle$ are the states $|\Psi^{\nu_+,\nu_-}_\nu\rangle$ in Eq. (A32), and hence e_{Y1}, η_1, s_1, e_{Y2}, η_2, s_2 belong to the valley/spin flavor which are not occupied. The scattering matrix in the first chiral limit does not depend on η_1, η_2

$$T_{e_{Y2};e_{Y1}}(\mathbf{k}+\mathbf{q},\mathbf{k};\mathbf{p}) = \delta_{\mathbf{q},0}(R_0(\mathbf{k}+\mathbf{p}) + R_0(-\mathbf{k})) + 2\sum_{\mathbf{G}} V(\mathbf{G}+\mathbf{q})M_{e_{Y2}}(\mathbf{k}+\mathbf{p},\mathbf{q}+\mathbf{G})M_{e_{Y1}}(-\mathbf{k},-\mathbf{q}-\mathbf{G}), \tag{E8}$$

where $M_{e_Y}(\mathbf{k},\mathbf{q}+\mathbf{G})$ is given in Eq. (A20) and $R^\eta_0(\mathbf{k})$ is given in Eq. (C12).

If condition Eq. (A30) is satisfied, the eigenstates $|\Psi^{\nu_+,\nu_-}_\nu\rangle$ are the ground states, and hence the states Eq. (E7) are the neutral excitations on top of the ground states. Without Eq. (A30), only $\nu = 0$ states are guaranteed to be the ground states, although the

others are still eigenstates. With condition Eq. (A30), we have

$$T_{e_{Y2};e_{Y1}}(\mathbf{k}+\mathbf{q},\mathbf{k};\mathbf{p}) = \delta_{\mathbf{q},0}\sum_{\mathbf{G},\mathbf{q}} V(\mathbf{G}+\mathbf{q})[\alpha_0(\mathbf{k},\mathbf{q}+\mathbf{G})^2+\alpha_2(\mathbf{k},\mathbf{q}+\mathbf{G})^2+\alpha_0(\mathbf{k}+\mathbf{p},\mathbf{q}+\mathbf{G})^2+\alpha_2(\mathbf{k}+\mathbf{p},\mathbf{q}+\mathbf{G})^2]$$
$$+2\sum_{\mathbf{G}} V(\mathbf{G}+\mathbf{q})(\alpha_0(\mathbf{k}+\mathbf{p},\mathbf{q}+\mathbf{G})+ie_{Y2}\alpha_2(\mathbf{k}+\mathbf{p},\mathbf{q}+\mathbf{G}))(\alpha_0(\mathbf{k},\mathbf{q}+\mathbf{G})+ie_{Y1}\alpha_2(\mathbf{k},\mathbf{q}+\mathbf{G})), \tag{E9}$$

where we have used the $\alpha_{0,2}(\mathbf{k},\mathbf{q}+\mathbf{G}) = \alpha_{0,2}(-\mathbf{k},-\mathbf{q}-\mathbf{G})$. Solving Eq. (E7) provides us with the expression for the charge $+2$ excitations at momentum $\mathbf{p}$ on top of the TBG ground states.

3. Absence of Cooper pairing in the projected Coulomb Hamiltonian

In Sec. V B, we have derived the sufficient conditions for the existence [Eq. (37)] and absence [Eq. (38)] of Cooper pairing binding energies. Now we prove that, in the projected Coulomb Hamiltonian with time-reversal symmetry T and the combined symmetry $PC_{2z}T$, where P is the unitary PH symmetry [43,108], $T^{(\eta_2,\eta_1)\prime\prime}_{m,m';m_2,m_1}(\mathbf{k}+\mathbf{q},\mathbf{k};\mathbf{p})$ is guaranteed to be positive semidefinite. Thus the condition (38) for the absence of Cooper pairing binding energy is always satisfied. We write $T^{(\eta_2,\eta_1)\prime\prime}_{m,m';m_2,m_1}(\mathbf{k}+\mathbf{q},\mathbf{k};\mathbf{p})$, which is defined as the third term in Eq. (E5), as

$$T^{(\eta_2,\eta_1)\prime\prime}_{m,m';m_2,m_1}(\mathbf{k}+\mathbf{q},\mathbf{k};\mathbf{p}) = 2\sum_{\mathbf{G}} V(\mathbf{G}+\mathbf{q})M^{(\eta_2)}_{mm_2}(\mathbf{k}+\mathbf{p},\mathbf{q}+\mathbf{G})M^{(\eta_1)}_{m'm_1}(-\mathbf{k},-\mathbf{q}-\mathbf{G}). \tag{E10}$$

We first consider the case $\eta_2 = -\eta_1 = \eta$. Due to the time-reversal symmetry $T|u_{n,\eta}(-\mathbf{k})\rangle = |u_{n,-\eta}(\mathbf{k})\rangle$ in the gauge Eq. (A10) [109], where $|u_{n,\eta}(\mathbf{k})\rangle$ is the $2N_{\mathbf{Q}}\times 1$ vector $u_{\mathbf{Q},\alpha;n\eta}(\mathbf{k})$ in Eq. (A3), and the definition of the M matrix (Eq. (A8)), we have

$$M^{(\eta)}_{mn}(\mathbf{k},\mathbf{q}+\mathbf{G}) = \langle u_{m,\eta}(\mathbf{k}+\mathbf{q}+\mathbf{G})|u_{n,\eta}(\mathbf{k})\rangle = \langle Tu_{m,-\eta}(-\mathbf{k}-\mathbf{q}-\mathbf{G})|Tu_{n,-\eta}(-\mathbf{k})\rangle$$
$$= \langle u_{n,-\eta}(-\mathbf{k})|u_{m,-\eta}(-\mathbf{k}-\mathbf{q}-\mathbf{G})\rangle = \langle u_{m,-\eta}(-\mathbf{k}-\mathbf{q}-\mathbf{G})|u_{n,-\eta}(-\mathbf{k})\rangle^* = M^{(-\eta)}_{mn}(-\mathbf{k},-\mathbf{q}-\mathbf{G}). \tag{E11}$$

Thus we can rewrite $T^{(\eta,-\eta)\prime\prime}_{m,m';m_2,m_1}(\mathbf{k}+\mathbf{q},\mathbf{k};\mathbf{p})$ as

$$T^{(\eta,-\eta)\prime\prime}_{m,m';m_2,m_1}(\mathbf{k}+\mathbf{q},\mathbf{k};\mathbf{p}) = 2\sum_{\mathbf{G}} V(\mathbf{G}+\mathbf{q})M^{(\eta)}_{mm_2}(\mathbf{k}+\mathbf{p},\mathbf{q}+\mathbf{G})M^{(\eta)*}_{m'm_1}(\mathbf{k},\mathbf{q}+\mathbf{G}). \tag{E12}$$

We consider the expectation value of $T^{(\eta,-\eta)\prime\prime}(\mathbf{k}+\mathbf{q},\mathbf{k};\mathbf{p})$ on a complex function $\phi_{m_2,m_1}(\mathbf{k})$:

$$\langle T''\rangle^{\eta}_{\phi}(\mathbf{p}) = \sum_{\mathbf{k}_1,\mathbf{k}_2}\sum_{mm'm_2m_2}\phi^*_{mm'}(\mathbf{k}_2)T^{(\eta,-\eta)\prime\prime}(\mathbf{k}_2,\mathbf{k}_1;\mathbf{p})\phi_{m_2,m_1}(\mathbf{k}_1)$$
$$= 2\sum_{\mathbf{k}_1,\mathbf{k}_2,\mathbf{G}} V(\mathbf{k}_2+\mathbf{G}-\mathbf{k}_1)\phi^*_{mm'}(\mathbf{k}_2)\langle u_{m\eta}(\mathbf{k}_2+\mathbf{p}+\mathbf{G})|u_{m_2\eta}(\mathbf{k}_1+\mathbf{p})\rangle\phi_{m_2,m_1}(\mathbf{k}_1)\langle u_{m_1}(\mathbf{k}_1)|u_{m'\eta}(\mathbf{k}_2+\mathbf{G})\rangle. \tag{E13}$$

Using Eq. (A4), we have $\langle u_{m_1}(\mathbf{k})|u_{m'\eta}(\mathbf{k}+\mathbf{q}+\mathbf{G})\rangle = \langle u_{m_1}(\mathbf{k}+\mathbf{G}')|u_{m'\eta}(\mathbf{k}+\mathbf{q}+\mathbf{G}+\mathbf{G}')\rangle$ and hence

$$\langle T''\rangle^{\eta}_{\phi}(\mathbf{p}) = \frac{2}{N_{\mathbf{G}}}\sum_{\mathbf{k}_1,\mathbf{k}_2,\mathbf{G}_1,\mathbf{G}_2}\sum_{mm'm_2m_1} V(\mathbf{k}_2+\mathbf{G}_2-\mathbf{k}_1-\mathbf{G}_1)$$
$$\times\phi^*_{mm'}(\mathbf{k}_2)\langle u_{m\eta}(\mathbf{k}_2+\mathbf{p}+\mathbf{G}_2)|u_{m_2\eta}(\mathbf{k}_1+\mathbf{p}+\mathbf{G}_1)\rangle\phi_{m_2,m_1}(\mathbf{k}_1)\langle u_{m_1}(\mathbf{k}_1+\mathbf{G}_1)|u_{m'\eta}(\mathbf{k}_2+\mathbf{G}_2)\rangle. \tag{E14}$$

We then define the matrix

$$W(\mathbf{k}_1+\mathbf{G}_1) = \sum_{m_2m_1}|u_{m_2\eta}(\mathbf{k}_1+\mathbf{p}+\mathbf{G}_1)\rangle\phi_{m_2,m_1}(\mathbf{k}_1)\langle u_{m_1}(\mathbf{k}_1+\mathbf{G}_1)| \tag{E15}$$

such that $\langle T''\rangle^{\eta}_{\phi}(\mathbf{p})$ can be written as

$$\langle T''\rangle^{\eta}_{\phi}(\mathbf{p}) = \frac{2}{N_{\mathbf{G}}}\sum_{\mathbf{k}_1,\mathbf{k}_2,\mathbf{G}_1,\mathbf{G}_2}\mathrm{Tr}[W^{\dagger}(\mathbf{k}_2+\mathbf{G}_2)W(\mathbf{k}_1+\mathbf{G}_1)]V(\mathbf{k}_2+\mathbf{G}_2-\mathbf{k}_1-\mathbf{G}_1)$$
$$= \frac{2}{N_{\mathbf{G}}}\sum_{ab}\sum_{\mathbf{k}_1,\mathbf{k}_2,\mathbf{G}_1,\mathbf{G}_2} W^*_{ab}(\mathbf{k}_2+\mathbf{G}_2)W_{ab}(\mathbf{k}_1+\mathbf{G}_1)V(\mathbf{k}_2+\mathbf{G}_2-\mathbf{k}_1-\mathbf{G}_1), \tag{E16}$$

where a and b are the indices of the matrix $W(\mathbf{k}+\mathbf{G})$. For each term with given a and b in Eq. (E16), we can view the summation over $\mathbf{k}_1$, $\mathbf{k}_2$, $\mathbf{G}_1$, and $\mathbf{G}_2$ as $W^\dagger_{ab}VW_{ab}$, where now $W_{ab}(\mathbf{k}+\mathbf{G})$ is viewed as a vector with the index $\mathbf{k}+\mathbf{G}$. Since $V(\mathbf{k}_2+\mathbf{G}_2-\mathbf{k}_1-\mathbf{G}_1)$ is a positive semidefinite matrix, $W^\dagger_{ab}VW_{ab}$ must be non-negative, and hence $\langle T''\rangle^{\eta}_{\phi}(\mathbf{p}) \geqslant 0$ for arbitrary ϕ. Therefore $T^{(\eta,-\eta)''}_{m,m';m_2,m_1}(\mathbf{k}+\mathbf{q},\mathbf{k};\mathbf{p})$ is positive semidefinite at every $\mathbf{p}$.

Then we prove that $T^{(\eta_2,\eta_1)''}_{m,m';m_2,m_1}(\mathbf{k}+\mathbf{q},\mathbf{k};\mathbf{p})$ with $\eta_2=\eta_1=\eta$ is also positive semidefinite. Due to the symmetry $PC_{2z}T|u_{n,\eta}(\mathbf{k})\rangle = n|u_{-n,\eta}(-\mathbf{k})\rangle$ in the gauge Eq. (A10) [109] and the definition of the M matrix [Eq. (A8)], we have

$$\begin{aligned} M^{(\eta)}_{mn}(\mathbf{k},\mathbf{q}+\mathbf{G}) &= \langle u_{m,\eta}(\mathbf{k}+\mathbf{q}+\mathbf{G})|u_{n,\eta}(\mathbf{k})\rangle = nm\langle PC_{2z}Tu_{-m,\eta}(-\mathbf{k}-\mathbf{q}-\mathbf{G})|PC_{2z}Tu_{-n,\eta}(-\mathbf{k})\rangle \\ &= nm\langle u_{-n,\eta}(-\mathbf{k})|u_{-m,\eta}(-\mathbf{k}-\mathbf{q}-\mathbf{G})\rangle = nmM^{(\eta)*}_{-m,-n}(-\mathbf{k},-\mathbf{q}-\mathbf{G}). \end{aligned} \tag{E17}$$

Thus we can rewrite $T^{(\eta,\eta)''}_{m,m';m_2,m_1}(\mathbf{k}+\mathbf{q},\mathbf{k};\mathbf{p})$ as

$$T^{(\eta,\eta)''}_{m,m';m_2,m_1}(\mathbf{k}+\mathbf{q},\mathbf{k};\mathbf{p}) = 2\sum_{\mathbf{G}} V(\mathbf{G}+\mathbf{q})M^{(\eta)}_{mm_2}(\mathbf{k}+\mathbf{p},\mathbf{q}+\mathbf{G})m'm_1M^{(\eta)*}_{-m',-m_1}(\mathbf{k},\mathbf{q}+\mathbf{G}). \tag{E18}$$

Repeating the calculations starting from Eq. (E13), one can show that $T^{(\eta,\eta)''}_{m,m';m_2,m_1}(\mathbf{k}+\mathbf{q},\mathbf{k};\mathbf{p})$ must be positive semidefinite. The only difference with the above proof is that the definition of the W matrix becomes

$$W(\mathbf{k}_1+\mathbf{G}_1) = \sum_{m_2m_1} |u_{m_2\eta}(\mathbf{k}_1+\mathbf{p}+\mathbf{G}_1)\rangle\phi_{m_2,m_1}(\mathbf{k}_1)\langle u_{-m_1}(\mathbf{k}_1+\mathbf{G}_1)|m_1. \tag{E19}$$

4. Charge −2 excitations

Based on the above, the charge -2 excitations are trivial to obtain. We do not give the details, but just the expression for the scattering elements

$$[H_I-\mu N, c_{\mathbf{k}+\mathbf{p},m_2,\eta_2,s_2}c_{-\mathbf{k},m_1,\eta_1,s_1}]|\Psi\rangle = \frac{1}{2\Omega_{\rm tot}}\sum_{m,m'}\sum_{\mathbf{q}}\widetilde{T}^{(\eta_2,\eta_1)}_{mm';m_2m_1}(\mathbf{k}+\mathbf{q},\mathbf{k};\mathbf{p})c_{\mathbf{k}+\mathbf{p}+\mathbf{q},m,\eta_2,s_2}c_{-\mathbf{k}-\mathbf{q},m',\eta_1,s_1}|\Psi\rangle, \tag{E20}$$

The $|\Psi\rangle$ are the states $|\Psi_\nu\rangle$ in Eq. (A35), and hence η_1, s_1, η_2, and s_2 belong to the valley/spin flavor which are not occupied. For a generic exact eigenstate $|\Psi\rangle$ at chemical potential μ satisfying $(O_{\mathbf{q},\mathbf{G}}-A_{\mathbf{G}}N_M\delta_{\mathbf{q},0})|\Psi\rangle=0$ for some coefficient $A_{\mathbf{G}}$, we find that the $\widetilde{T}^{(\eta_2,\eta_1)}_{m_2,m;m_1m'}(\mathbf{k}_1,\mathbf{k}_2;\mathbf{q})$ matrix reads

$$\begin{aligned} \widetilde{T}^{(\eta_2,\eta_1)}_{mm';m_2m_1}(\mathbf{k}+\mathbf{q},\mathbf{k};\mathbf{p}) &= \delta_{\mathbf{q},0}\big(\delta_{m,m_2}\widetilde{R}^{\eta_1}_{m'm_1}(-\mathbf{k}) + \delta_{m',m_1}\widetilde{R}^{\eta_2}_{mm_2}(\mathbf{k}+\mathbf{p})\big) \\ &\quad + 2\sum_{\mathbf{G}} V(\mathbf{G}+\mathbf{q})M^{(\eta_2)*}_{m,m_2}(\mathbf{k}+\mathbf{p},\mathbf{q}+\mathbf{G})M^{(\eta_1)*}_{m',m_1}(-\mathbf{k},-\mathbf{q}-\mathbf{G}), \end{aligned} \tag{E21}$$

where $\widetilde{R}^{\eta}_{mn}(\mathbf{k})$ are the -1 excitation matrices in Eq. (C16). We see that the charge -2 energy is a sum of the two single-particle energies [first row of Eq. (E21)] plus an interaction energy [second row of Eq. (E21)]. In particular, for the chiral limit, the scattering matrix elements are identical to those of charge $+2$, i.e.,Eq. (E9).

5. Charge ±2 excitation spectra for different parameters

In Figs. 9 and 10, the charge ±2 excitations are plotted at different fillings and w_0/w_1's for two different screening lengths of the Coulomb interaction (Eq. (A7)), i.e.,$\xi=10$ and 20 nm, respectively. The corresponding interaction strengths are $U_{10\,\rm nm}=26$ meV and $U_{20\,\rm nm}=13$ meV. We have used $w_1=110$ meV in all the calculations and $w_0/w_1=0$, 0.4, and 0.8 for $\nu=0,\ -2$ and $w_0/w_1=0$ for $\nu=-1,\ -3$.

The charge $+2$ (-2) spectrum consists of a two-particle (two-hole) continuum [the blue (red) area in Figs. 9 and 10] and a set of gapped charge $+2$ (-2) collective modes. The energies in the two-particle (hole) continuum are just sums of two charge $+1$ (-1) excitation energies. Note that all the charge $+2$ (-2) collective modes appear above the two-particle (two-hole) continuum, implying the absence of Cooper pairing binding energy, as proved in Sec. V B.

APPENDIX F: APPROXIMATE CHARGE ±1 AND NEUTRAL EXITATIONS AT ODD FILLINGS IN THE NONCHIRAL-FLAT U(4) LIMIT

1. Approximate charge +1 excitations at odd fillings in the nonchiral-flat U(4) limit

In the nonchiral-flat limit, the states $|\Psi^{\nu_+,\nu_-}_{\nu}\rangle$ at odd fillings $\nu=\pm1,\ \pm3$ are no longer exact eigenstates of the Hamiltonian. However, in Ref. [110], we have shown that the states $|\Psi^{1,0}_{-3}\rangle$ [or its U(4) rotations] and $|\Psi^{2,1}_{-1}\rangle$ [or its U(4) rotations] are the

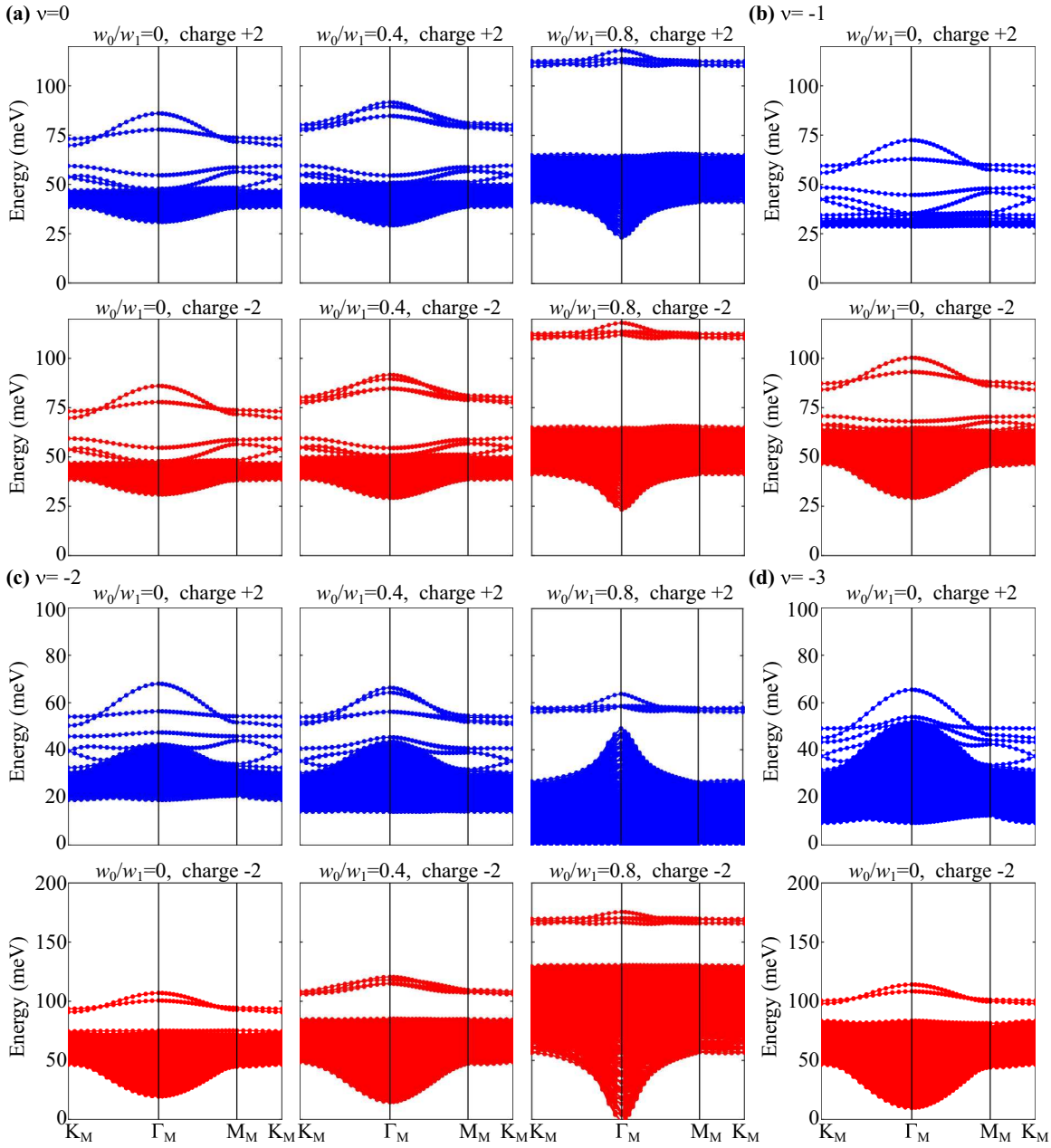

FIG. 9. Exact charge +2 (blue) and −2 (red) excitations at $\theta = 1.05^\circ$. The flat metric condition is *not* imposed. In this plot we have used the parameters defined in Appendix A: $v_F = 5.944$ eV Å, $|K| = 1.703$ Å^{-1}, $w_1 = 110$ meV, $U_\xi = 26$ meV, and $\xi = 10$ nm.

lowest states at fillings $\nu = -3, -1$ to the first-order perturbation of the (first) chiral symmetry breaking. In this section, we derive the approximate charge 1 excitations above these perturbative lowest states.

Since these states have fully occupied Chern bands, it is convenient to work in the Chern band basis. We write the $O_{\mathbf{q},\mathbf{G}}$ operator as a sum of a (first) chiral preserving term

$$O^0_{\mathbf{q},\mathbf{G}} = \sum_{\mathbf{k},e_Y,\eta,s} \sqrt{V(\mathbf{q}+\mathbf{G})} M^{(\eta)}_{e_Y,e_Y}(\mathbf{k},\mathbf{q}+\mathbf{G}) \left(d^\dagger_{\mathbf{k}+\mathbf{q},e_Y,\eta,s} d_{\mathbf{k},e_Y,\eta,s} - \frac{1}{2}\delta_{\mathbf{q},0} \right)$$
$$= \sum_{\mathbf{k},e_Y,\eta,s} \sqrt{V(\mathbf{q}+\mathbf{G})} M_{e_Y}(\mathbf{k},\mathbf{q}+\mathbf{G}) \left(d^\dagger_{\mathbf{k}+\mathbf{q},e_Y,\eta,s} d_{\mathbf{k},e_Y,\eta,s} - \frac{1}{2}\delta_{\mathbf{q},0} \right) \quad \text{(F1)}$$

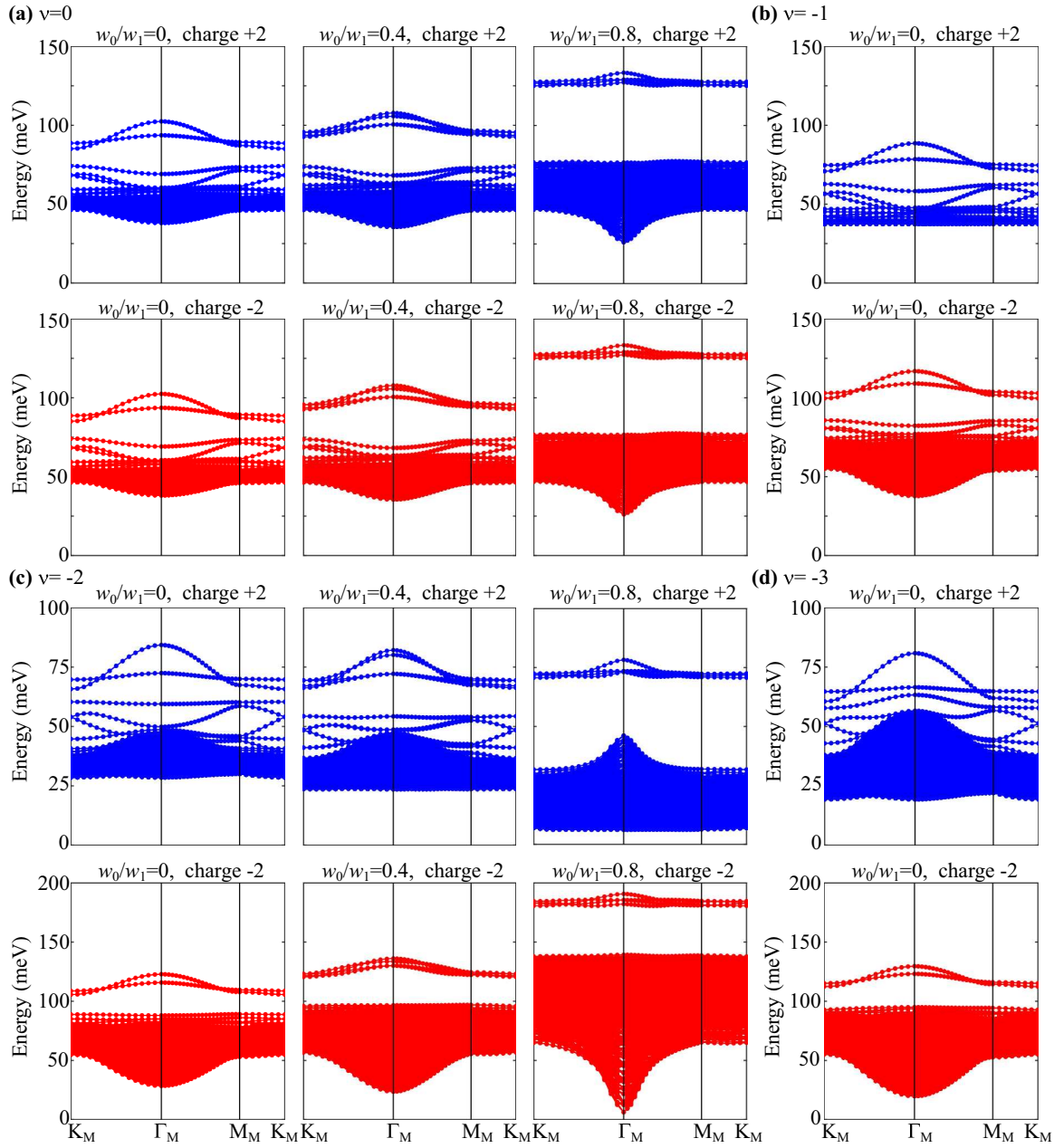

FIG. 10. Exact charge $+2$ (blue) and -2 (red) excitations at $\theta = 1.05^\circ$. The flat metric condition is *not* imposed. In this plot, we use the screening length $\xi = 20$ nm and the interaction strength $U_\xi = 13$ meV accordingly. The other parameters are same as in Appendix A: $v_F = 5.944$ eV Å, $|K| = 1.703$ Å^{-1}, and $w_1 = 110$ meV.

and a chiral breaking term

$$O^1_{\mathbf{q},\mathbf{G}} = \sum_{\mathbf{k},e_Y,\eta,s} \sqrt{V(\mathbf{q}+\mathbf{G})} M^{(\eta)}_{-e_Y,e_Y}(\mathbf{k},\mathbf{q}+\mathbf{G}) d^\dagger_{\mathbf{k}+\mathbf{q},-e_Y,\eta,s} d_{\mathbf{k},e_Y,\eta,s},$$
$$= \sum_{\mathbf{k},e_Y,\eta,s} \sqrt{V(\mathbf{q}+\mathbf{G})} \eta F_{e_Y}(\mathbf{k},\mathbf{q}+\mathbf{G}) d^\dagger_{\mathbf{k}+\mathbf{q},-e_Y,\eta,s} d_{\mathbf{k},e_Y,\eta,s}, \tag{F2}$$

where the M matrix $M^{(\eta)}_{e'_Y,e_Y}$ and the factors M_{e_Y} and F_{e_Y} are defined in Eqs. (A20) and (A21). We assume the initial state as $d^\dagger_{\mathbf{k},e_Y,\eta,s}|\Psi^{\nu_+,\nu_-}_\nu\rangle$. Acting the Hamiltonian on the initial state, we obtain two terms: $[H_I - \mu N, d^\dagger_{\mathbf{k},e_Y,\eta,s}]|\Psi^{\nu_+,\nu_-}_\nu\rangle$ and $d^\dagger_{\mathbf{k},e_Y,\eta,s}(H_I - \mu N)|\Psi^{\nu_+,\nu_-}_\nu\rangle$. In the (first) chiral-flat limit, the second term is simply $E_0 d^\dagger_{\mathbf{k},e_Y,\eta,s}|\Psi^{\nu_+,\nu_-}_\nu\rangle$ with E_0 being the ground state energy.

However, the second term also involve excited states when the (first) chiral symmetry is broken. To be specific, we have

$$d^\dagger_{\mathbf{k},e_Y,\eta,s}H_I\big|\Psi_\nu^{\nu_+,\nu_-}\big\rangle = \frac{1}{2\Omega_{\rm tot}}\sum_{\mathbf{q},\mathbf{G}} d^\dagger_{\mathbf{k},e_Y,\eta,s}\big(O^0_{-\mathbf{q},-\mathbf{G}}+O^1_{-\mathbf{q},-\mathbf{G}}\big)\big(O^0_{\mathbf{q},\mathbf{G}}+O^1_{\mathbf{q},\mathbf{G}}\big)\big|\Psi_\nu^{\nu_+,\nu_-}\big\rangle$$
$$= \frac{1}{2\Omega_{\rm tot}}\sum_{\mathbf{q},\mathbf{G}} d^\dagger_{\mathbf{k},e_Y,\eta,s}\big(\delta_{\mathbf{q},0}A_{-\mathbf{G}}A_{\mathbf{G}}N_M^2+O^1_{-\mathbf{q},-\mathbf{G}}O^0_{\mathbf{q},\mathbf{G}}+O^0_{-\mathbf{q},-\mathbf{G}}O^1_{\mathbf{q},\mathbf{G}}+O^1_{-\mathbf{q},-\mathbf{G}}O^1_{\mathbf{q},\mathbf{G}}\big)\big|\Psi_\nu^{\nu_+,\nu_-}\big\rangle. \quad \text{(F3)}$$

The first term on the right-hand side will give the unperturbed ground state energy E_0, whereas the other three terms yield excited states. Now we approximate it by projecting it into the Hilbert space with a single-particle excitation. Notice that $d^\dagger_{\mathbf{k},e_Y,\eta,s}$ generates a particle in an empty Chern band and the O^1 operator, by definition, generates particles in the empty Chern bands and holes in occupied Chern bands. Thus the terms $d^\dagger_{\mathbf{k},e_Y,\eta,s}O^1_{-\mathbf{q},-\mathbf{G}}O^0_{\mathbf{q},\mathbf{G}}$ and $d^\dagger_{\mathbf{k},e_Y,\eta,s}O^0_{-\mathbf{q},-\mathbf{G}}O^1_{\mathbf{q},\mathbf{G}}$ will at least generate two particles plus one hole. Hence they do not contribute to the projected equation. Now we consider the term $d^\dagger_{\mathbf{k},e_Y,\eta,s}O^1_{-\mathbf{q},-\mathbf{G}}O^1_{\mathbf{q},\mathbf{G}}$

$$d^\dagger_{\mathbf{k},e_Y,\eta,s}O^1_{-\mathbf{q},-\mathbf{G}}O^1_{\mathbf{q},\mathbf{G}} = \sum_{\mathbf{k}_1,\mathbf{k}_2}\sum_{e_{Y1},e_{Y2}}\sum_{\eta_1 s_1\eta_2 s_2} V(\mathbf{q}+\mathbf{G})\eta_1 F^{(\eta_1)}_{e_{Y1}}(\mathbf{k}_1,-\mathbf{q}-\mathbf{G})\eta_2 F^{(\eta_2)}_{e_{Y2}}(\mathbf{k}_2,\mathbf{q}+\mathbf{G})$$
$$\times d^\dagger_{\mathbf{k},e_Y,\eta,s}d^\dagger_{\mathbf{k}_1-\mathbf{q},-e_{Y1},\eta_1,s_1}d_{\mathbf{k}_1,e_{Y1},\eta_1,s_1}d^\dagger_{\mathbf{k}_2+\mathbf{q},-e_{Y2},\eta_2,s_2}d_{\mathbf{k}_2,e_{Y2},\eta_2,s_2}. \quad \text{(F4)}$$

According to the Wick's theorem, we have

$$\begin{aligned}
&d^\dagger_{\mathbf{k},e_Y,\eta,s}d^\dagger_{\mathbf{k}_1-\mathbf{q},-e_{Y1},\eta_1,s_1}d_{\mathbf{k}_1,e_{Y1},\eta_1,s_1}d^\dagger_{\mathbf{k}_2+\mathbf{q},-e_{Y2},\eta_2,s_2}d_{\mathbf{k}_2,e_{Y2},\eta_2,s_2}\\
&=: d^\dagger_{\mathbf{k},e_Y,\eta,s}d^\dagger_{\mathbf{k}_1-\mathbf{q},-e_{Y1},\eta_1,s_1}d_{\mathbf{k}_1,e_{Y1},\eta_1,s_1}d^\dagger_{\mathbf{k}_2+\mathbf{q},-e_{Y2},\eta_2,s_2}d_{\mathbf{k}_2,e_{Y2},\eta_2,s_2} : +\cdots\\
&\quad+\big\langle\Psi_\nu^{\nu_+,\nu_-}\big|d^\dagger_{\mathbf{k},e_Y,\eta,s}d_{\mathbf{k}_1,e_{Y1},\eta_1,s_1}\big|\Psi_\nu^{\nu_+,\nu_-}\big\rangle\big\langle\Psi_\nu^{\nu_+,\nu_-}\big|d^\dagger_{\mathbf{k}_1-\mathbf{q},-e_{Y1},\eta_1,s_1}d_{\mathbf{k}_2,e_{Y2},\eta_2,s_2}\big|\Psi_\nu^{\nu_+,\nu_-}\big\rangle d^\dagger_{\mathbf{k}_2+\mathbf{q},-e_{Y2},\eta_2,s_2}\\
&\quad-\big\langle\Psi_\nu^{\nu_+,\nu_-}\big|d^\dagger_{\mathbf{k},e_Y,\eta,s}d_{\mathbf{k}_2,e_{Y2},\eta_2,s_2}\big|\Psi_\nu^{\nu_+,\nu_-}\big\rangle\big\langle\Psi_\nu^{\nu_+,\nu_-}\big|d_{\mathbf{k}_1,e_{Y1},\eta_1,s_1}d^\dagger_{\mathbf{k}_2+\mathbf{q},-e_{Y2},\eta_2,s_2}\big|\Psi_\nu^{\nu_+,\nu_-}\big\rangle d^\dagger_{\mathbf{k}_1-\mathbf{q},-e_{Y1},\eta_1,s_1}\\
&\quad+\big\langle\Psi_\nu^{\nu_+,\nu_-}\big|d^\dagger_{\mathbf{k}_1-\mathbf{q},-e_{Y1},\eta_1,s_1}d_{\mathbf{k}_2,e_{Y2},\eta_2,s_2}\big|\Psi_\nu^{\nu_+,\nu_-}\big\rangle\big\langle\Psi_\nu^{\nu_+,\nu_-}\big|d_{\mathbf{k}_1,e_{Y1},\eta_1,s_1}d^\dagger_{\mathbf{k}_2+\mathbf{q},-e_{Y2},\eta_2,s_2}\big|\Psi_\nu^{\nu_+,\nu_-}\big\rangle d^\dagger_{\mathbf{k},e_Y,\eta,s}. \quad \text{(F5)}
\end{aligned}$$

Here $:A:=A$ represents the normal ordered form of the operator A with respect to $|\Psi_\nu^{\nu_+,\nu_-}\rangle$, where the operators that annihilate $|\Psi_\nu^{\nu_+,\nu_-}\rangle$ is ordered on the right-hand side of the operators that do not. The second term ("$\cdots$") represent the normal ordered terms with one contraction. The first (second) term either annihilate $|\Psi_\nu^{\nu_+,\nu_-}\rangle$ or generate three (two) particles plus two (one) holes. We hence will omit them. The third and fourth terms must vanish since we require the flavor $\{e_Y,\eta,s\}$ to be empty and hence $\langle\Psi_\nu^{\nu_+,\nu_-}|d^\dagger_{\mathbf{k},e_Y,\eta,s}=0$. The last term is the Fock energy correction to the ground state energy. Therefore we conclude

$$d^\dagger_{\mathbf{k},e_Y,\eta,s}H_I\big|\Psi_\nu^{\nu_+,\nu_-}\big\rangle \approx (E_0+\Delta E_0)d^\dagger_{\mathbf{k},e_Y,\eta,s}\big|\Psi_\nu^{\nu_+,\nu_-}\big\rangle, \quad \text{(F6)}$$

where E_0 is the unperturbed ground state energy and ΔE_0 is the Fock energy correct.

The excitation energy is hence given by the spectrum of $[H_I-\mu N, d^\dagger_{\mathbf{k},e_Y,\eta,s}]$. Following the calculation in Appendix B, we obtain

$$[O_{-\mathbf{q},-\mathbf{G}}O_{\mathbf{q},\mathbf{G}}, d^\dagger_{\mathbf{k},e_Y,\eta,s}] = V(\mathbf{q}+\mathbf{G})P^\eta_{e'_Y,e_Y}(\mathbf{k},\mathbf{q}+\mathbf{G})d^\dagger_{\mathbf{k},e'_Y,\eta,s}$$
$$+\sqrt{V(\mathbf{G}+\mathbf{q})}\big(M^{(\eta)}_{e'_Y,e_Y}(\mathbf{k},\mathbf{q}+\mathbf{G})d^\dagger_{\mathbf{k}+\mathbf{q},e'_Y,\eta,s}O_{-\mathbf{q},-\mathbf{G}}+M^{(\eta)}_{e'_Y,e_Y}(\mathbf{k},-\mathbf{q}-\mathbf{G})d^\dagger_{\mathbf{k}-\mathbf{q},e'_Y,\eta,s}O_{\mathbf{q},\mathbf{G}}\big), \quad \text{(F7)}$$

where

$$P^\eta_{e'_Y,e_Y}(\mathbf{k},\mathbf{q}+\mathbf{G}) = \sum_{e''_Y} M^{(\eta)*}_{e''_Y,e'_Y}(\mathbf{k},\mathbf{q}+\mathbf{G})M^{(\eta)}_{e''_Y,e_Y}(\mathbf{k},\mathbf{q}+\mathbf{G}). \quad \text{(F8)}$$

Acting the commutator of the interaction Hamiltonian and $d^\dagger_{\mathbf{k},e_Y,\eta,s}$ on the state $|\Psi_\nu^{\nu_+,\nu_-}\rangle$, we have

$$\big[H_I-\mu N, d^\dagger_{\mathbf{k},e_Y,\eta,s}\big]\big|\Psi_\nu^{\nu_+,\nu_-}\big\rangle = \frac{1}{2\Omega_{\rm tot}}\sum_{\mathbf{q},\mathbf{G},e'_Y}\big(V(\mathbf{q}+\mathbf{G})P^\eta_{e'_Y,e_Y}(\mathbf{k},\mathbf{q}+\mathbf{G})d^\dagger_{\mathbf{k},e'_Y,\eta,s}$$
$$+2\sqrt{V(\mathbf{G}+\mathbf{q})}M^{(\eta)}_{e'_Y,e_Y}(\mathbf{k},\mathbf{q}+\mathbf{G})d^\dagger_{\mathbf{k}+\mathbf{q},e'_Y,\eta,s}O_{-\mathbf{q},-\mathbf{G}}\big)\big|\Psi_\nu^{\nu_+,\nu_-}\big\rangle-\mu d^\dagger_{\mathbf{k},e_Y,\eta,s}\big|\Psi_\nu^{\nu_+,\nu_-}\big\rangle. \quad \text{(F9)}$$

In the (first) chiral limit, where $O_{-\mathbf{q},-\mathbf{G}}|\Psi_\nu^{\nu_+,\nu_-}\rangle=\delta_{\mathbf{q},0}A_{-\mathbf{G}}N_M|\Psi_\nu^{\nu_+,\nu_-}\rangle$, the right-hand side of the above equation only has one particle excitations. However, when the (first) chiral symmetry is broken, $d^\dagger_{\mathbf{k},e_Y,\eta,s}O_{-\mathbf{q},-\mathbf{G}}|\Psi_\nu^{\nu_+,\nu_-}\rangle$ will yield excitations with two

particles plus one hole

$$d^\dagger_{\mathbf{k}+\mathbf{q},e'_Y,\eta,s}O_{-\mathbf{q},-\mathbf{G}}\left|\Psi_\nu^{\nu_+,\nu_-}\right\rangle = d^\dagger_{\mathbf{k}+\mathbf{q},e'_Y,\eta,s}\left(O^0_{-\mathbf{q},-\mathbf{G}}+O^1_{-\mathbf{q},-\mathbf{G}}\right)\left|\Psi_\nu^{\nu_+,\nu_-}\right\rangle = \delta_{\mathbf{q},0}A_{-\mathbf{G}}N_M d^\dagger_{\mathbf{k},e'_Y,\eta,s}\left|\Psi_\nu^{\nu_+,\nu_-}\right\rangle + \sum_{\mathbf{k}',e''_Y,\eta',s'}\sqrt{V(\mathbf{q}+\mathbf{G})}\eta' F_{e''_Y}(\mathbf{k}',-\mathbf{q}-\mathbf{G})d^\dagger_{\mathbf{k}+\mathbf{q},e'_Y,\eta,s}d^\dagger_{\mathbf{k}'-\mathbf{q},-e''_Y,\eta',s'}d_{\mathbf{k}',e''_Y,\eta',s'}\left|\Psi_\nu^{\nu_+,\nu_-}\right\rangle \quad \text{(F10)}$$

We now approximate the right-hand side by projecting it into the one particle Hilbert space: We only keep the term satisfying $\mathbf{k}'=\mathbf{k}+\mathbf{q}$, $e''_Y=e'_Y$, $\eta'=\eta$, and $s'=s$:

$$d^\dagger_{\mathbf{k}+\mathbf{q},e'_Y,\eta,s}O_{-\mathbf{q},-\mathbf{G}}\left|\Psi_\nu^{\nu_+,\nu_-}\right\rangle \approx \delta_{\mathbf{q},0}A_{-\mathbf{G}}N_M d^\dagger_{\mathbf{k},e'_Y,\eta,s}\left|\Psi_\nu^{\nu_+,\nu_-}\right\rangle - \sqrt{V(\mathbf{q}+\mathbf{G})}\eta F_{e'_Y}(\mathbf{k}+\mathbf{q},-\mathbf{q}-\mathbf{G})n_{e'_Y,\eta,s}d^\dagger_{\mathbf{k},-e'_Y,\eta,s}\left|\Psi_\nu^{\nu_+,\nu_-}\right\rangle, \quad \text{(F11)}$$

where $n_{e'_Y,\eta,s}$ equals to 1 if the flavor $\{e'_Y,\eta,s\}$ is occupied and equals to 0 otherwise. If e'_Y in the second term equals to e_Y, then there must be $n_{e'_Y,\eta,s}=0$ because we require $\{e_Y,\eta,s\}$ to be empty such that $d^\dagger_{\mathbf{k},e_Y,\eta,s}|\Psi_\nu^{\nu_+,\nu_-}\rangle$ is nonvanishing. Hence we only need to keep the $e'_Y=-e_Y$ in the second term. Then we can rewrite the second term in Eq. (F9) as

$$\begin{aligned}
&\sum_{e'_Y}M^{(\eta)}_{e'_Y,e_Y}(\mathbf{k},\mathbf{q}+\mathbf{G})d^\dagger_{\mathbf{k}+\mathbf{q},e'_Y,\eta,s}O_{-\mathbf{q},-\mathbf{G}}\left|\Psi_\nu^{\nu_+,\nu_-}\right\rangle\\
&\approx\sum_{e'_Y}\delta_{\mathbf{q},0}A_{-\mathbf{G}}N_M M^{(\eta)}_{e'_Y,e_Y}(\mathbf{k},\mathbf{G})d^\dagger_{\mathbf{k},e'_Y,\eta,s}\left|\Psi_\nu^{\nu_+,\nu_-}\right\rangle - \sqrt{V(\mathbf{q}+\mathbf{G})}M^{\eta}_{-e_Y,e_Y}(\mathbf{k},\mathbf{q}+\mathbf{G})\\
&\quad\times\eta F_{-e_Y}(\mathbf{k}+\mathbf{q},-\mathbf{q}-\mathbf{G})n_{-e_Y,\eta,s}d^\dagger_{\mathbf{k},e_Y,\eta,s}\left|\Psi_\nu^{\nu_+,\nu_-}\right\rangle\\
&\approx\sum_{e'_Y}\delta_{\mathbf{q},0}A_{-\mathbf{G}}N_M M^{(\eta)}_{e'_Y,e_Y}(\mathbf{k},\mathbf{G})d^\dagger_{\mathbf{k},e'_Y,\eta,s}\left|\Psi_\nu^{\nu_+,\nu_-}\right\rangle - n_{-e_Y,\eta,s}\sqrt{V(\mathbf{q}+\mathbf{G})}\left|F_{e_Y}(\mathbf{k},\mathbf{q}+\mathbf{G})\right|^2 d^\dagger_{e_Y,\eta,s}\left|\Psi_\nu^{\nu_+,\nu_-}\right\rangle. \quad \text{(F12)}
\end{aligned}$$

Here we have made use of Eqs. (A21) and (A12). With the above approximation, we can write the excitation equation as

$$\left[H_I-\mu N, d^\dagger_{\mathbf{k},e_Y,\eta,s}\right]\left|\Psi_\nu^{\nu_+,\nu_-}\right\rangle \approx \sum_{e'_Y}R^{\eta,s}_{e'_Y,e_Y}d^\dagger_{\mathbf{k},e'_Y,\eta,s}\left|\Psi_\nu^{\nu_+,\nu_-}\right\rangle, \quad \text{(F13)}$$

where

$$\begin{aligned}
R^{\eta,s}_{e'_Y,e_Y} =& \frac{1}{2\Omega_{\text{tot}}}\sum_{\mathbf{q},\mathbf{G}}\Big(V(\mathbf{q}+\mathbf{G})P^{\eta}_{e'_Y,e_Y}(\mathbf{k},\mathbf{q}+\mathbf{G}) + 2\delta_{\mathbf{q},0}\sqrt{V(\mathbf{G})}A_{-\mathbf{G}}N_M M^{(\eta)}_{e'_Y,e_Y}(\mathbf{k},\mathbf{G})\\
&- 2\delta_{e'_Y,e_Y}n_{-e_Y,\eta,s}V(\mathbf{q}+\mathbf{G})|F_{e_Y}(\mathbf{k},\mathbf{q}+\mathbf{G})|^2\Big) - \mu\delta_{e'_Y,e_Y}. \quad \text{(F14)}
\end{aligned}$$

Notice that both e_Y and e'_Y are limited to empty Chern bands in the valley-spin flavor η, s.

Let us first consider the charge $+1$ excitation at $\nu=-3$. Without loss of generality, we assume the occupied flavor is $\{+1,\uparrow,+1\}$. For the excitation in the half-filled valley-spin sector ($\{+1,\uparrow\}$), the e_Y and e'_Y indices in $R^{\eta,s}_{e'_Y,e_Y}$ are limited for the empty Chern band (-1). In this case the R matrix is one-by-one with $n_{-e_Y,\eta,s}=1$. For the excitation in the other (fully empty) valley-spin sectors, the e_Y and e'_Y indices can be either 1 or -1. Hence the R matrix is a two-by-two matrix with $n_{-e_Y,\eta,s}=0$. The calculation for $\nu=-1$ is similar. Due to Ref. [110], the perturbative ground state in the nonchiral-flat limit at $\nu=-1$ is $|\Psi^{2,1}_{-1}\rangle$ [or its U(4) rotations]. There is a fully occupied valley-spin sector and a half-filled valley-spin sector. In the half-filled valley-spin sector, R is one-by-one with $n_{-e_Y,\eta,s}=1$, and in the empty valley-spin sectors, R is two-by-two with $n_{-e_Y,\eta,s}=0$. The approximate charge $+1$ excitations are shown in Fig. 11.

2. Approximate charge −1 excitations at odd fillings in the nonchiral-flat limit

In the nonchiral-flat limit, the states $|\Psi_\nu^{\nu_+,\nu_-}\rangle$ at odd fillings $\nu=\pm1,\ \pm3$ are no longer exact eigenstates of the Hamiltonian. However, in Ref. [110] we have shown that the states $|\Psi^{1,0}_{-3}\rangle$ [or its U(4) rotations] and $|\Psi^{2,1}_{-1}\rangle$ [or its U(4) rotations] are the lowest states at fillings $\nu=-3,-1$ to the first-order perturbation of the (first) chiral symmetry breaking. Using the same method as in Appendix F 1, in this section, we derive the approximate charge -1 excitations above these perturbative lowest states.

For the same reason in Appendix F 1, the spectrum of excitation is given by the eigenvalues of $[H_I-\mu N, d_{\mathbf{k},e_Y,\eta,s}]$. Following the calculation in Appendix F 1, we have

$$\begin{aligned}
\left[H_I-\mu N, d_{\mathbf{k},e_Y,\eta,s}\right]\left|\Psi_\nu^{\nu_+,\nu_-}\right\rangle =& \frac{1}{2\Omega_{\text{tot}}}\sum_{\mathbf{q},\mathbf{G},e'_Y}\Big(V(\mathbf{q}+\mathbf{G})P^{\eta*}_{e'_Y,e_Y}(\mathbf{k},\mathbf{q}+\mathbf{G})d_{\mathbf{k},e'_Y,\eta,s}\\
&- 2\sqrt{V(\mathbf{G}+\mathbf{q})}M^{(\eta)*}_{e'_Y,e_Y}(\mathbf{k},\mathbf{q}+\mathbf{G})d_{\mathbf{k}+\mathbf{q},e'_Y,\eta,s}O_{\mathbf{q},\mathbf{G}}\Big)\left|\Psi_\nu^{\nu_+,\nu_-}\right\rangle + \mu d_{\mathbf{k},e_Y,\eta,s}\left|\Psi_\nu^{\nu_+,\nu_-}\right\rangle, \quad \text{(F15)}
\end{aligned}$$

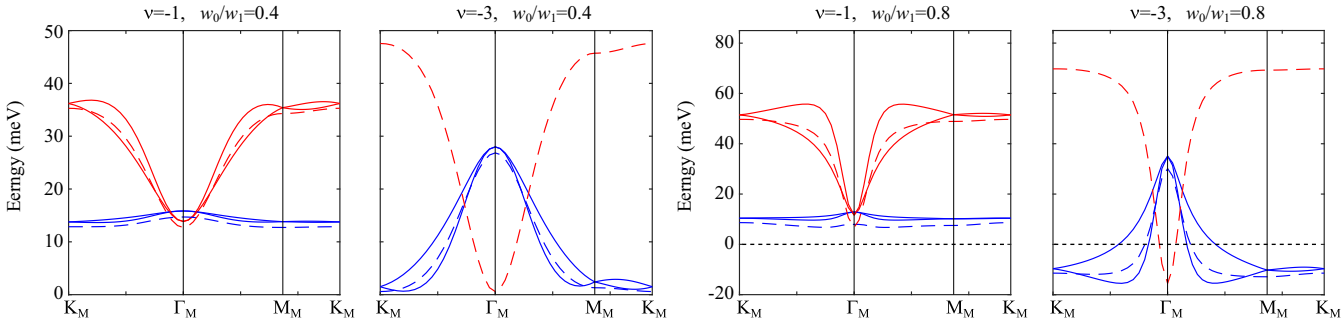

FIG. 11. Approximate charge $+1$ (blue) and -1 (red) excitations at $\theta = 1.05^\circ$ at odd fillings in the nonchiral-flat limit. The dashed bands are the excitations in the half-filled valley-spin sectors. The solid blue (red) bands are the $+1$ (-1) excitations in the fully empty (occupied) valley-spin sectors. The flat metric condition is *not* imposed. In this plot we set the screening length as $\xi = 10$ nm and accordingly the interaction strength as $U_\xi = 13$ meV. The other parameters are same as in Appendix A: $v_F = 5.944$ eV Å, $|K| = 1.703$ Å^{-1}, and $w_1 = 110$ meV.

where P^η is defined in Eq. (F8). When the (first) chiral symmetry is broken, the term $d_{\mathbf{k}+\mathbf{q},e'_Y,\eta,s}O_{\mathbf{q},\mathbf{G}}|\Psi_\nu^{\nu_+,\nu_-}\rangle$ yields excitations with two holes plus one particle

$$\begin{aligned} &d_{\mathbf{k}+\mathbf{q},e'_Y,\eta,s}O_{\mathbf{q},\mathbf{G}}\left|\Psi_\nu^{\nu_+,\nu_-}\right\rangle \\ &\quad= d_{\mathbf{k}+\mathbf{q},e'_Y,\eta,s}\left(O^0_{\mathbf{q},\mathbf{G}}+O^1_{\mathbf{q},\mathbf{G}}\right)\left|\Psi_\nu^{\nu_+,\nu_-}\right\rangle \\ &\quad= \delta_{\mathbf{q},0}A_{\mathbf{G}}N_M d_{\mathbf{k},e'_Y,\eta,s}\left|\Psi_\nu^{\nu_+,\nu_-}\right\rangle + \sum_{\mathbf{k}',e''_Y,\eta',s'}\sqrt{V(\mathbf{q}+\mathbf{G})}\eta' F_{e''_Y}(\mathbf{k}',\mathbf{q}+\mathbf{G})d_{\mathbf{k}+\mathbf{q},e'_Y,\eta,s}d^\dagger_{\mathbf{k}'+\mathbf{q},-e''_Y,\eta',s'}d_{\mathbf{k}',e''_Y,\eta',s'}\left|\Psi_\nu^{\nu_+,\nu_-}\right\rangle. \end{aligned} \tag{F16}$$

We now approximate the right-hand side by projecting it into the one hole Hilbert space: We only keep the term satisfying $\mathbf{k}' = \mathbf{k}$, $e''_Y = -e'_Y$, $\eta' = \eta$, and $s' = s$:

$$\begin{aligned} d_{\mathbf{k}+\mathbf{q},e'_Y,\eta,s}O_{\mathbf{q},\mathbf{G}}\left|\Psi_\nu^{\nu_+,\nu_-}\right\rangle =& d_{\mathbf{k}+\mathbf{q},e'_Y,\eta,s}\left(O^0_{\mathbf{q},\mathbf{G}}+O^1_{\mathbf{q},\mathbf{G}}\right)\left|\Psi_\nu^{\nu_+,\nu_-}\right\rangle \\ =& \delta_{\mathbf{q},0}A_{\mathbf{G}}N_M d_{\mathbf{k},e'_Y,\eta,s}\left|\Psi_\nu^{\nu_+,\nu_-}\right\rangle + \sqrt{V(\mathbf{q}+\mathbf{G})}\eta F_{-e'_Y}(\mathbf{k},\mathbf{q}+\mathbf{G})\left(1-n_{e'_Y,\eta,s}\right)d_{\mathbf{k},-e'_Y,\eta,s}\left|\Psi_\nu^{\nu_+,\nu_-}\right\rangle, \end{aligned} \tag{F17}$$

where $n_{e'_Y,\eta,s}$ equals to 1 if the flavor $\{e'_Y,\eta,s\}$ is occupied and equals to 0 otherwise. If e'_Y in the second term equals to e_Y, then there must be $n_{e'_Y,\eta,s} = 1$ because we require $\{e_Y,\eta,s\}$ to be occupied such that $d_{\mathbf{k},e_Y,\eta,s}|\Psi_\nu^{\nu_+,\nu_-}\rangle$ is nonvanishing. Hence we only need to keep the $e'_Y = -e_Y$ in the second term. Then we can rewrite the second term in Eq. (F15) as

$$\begin{aligned} &\sum_{e'_Y}M^{(\eta)*}_{e'_Y,e_Y}(\mathbf{k},\mathbf{q}+\mathbf{G})d_{\mathbf{k}+\mathbf{q},e'_Y,\eta,s}O_{\mathbf{q},\mathbf{G}}\left)\left|\Psi_\nu^{\nu_+,\nu_-}\right\rangle\right. \\ &\quad= \sum_{e'_Y}\delta_{\mathbf{q},0}A_{\mathbf{G}}N_M M^{(\eta)*}_{e'_Y,e_Y}(\mathbf{k},\mathbf{G})d_{\mathbf{k},e'_Y,\eta,s}\left|\Psi_\nu^{\nu_+,\nu_-}\right\rangle + \left(1-n_{-e_Y,\eta,s}\right)\sqrt{V(\mathbf{q}+\mathbf{G})}\left|F_{e_Y}(\mathbf{k},\mathbf{q}+\mathbf{G})\right|^2 d_{\mathbf{k},e_Y,\eta,s}\left|\Psi_\nu^{\nu_+,\nu_-}\right\rangle. \end{aligned} \tag{F18}$$

Here we have made use of Eqs. (A21) and (A12). With the above approximation, we can write the excitation equation as

$$\left[H_I-\mu N, d_{\mathbf{k},e_Y,\eta,s}\right]\left|\Psi_\nu^{\nu_+,\nu_-}\right\rangle \approx \sum_{e'_Y}\widetilde{R}^{\eta,s}_{e'_Y,e_Y}d_{\mathbf{k},e'_Y,\eta,s}\left|\Psi_\nu^{\nu_+,\nu_-}\right\rangle, \tag{F19}$$

where

$$\begin{aligned} \widetilde{R}^{\eta,s}_{e'_Y,e_Y} =& \frac{1}{2\Omega_{\text{tot}}}\sum_{\mathbf{q},\mathbf{G}}\Big(V(\mathbf{q}+\mathbf{G})P^{\eta*}_{e'_Y,e_Y}(\mathbf{k},\mathbf{q}+\mathbf{G}) - 2\delta_{\mathbf{q},0}\sqrt{V(\mathbf{G})}A_{\mathbf{G}}N_M M^{(\eta)*}_{e'_Y,e_Y}(\mathbf{k},\mathbf{G}) \\ &- 2\delta_{e'_Y,e_Y}(1-n_{-e_Y,\eta,s})V(\mathbf{q}+\mathbf{G})|F_{e_Y}(\mathbf{k},\mathbf{q}+\mathbf{G})|^2\Big) + \mu\delta_{e'_Y,e_Y}. \end{aligned} \tag{F20}$$

Notice that both e_Y and e'_Y are limited to fully filled Chern bands in the valley-spin flavor η, s.

Let us first consider the charge -1 excitation at $\nu = -3$. Without loss of generality, we assume the occupied flavor is $\{+1,\uparrow,+1\}$. For the excitation in the half-filled valley-spin sector ($\{+1,\uparrow\}$), the e_Y and e'_Y indices in $\widetilde{R}^{\eta,s}_{e'_Y,e_Y}$ are limited for the occupied Chern band ($+1$). In this case the $\widetilde{R}$ matrix is one-by-one with $n_{-e_Y,\eta,s} = 0$. And there is no hole excitation in the other (fully empty) valley-spin sectors. The calculation for $\nu = -1$ is similar. Due to Ref. [110], the perturbative ground state in the nonchiral-flat limit at $\nu = -1$ is $|\Psi^{2,1}_{-1}\rangle$ (or its U(4) rotations). There is a fully occupied valley-spin sector and a half-filled valley-spin sector. In the half-filled valley-spin sector $\widetilde{R}$ is one-by-one with $n_{-e_Y,\eta,s} = 0$ and in the fully occupied valley-spin sector $\widetilde{R}$ is two-by-two with $n_{-e_Y,\eta,s} = 1$. The approximate charge -1 excitations are shown in Fig. 11.

3. Approximate charge neutral excitations at odd fillings in the nonchiral-flat U(4) limit

In the nonchiral-flat limit, the states $|\Psi_\nu^{\nu_+,\nu_-}\rangle$ at odd fillings $\nu=\pm1,\pm3$ are no longer exact eigenstates of the Hamiltonian. However, in Ref. [110], we have shown that the states $|\Psi_{-3}^{1,0}\rangle$ (or its U(4) rotations) and $|\Psi_{-1}^{2,1}\rangle$ (or its U(4) rotations] are the lowest states at fillings $\nu=-3,-1$ to the first-order perturbation of the (first) chiral symmetry breaking. In this section, we derive the approximate charge neutral excitations above these perturbative lowest states.

Since these states have fully occupied Chern bands, it is convenient to work in the Chern band basis. Following the calculations in Appendix D 1, we have

$$\begin{aligned}
&\left[H_I-\mu N, d^\dagger_{\mathbf{k}+\mathbf{p},e_{Y2},\eta_2,s_2}d_{\mathbf{k},e_{Y1},\eta_1,s_1}\right]\left|\Psi_\nu^{\nu_+,\nu_-}\right\rangle\\
&=\frac{1}{2\Omega_{\rm tot}}\sum_{\mathbf{q},\mathbf{G}}\Bigg(\sum_{e_Y}P^{\eta_2}_{e_Y,e_{Y2}}(\mathbf{k}+\mathbf{p},\mathbf{q}+\mathbf{G})d^\dagger_{\mathbf{k}+\mathbf{p},e_Y,\eta_2,s_2}d_{\mathbf{k},e_{Y1},\eta_1,s_1}+\sum_{e'_Y}P^{\eta_1*}_{e'_Y,e_{Y1}}(\mathbf{k},\mathbf{q}+\mathbf{G})d^\dagger_{\mathbf{k}+\mathbf{p},e_{Y2},\eta_2,s_2}d_{\mathbf{k},e'_Y,\eta_1,s_1}\\
&\quad+2\sqrt{V(\mathbf{G}+\mathbf{q})}\sum_{e_Y}M^{(\eta_2)}_{e_Y,e_{Y2}}(\mathbf{k}+\mathbf{p},\mathbf{q}+\mathbf{G})d^\dagger_{\mathbf{k}+\mathbf{p}+\mathbf{q},e_Y,\eta_2,s_2}d_{\mathbf{k},e_{Y1},\eta_1,s_1}O_{-\mathbf{q},-\mathbf{G}}\\
&\quad-2\sqrt{V(\mathbf{G}+\mathbf{q})}\sum_{e'_Y}M^{(\eta_1)*}_{e'_Y,e_{Y1}}(\mathbf{k},-\mathbf{q}-\mathbf{G})d^\dagger_{\mathbf{k}+\mathbf{p},e_{Y2},\eta_2,s_2}d_{\mathbf{k}-\mathbf{q},e'_Y,\eta_1,s_1}O_{-\mathbf{q},-\mathbf{G}}\\
&\quad-2V(\mathbf{G}+\mathbf{q})\sum_{e_Y,e'_Y}M^{(\eta_2)}_{e_Y,e_{Y2}}(\mathbf{k}+\mathbf{p},\mathbf{q}+\mathbf{G})M^{(\eta_1)*}_{e'_Y,e_{Y1}}(\mathbf{k},\mathbf{q}+\mathbf{G})d^\dagger_{\mathbf{k}+\mathbf{p}+\mathbf{q},e_Y,\eta_2,s_2}d_{\mathbf{k}+\mathbf{q},e'_Y,\eta_1,s_1}\Bigg)\left|\Psi_\nu^{\nu_+,\nu_-}\right\rangle. \qquad \text{(F21)}
\end{aligned}$$

In the (first) chiral limit, where $O_{-\mathbf{q},-\mathbf{G}}|\Psi_\nu^{\nu_+,\nu_-}\rangle=\delta_{\mathbf{q},0}A_{-\mathbf{G}}N_M|\Psi_\nu^{\nu_+,\nu_-}\rangle$, the right-hand side of the above equation only involve excitations with one pair of a particle and a hole. However, when the (first) chiral symmetry is broken, $O_{-\mathbf{q},-\mathbf{G}}|\Psi_\nu^{\nu_+,\nu_-}\rangle$ will yield additional particle-hole excitations:

$$\begin{aligned}
d^\dagger_{\mathbf{k}+\mathbf{p}+\mathbf{q},e_Y,\eta_2,s_2}d_{\mathbf{k},e_{Y1},\eta_1,s_1}O_{-\mathbf{q},-\mathbf{G}}\left|\Psi_\nu^{\nu_+,\nu_-}\right\rangle&=d^\dagger_{\mathbf{k}+\mathbf{p}+\mathbf{q},e_Y,\eta_2,s_2}d_{\mathbf{k},m_1,\eta_1,s_1}\left(O^0_{-\mathbf{q},-\mathbf{G}}+O^1_{-\mathbf{q},-\mathbf{G}}\right)\left|\Psi_\nu^{\nu_+,\nu_-}\right\rangle\\
&=\delta_{\mathbf{q},0}A_{-\mathbf{G}}N_Md^\dagger_{\mathbf{k}+\mathbf{p},e_Y,\eta_2,s_2}d_{\mathbf{k},e_{Y1},\eta_1,s_1}\left|\Psi_\nu^{\nu_+,\nu_-}\right\rangle+\sum_{\mathbf{k}'',e''_Y,\eta'',s''}\sqrt{V(\mathbf{q}+\mathbf{G})}\eta''F_{e''_Y}(\mathbf{k}'',-\mathbf{q}-\mathbf{G})\\
&\quad\times d^\dagger_{\mathbf{k}+\mathbf{p}+\mathbf{q},e_Y,\eta_2,s_2}d_{\mathbf{k},e_{Y1},\eta_1,s_1}d^\dagger_{\mathbf{k}''-\mathbf{q},-e''_Y,\eta'',s''}d_{\mathbf{k}'',e''_Y,\eta'',s''}\left|\Psi_\nu^{\nu_+,\nu_-}\right\rangle. \qquad \text{(F22)}
\end{aligned}$$

We approximate the above equation by projecting it into the Hilbert space of excitations with only one pair of particle and hole. According to the Wick's theorem, we have

$$\begin{aligned}
&d^\dagger_{\mathbf{k}+\mathbf{p}+\mathbf{q},e_Y,\eta_2,s_2}d_{\mathbf{k},e_{Y1},\eta_1,s_1}d^\dagger_{\mathbf{k}''-\mathbf{q},-e''_Y,\eta'',s''}d_{\mathbf{k}'',e''_Y,\eta'',s''}\\
&=:d^\dagger_{\mathbf{k}+\mathbf{p}+\mathbf{q},e_Y,\eta_2,s_2}d_{\mathbf{k},e_{Y1},\eta_1,s_1}d^\dagger_{\mathbf{k}''-\mathbf{q},-e''_Y,\eta'',s''}d_{\mathbf{k}'',e''_Y,\eta'',s''}:\\
&\quad+\left\langle\Psi_\nu^{\nu_+,\nu_-}\right|d^\dagger_{\mathbf{k}+\mathbf{p}+\mathbf{q},e_Y,\eta_2,s_2}d_{\mathbf{k},e_{Y1},\eta_1,s_1}\left|\Psi_\nu^{\nu_+,\nu_-}\right\rangle d^\dagger_{\mathbf{k}''-\mathbf{q},-e''_Y,\eta'',s''}d_{\mathbf{k}'',e''_Y,\eta'',s''}\\
&\quad+\left\langle\Psi_\nu^{\nu_+,\nu_-}\right|d^\dagger_{\mathbf{k}+\mathbf{p}+\mathbf{q},e_Y,\eta_2,s_2}d_{\mathbf{k}'',e''_Y,\eta'',s''}\left|\Psi_\nu^{\nu_+,\nu_-}\right\rangle d_{\mathbf{k},e_{Y1},\eta_1,s_1}d^\dagger_{\mathbf{k}''-\mathbf{q},-e''_Y,\eta'',s''}\\
&\quad+\left\langle\Psi_\nu^{\nu_+,\nu_-}\right|d_{\mathbf{k},e_{Y1},\eta_1,s_1}d^\dagger_{\mathbf{k}''-\mathbf{q},-e''_Y,\eta'',s''}\left|\Psi_\nu^{\nu_+,\nu_-}\right\rangle d^\dagger_{\mathbf{k}+\mathbf{p}+\mathbf{q},e_Y,\eta_2,s_2}d_{\mathbf{k}'',e''_Y,\eta'',s''}\\
&\quad-\left\langle\Psi_\nu^{\nu_+,\nu_-}\right|d_{\mathbf{k},e_{Y1},\eta_1,s_1}d^\dagger_{\mathbf{k}''-\mathbf{q},-e''_Y,\eta'',s''}\left|\Psi_\nu^{\nu_+,\nu_-}\right\rangle\left\langle\Psi_\nu^{\nu_+,\nu_-}\right|d^\dagger_{\mathbf{k}+\mathbf{p}+\mathbf{q},e_Y,\eta_2,s_2}d_{\mathbf{k}'',e''_Y,\eta'',s''}\left|\Psi_\nu^{\nu_+,\nu_-}\right\rangle. \qquad \text{(F23)}
\end{aligned}$$

Here $:A:$ represents the normal ordered form of the operator A with respect to $|\Psi_\nu^{\nu_+,\nu_-}\rangle$, where all the creation operators of occupied states and annihilation operators of empty states are on the right-hand side of the creation operators of empty states and annihilation operators of occupied states. The first (normal ordered) term is nonvanishing when acted on $|\Psi_\nu^{\nu_+,\nu_-}\rangle$ if the two creation operators are of empty states and the two annihilation operators are of occupied states. However, we will omit this term because it yields two particle-hole pairs. Since we require $d_{\mathbf{k},e_{Y1},\eta_1,s_1}$ to be occupied such that the initial state is nonvanishing, there must be $\langle\Psi_\nu^{\nu_+,\nu_-}|d_{\mathbf{k},e_{Y1},\eta_1,s_1}=0$ and hence the last two terms in the above equation vanish. Then we obtain

$$\begin{aligned}
&d^\dagger_{\mathbf{k}+\mathbf{p}+\mathbf{q},e_Y,\eta_2,s_2}d_{\mathbf{k},e_{Y1},\eta_1,s_1}d^\dagger_{\mathbf{k}''-\mathbf{q},-e''_Y,\eta'',s''}d_{\mathbf{k}'',e''_Y,\eta'',s''}\\
&\approx\delta_{\mathbf{p}+\mathbf{q},0}\delta_{e_Y,e_{Y1}}\delta_{\eta_2,\eta_1}\delta_{s_2,s_1}d^\dagger_{\mathbf{k}''-\mathbf{q},-e''_Y,\eta'',s''}d_{\mathbf{k}'',e''_Y,\eta'',s''}-\delta_{\mathbf{k}+\mathbf{p}+\mathbf{q},\mathbf{k}''}\delta_{e_Y,e''_Y}\delta_{\eta_2,\eta''}\delta_{s_2,s''}n_{e_Y,\eta_2,s_2}d^\dagger_{\mathbf{k}+\mathbf{p},-e_Y,\eta,s}d_{\mathbf{k},e_{Y1},\eta_1,s_1}, \qquad \text{(F24)}
\end{aligned}$$

where $n_{e_Y,\eta,s}$ equals to 1 if the flavor $\{e_Y,\eta,s\}$ is occupied and equals to 0 otherwise. Here we have made use of $\{d^\dagger_{\mathbf{k}+\mathbf{p},-e_Y,\eta,s},d_{\mathbf{k},e_{Y1},\eta_1,s_1}\}=0$, which is because $\{e_{Y1},\eta_1,s_1\}$ is required to be occupied and $\{-e_Y,\eta,s\}$ is required to be empty

and hence $\{e_{Y1}, \eta_1, s_1\} \neq \{-e_Y, \eta, s\}$. Then we obtain

$$\begin{aligned}
&d^\dagger_{\mathbf{k}+\mathbf{p}+\mathbf{q},e_Y,\eta_2,s_2} d_{\mathbf{k},e_{Y1},\eta_1,s_1} O_{-\mathbf{q},-\mathbf{G}} \left|\Psi_\nu^{\nu_+,\nu_-}\right\rangle \\
&\quad\approx \delta_{\mathbf{q},0} A_{-\mathbf{G}} N_M d^\dagger_{\mathbf{k}+\mathbf{p},e_Y,\eta_2,s_2} d_{\mathbf{k},e_{Y1},\eta_1,s_1} \left|\Psi_\nu^{\nu_+,\nu_-}\right\rangle - \sqrt{V(\mathbf{q}+\mathbf{G})}\eta_2 F_{e_Y}(\mathbf{k}+\mathbf{p}+\mathbf{q}, -\mathbf{q}-\mathbf{G}) n_{e_Y,\eta_2,s_2} d^\dagger_{\mathbf{k}+\mathbf{p},-e_Y,\eta,s} d_{\mathbf{k},e_{Y1},\eta_1,s_1} \\
&\qquad+ \delta_{\mathbf{p}+\mathbf{q},0}\delta_{e_Y,e_{Y1}}\delta_{\eta_2,\eta_1}\delta_{s_2,s_1} \sum_{\mathbf{k}'',e''_Y,\eta'',s''} \sqrt{V(\mathbf{q}+\mathbf{G})}\eta'' F_{e''_Y}(\mathbf{k}'', -\mathbf{q}-\mathbf{G}) d^\dagger_{\mathbf{k}''-\mathbf{q},-e''_Y,\eta'',s''} d_{\mathbf{k}'',e''_Y,\eta'',s''}. \qquad \text{(F25)}
\end{aligned}$$

Similarly, we have

$$\begin{aligned}
&d^\dagger_{\mathbf{k}+\mathbf{p},e_{Y2},\eta_2,s_2} d_{\mathbf{k}-\mathbf{q},e'_Y,\eta_1,s_1} d^\dagger_{\mathbf{k}''-\mathbf{q},-e''_Y,\eta'',s''} d_{\mathbf{k}'',e''_Y,\eta'',s''} \\
&\quad\approx \left\langle \Psi_\nu^{\nu_+,\nu_-}\right| d^\dagger_{\mathbf{k}+\mathbf{p},e_{Y2},\eta_2,s_2} d_{\mathbf{k}-\mathbf{q},e'_Y,\eta_1,s_1} \left|\Psi_\nu^{\nu_+,\nu_-}\right\rangle d^\dagger_{\mathbf{k}''-\mathbf{q},-e''_Y,\eta'',s''} d_{\mathbf{k}'',e''_Y,\eta'',s''} \\
&\qquad+ \left\langle \Psi_\nu^{\nu_+,\nu_-}\right| d^\dagger_{\mathbf{k}+\mathbf{p},e_{Y2},\eta_2,s_2} d_{\mathbf{k}'',e''_Y,\eta'',s''} \left|\Psi_\nu^{\nu_+,\nu_-}\right\rangle d_{\mathbf{k}-\mathbf{q},e'_Y,\eta_1,s_1} d^\dagger_{\mathbf{k}''-\mathbf{q},-e''_Y,\eta'',s''} \\
&\qquad+ \left\langle \Psi_\nu^{\nu_+,\nu_-}\right| d_{\mathbf{k}-\mathbf{q},e'_Y,\eta_1,s_1} d^\dagger_{\mathbf{k}''-\mathbf{q},-e''_Y,\eta'',s''} \left|\Psi_\nu^{\nu_+,\nu_-}\right\rangle d^\dagger_{\mathbf{k}+\mathbf{p},e_{Y2},\eta_2,s_2} d_{\mathbf{k}'',e''_Y,\eta'',s''} \\
&\qquad- \left\langle \Psi_\nu^{\nu_+,\nu_-}\right| d_{\mathbf{k}-\mathbf{q},e'_Y,\eta_1,s_1} d^\dagger_{\mathbf{k}''-\mathbf{q},-e''_Y,\eta'',s''} \left|\Psi_\nu^{\nu_+,\nu_-}\right\rangle \left\langle \Psi_\nu^{\nu_+,\nu_-}\right| d^\dagger_{\mathbf{k}+\mathbf{p},e_{Y2},\eta_2,s_2} d_{\mathbf{k}'',e''_Y,\eta'',s''} \left|\Psi_\nu^{\nu_+,\nu_-}\right\rangle \\
&\quad\approx \delta_{\mathbf{k},\mathbf{k}''}\delta_{e'_Y,-e''_Y}\delta_{\eta_1,\eta''}\delta_{s_1,s''}(1-n_{e'_Y,\eta_1,s_1}) d^\dagger_{\mathbf{k}+\mathbf{p},e_{Y2},\eta_2,s_2} d_{\mathbf{k}'',e''_Y,\eta'',s''}, \qquad \text{(F26)}
\end{aligned}$$

where we have made use of $\langle\Psi_\nu^{\nu_+,\nu_-}| d^\dagger_{\mathbf{k}+\mathbf{p},e_{Y2},\eta_2,s_2} = 0$, and hence

$$\begin{aligned}
&d^\dagger_{\mathbf{k}+\mathbf{p},e_{Y2},\eta_2,s_2} d_{\mathbf{k}-\mathbf{q},e'_Y,\eta_1,s_1} O_{-\mathbf{q},-\mathbf{G}} \left|\Psi_\nu^{\nu_+,\nu_-}\right\rangle \\
&\quad\approx \delta_{\mathbf{q},0} A_{-\mathbf{G}} N_M d^\dagger_{\mathbf{k}+\mathbf{p},e_Y,\eta_2,s_2} d_{\mathbf{k},e_{Y1},\eta_1,s_1} \left|\Psi_\nu^{\nu_+,\nu_-}\right\rangle + \sqrt{V(\mathbf{q}+\mathbf{G})}\eta_1 F_{-e_{Y1}}(\mathbf{k}, -\mathbf{q}-\mathbf{G})(1-n_{e'_Y,\eta_1,s_1}) d^\dagger_{\mathbf{k}+\mathbf{p},e_{Y2},\eta,s} d_{\mathbf{k},-e'_Y,\eta_1,s_1}. \qquad \text{(F27)}
\end{aligned}$$

Substituting Eqs. (F25) and (F27) into Eq. (F21), we obtain

$$\begin{aligned}
&\left[H_I - \mu N, d^\dagger_{\mathbf{k}+\mathbf{p},e_{Y2},\eta_2,s_2} d_{\mathbf{k},e_{Y1},\eta_1,s_1}\right] \left|\Psi_\nu^{\nu_+,\nu_-}\right\rangle \\
&\quad\approx \left(\sum_{e_Y} R^{\eta_2,s_2}_{e_Y,e_{Y2}}(\mathbf{k}+\mathbf{p}) d^\dagger_{\mathbf{k}+\mathbf{p},e_Y,\eta_2,s_2} d_{\mathbf{k},e_{Y1},\eta_1,s_1} + \sum_{e'_Y} \widetilde{R}^{\eta_1,s_1 *}_{e'_Y,e_{Y1}}(\mathbf{k}) d^\dagger_{\mathbf{k}+\mathbf{p},e_{Y2},\eta_2,s_2} d_{\mathbf{k},e'_Y,\eta_1,s_1}\right) \left|\Psi_\nu^{\nu_+,\nu_-}\right\rangle \\
&\qquad- \frac{1}{\Omega_{\text{tot}}} \sum_{\mathbf{q},\mathbf{G}} V(\mathbf{G}+\mathbf{q}) \sum_{e_Y,e'_Y} M^{(\eta_2)}_{e_Y,e_{Y2}}(\mathbf{k}+\mathbf{p}, \mathbf{q}+\mathbf{G}) M^{(\eta_1)*}_{e'_Y,e_{Y1}}(\mathbf{k}, \mathbf{q}+\mathbf{G}) d^\dagger_{\mathbf{k}+\mathbf{p}+\mathbf{q},e_Y,\eta_2,s_2} d_{\mathbf{k}+\mathbf{q},e'_Y,\eta_1,s_1} \left|\Psi_\nu^{\nu_+,\nu_-}\right\rangle \\
&\qquad+ \frac{\delta_{\eta_2\eta_1}\delta_{s_2,s_1}}{\Omega_{\text{tot}}} \sum_{\mathbf{G}} \sum_{\mathbf{k}''e''_Y\eta''s''} V(-\mathbf{p}+\mathbf{G}) M^{(\eta_2)}_{e_{Y1},e_{Y2}}(\mathbf{k}+\mathbf{p}, -\mathbf{p}+\mathbf{G}) \eta'' F_{e''_Y}(\mathbf{k}'', \mathbf{p}-\mathbf{G}) d^\dagger_{\mathbf{k}''+\mathbf{p},-e''_Y,\eta'',s''} d_{\mathbf{k}'',e''_Y,\eta'',s''} \left|\Psi_\nu^{\nu_+,\nu_-}\right\rangle, \qquad \text{(F28)}
\end{aligned}$$

where R^{η_2,s_2} and $\widetilde{R}^{\eta_1,s_1}$ are given by Eqs. (F14) and (F20), respectively. The last term is nonzero only if $\{e_{Y1}, \eta_1, s_1\}$ is occupied and $\{e_{Y2}, \eta_2, s_2\}$ is empty, which, provided $\eta_2 = \eta_1$ and $s_2 = s_1$, also implies e_{Y1} must equal to $-e_{Y2}$. Thus we can rewrite the last term as

$$\begin{aligned}
&\frac{\delta_{e_{Y2},-e_{Y1}}\delta_{\eta_2\eta_1}\delta_{s_2,s_1}}{\Omega_{\text{tot}}} \sum_{\mathbf{G}} \sum_{\mathbf{k}''e_Y\eta s} V(-\mathbf{p}+\mathbf{G})\eta_2 F_{e_{Y2}}(\mathbf{k}+\mathbf{p}, -\mathbf{p}+\mathbf{G})\eta F_{-e_Y}(\mathbf{k}'', \mathbf{p}-\mathbf{G}) d^\dagger_{\mathbf{k}''+\mathbf{p},e_Y,\eta,s} d_{\mathbf{k}'',-e_Y,\eta,s} \left|\Psi_\nu^{\nu_+,\nu_-}\right\rangle \\
&\quad= \frac{\delta_{e_{Y2},-e_{Y1}}\delta_{\eta_2\eta_1}\delta_{s_2,s_1}}{\Omega_{\text{tot}}} \sum_{\mathbf{G}} \sum_{\mathbf{k}''e_Y\eta s} V(-\mathbf{p}+\mathbf{G})\eta_2 F_{e_{Y2}}(\mathbf{k}, \mathbf{p}-\mathbf{G})\eta F^*_{e_Y}(\mathbf{k}'', \mathbf{p}-\mathbf{G}) d^\dagger_{\mathbf{k}''+\mathbf{p},e_Y,\eta,s} d_{\mathbf{k}'',-e_Y,\eta,s} \left|\Psi_\nu^{\nu_+,\nu_-}\right\rangle, \qquad \text{(F29)}
\end{aligned}$$

where we have made use of Eqs. (A21) and (A12). Therefore we can write the scattering equation as

$$\begin{aligned}
&\left[H_I - \mu N, d^\dagger_{\mathbf{k}+\mathbf{p},e_{Y2},\eta_2,s_2} d_{\mathbf{k},e_{Y1},\eta_1,s_1}\right] \left|\Psi_\nu^{\nu_+,\nu_-}\right\rangle \\
&\quad\approx \sum_{\eta,s,\eta',s'} \sum_{e_Y,e'_Y} \sum_{\mathbf{q}} S^{\eta,s,\eta',s';\eta_2,s_2,\eta_1,s_1}_{e_Y,e'_Y;e_{Y2},e_{Y1}}(\mathbf{k}+\mathbf{q}, \mathbf{k}; \mathbf{p}) d^\dagger_{\mathbf{k}+\mathbf{q}+\mathbf{p},e_Y,\eta,s} d_{\mathbf{k}+\mathbf{q},e'_Y,\eta',s'} \left|\Psi_\nu^{\nu_+,\nu_-}\right\rangle, \qquad \text{(F30)}
\end{aligned}$$

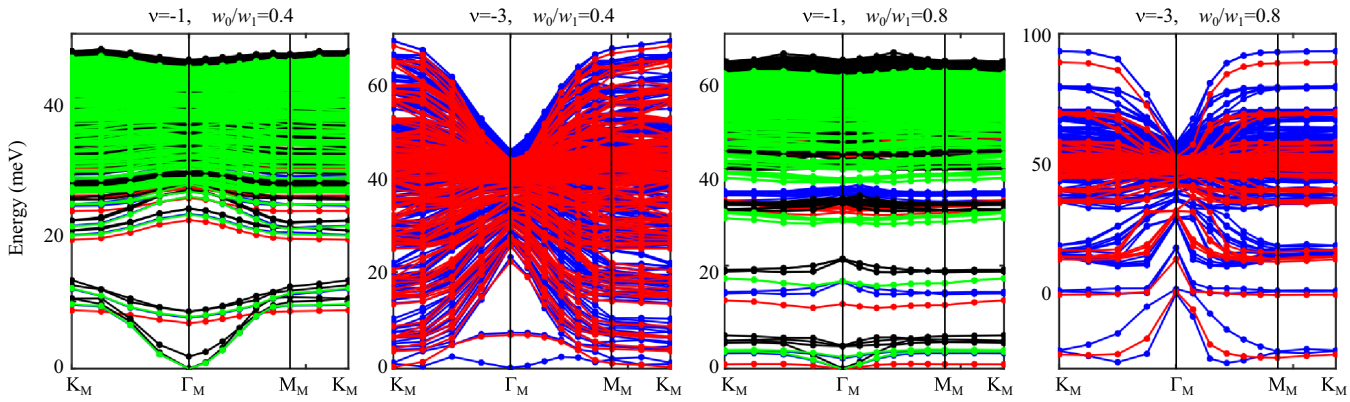

FIG. 12. Approximate charge neutral excitations at $\theta = 1.05^\circ$ at odd fillings in the nonchiral-flat limit. The flat metric condition is *not* imposed. Blue, red, black, and green bands are in the empty-half, half-half, empty-filled, and half-filled sectors, respectively. (See the text for the definition of sectors.) In this plot, we set the screening length as $\xi = 10$ nm and accordingly the interaction strength as $U_\xi = 13$ meV. The other parameters are same as in Appendix A: $v_F = 5.944$ eV Å, $|K| = 1.703$ Å^{-1}, and $w_1 = 110$ meV.

where the scattering matrix is

$$S^{\eta,s,\eta',s';\eta_2,s_2,\eta_1,s_1}_{e_Y,e'_Y;e_{Y2},e_{Y1}}(\mathbf{k}+\mathbf{q},\mathbf{k};\mathbf{p}) = \delta_{\eta,\eta_2}\delta_{s,s_2}\delta_{\eta',\eta_1}\delta_{s',s_1}\Big(\delta_{\mathbf{q},0}\big(R^{\eta_2,s_2}_{e_Y,e_{Y2}}(\mathbf{k}+\mathbf{p})\delta_{e'_Y,e_{Y1}} + \delta_{e_Y,e_{Y2}}\widetilde{R}^{\eta_1,s_1}_{e'_Y,e_{Y1}}(\mathbf{k})\big)$$
$$- \frac{1}{\Omega_{\rm tot}}\sum_{\mathbf{G}} V(\mathbf{G}+\mathbf{q})M^{(\eta_2)}_{e_Y,e_{Y2}}(\mathbf{k}+\mathbf{p},\mathbf{q}+\mathbf{G})M^{(\eta_1)*}_{e'_Y,e_{Y1}}(\mathbf{k},\mathbf{q}+\mathbf{G})\Big)$$
$$+ \delta_{e_{Y2},-e_{Y1}}\delta_{\eta_2\eta_1}\delta_{s_2,s_1}\delta_{e_Y,-e'_Y}\delta_{\eta\eta'}\delta_{ss'}\frac{1}{\Omega_{\rm tot}}\sum_{\mathbf{G}} V(-\mathbf{p}+\mathbf{G})\eta F^*_{e_Y}(\mathbf{k}+\mathbf{q},\mathbf{p}-\mathbf{G})\eta_2 F_{e_{Y2}}(\mathbf{k},\mathbf{p}-\mathbf{G}). \tag{F31}$$

The last term is nonzero if both the $\{\eta_2, s_2\}$ and $\{\eta, s\}$ valley-spin flavors are half filled. It couples all the half filled valley-spin flavors, which are independent in the (first) chiral-flat limit, to each other.

According to [110], in the nonchiral-flat limit the state $\Psi^{1,0}_{-3}$ (or its U(4) rotations) is still the perturbative ground state at $\nu = -3$. Without loss of generality, we assume the occupied flavor is $\{+1, \uparrow, +1\}$. Then we can divide the neutral excitations into the following sectors.

(1) The half-half sector, where $\eta_2 = \eta_1 = +1$, $s_2 = s_1 = \uparrow$. The delta functions in the first term of Eq. (F31) require $\eta = \eta' = +1$, $s = s' = \uparrow$. The delta functions in the second term require $\eta = \eta'$ and $s = s'$. Since $d^\dagger_{\eta,s,e_Y}$ and d_{η',s',e'_Y} must belong to empty and occupied bands, there must also be $\eta = \eta' = +1$, $s = s' = \uparrow$ in the second term. Then it follows that $e_Y = e_{Y2} = -1$, $e'_Y = e_{Y1} = +1$. At given $\mathbf{k}$, $\mathbf{p}$, $\mathbf{q}$, the S matrix is a one-by-one matrix.

(2) The empty-half sector, where $\{\eta_2, s_2\}$ is an empty valley-spin sector and $\{\eta_1, s_1\}$ is a half-filled valley-spin sector. The second term of Eq. (F31) vanish due to the delta function $\delta_{\eta_2\eta_1}\delta_{s_2s_1}$. The delta functions in the first term require $\eta = \eta_2$, $s = s_2$, $\eta' = \eta_1$, and $s' = s_1$. It follows that $e'_Y = e_{Y1} = +1$ and e_Y, e_{Y2} take values in ± 1. At given $\mathbf{k}$, $\mathbf{p}$, and $\mathbf{q}$, the S matrix is a two-by-two matrix.

According to Ref. [110], in the nonchiral-flat limit the state $\Psi^{2,1}_{-1}$ [or its U(4) rotations] is still the perturbative ground state at $\nu = -1$. There is a fully occupied valley-spin sector and a half filled valley-spin sector. Without loss of generality, we assume the occupied flavors as $\{+1, \uparrow, +1\}$, $\{+1, \uparrow, -1\}$, and $\{+1, \downarrow, +1\}$. Then we can divide the neutral excitations into the following sectors.

(1) The half-half sector, where $\eta_2 = \eta_1 = +1$, $s_2 = s_1 = \downarrow$. The delta functions in the first term of Eq. (F31) require $\eta = \eta' = +1$ and $s = s' = \downarrow$. The delta functions in the second term require $\eta = \eta'$ and $s = s'$. Since $d^\dagger_{\eta,s,e_Y}$ and d_{η',s',e'_Y} must belong to empty and occupied bands, there must also be $\eta = \eta' = +1$, $s = s' = \downarrow$ (the half filled valley-spin sector) in the second term. Then it follows that $e_Y = e_{Y2} = -1$, $e'_Y = e_{Y1} = +1$. At given $\mathbf{k}$, $\mathbf{p}$, $\mathbf{q}$, the S matrix is a one-by-one matrix.

(2) The empty-half sector, where $\{\eta_2, s_2\}$ is an empty valley-spin sector and $\{\eta_1, s_1\}$ is a half-filled valley-spin sector. The second term of Eq. (F31) vanish due to the delta function $\delta_{\eta_2\eta_1}\delta_{s_2s_1}$. The delta functions in the first term require $\eta = \eta_2$, $s = s_2$, $\eta' = \eta_1$, and $s' = s_1$. It follows that $e'_Y = e_{Y1} = +1$ and e_Y, e_{Y2} take values in ± 1. At given $\mathbf{k}$, $\mathbf{p}$, and $\mathbf{q}$, the S matrix is a two-by-two matrix.

(3) The half-occupied sector, where $\{\eta_2, s_2\}$ is the half filled valley-spin sector $\{+1, \downarrow\}$ and $\{\eta_1, s_1\}$ is the fully occupied valley-spin sector $\{+1, \uparrow\}$. The second term of Eq. (F31) vanish due to the delta function $\delta_{\eta_2\eta_1}\delta_{s_2s_1}$. The delta functions in the first term require $\eta = \eta_2$, $s = s_2$, $\eta' = \eta_1$, and $s' = s_1$. It follows that e'_Y, e_{Y1} take values in ± 1 and $e_Y = e_{Y2} = -1$. At given $\mathbf{k}$, $\mathbf{p}$, and $\mathbf{q}$, the S matrix is a two-by-two matrix.

(4) The empty-occupied sector, where $\{\eta_2, s_2\}$ is an empty valley-spin sector and $\{\eta_1, s_1\}$ is the fully occupied valley-spin sector $\{+1, \uparrow\}$. The second term of Eq. (F31) vanish due to the delta function $\delta_{\eta_2\eta_1}\delta_{s_2s_1}$. The delta functions in the first term require $\eta = \eta_2$, $s = s_2$, $\eta' = \eta_1$, $s' = s_1$. It follows that e'_Y, e_{Y1}, e_Y, and e_{Y2} all take values in ± 1. At given $\mathbf{k}$, $\mathbf{p}$, and $\mathbf{q}$, the S matrix is a four-by-four matrix.

The numerical results are shown in Fig. 12.

[1] R. Bistritzer and A. H. MacDonald, Moiré bands in twisted double-layer graphene, Proc. Natl. Acad. Sci. USA **108**, 12233 (2011).

[2] Y. Cao, V. Fatemi, A. Demir, S. Fang, S. L. Tomarken, J. Y. Luo, J. D. Sanchez-Yamagishi, K. Watanabe, T. Taniguchi, E. Kaxiras, R. C. Ashoori, and P. Jarillo-Herrero, Correlated insulator behaviour at half-filling in magic-angle graphene superlattices, Nature (London) **556**, 80 (2018).

[3] Y. Cao, V. Fatemi, S. Fang, K. Watanabe, T. Taniguchi, E. Kaxiras, and P. Jarillo-Herrero, Unconventional superconductivity in magic-angle graphene superlattices, Nature (London) **556**, 43 (2018).

[4] X. Lu, P. Stepanov, W. Yang, M. Xie, M. A. Aamir, I. Das, C. Urgell, K. Watanabe, T. Taniguchi, G. Zhang *et al.*, Superconductors, orbital magnets and correlated states in magic-angle bilayer graphene, Nature (London) **574**, 653 (2019).

[5] M. Yankowitz, S. Chen, H. Polshyn, Y. Zhang, K. Watanabe, T. Taniguchi, D. Graf, A. F. Young, and C. R. Dean, Tuning superconductivity in twisted bilayer graphene, Science **363**, 1059 (2019).

[6] A. L. Sharpe, E. J. Fox, A. W. Barnard, J. Finney, K. Watanabe, T. Taniguchi, M. A. Kastner, and D. Goldhaber-Gordon, Emergent ferromagnetism near three-quarters filling in twisted bilayer graphene, Science **365**, 605 (2019).

[7] Y. Saito, J. Ge, K. Watanabe, T. Taniguchi, and A. F. Young, Independent superconductors and correlated insulators in twisted bilayer graphene, Nat. Phys. **16**, 926 (2020).

[8] P. Stepanov, I. Das, X. Lu, A. Fahimniya, K. Watanabe, T. Taniguchi, F. H. L. Koppens, J. Lischner, L. Levitov, and D. K. Efetov, Untying the insulating and superconducting orders in magic-angle graphene, Nature (London) **583**, 375 (2020).

[9] X. Liu, Z. Wang, K. Watanabe, T. Taniguchi, O. Vafek, and J. I. A. Li, Tuning electron correlation in magic-angle twisted bilayer graphene using coulomb screening, Science **371**, 1261 (2021).

[10] H. S. Arora, R. Polski, Y. Zhang, A. Thomson, Y. Choi, H. Kim, Z. Lin, I. Z. Wilson, X. Xu, J.-H. Chu *et al.*, Superconductivity in metallic twisted bilayer graphene stabilized by wse2, Nature (London) **583**, 379 (2020).

[11] M. Serlin, C. L. Tschirhart, H. Polshyn, Y. Zhang, J. Zhu, K. Watanabe, T. Taniguchi, L. Balents, and A. F. Young, Intrinsic quantized anomalous hall effect in a moiré heterostructure, Science **367**, 900 (2019).

[12] Y. Cao, D. Chowdhury, D. Rodan-Legrain, O. Rubies-Bigorda, K. Watanabe, T. Taniguchi, T. Senthil, and P. Jarillo-Herrero, Strange Metal in Magic-Angle Graphene with Near Planckian Dissipation, Phys. Rev. Lett. **124**, 076801 (2020).

[13] H. Polshyn, M. Yankowitz, S. Chen, Y. Zhang, K. Watanabe, T. Taniguchi, C. R. Dean, and A. F. Young, Large linear-in-temperature resistivity in twisted bilayer graphene, Nat. Phys. **15**, 1011 (2019).

[14] Y. Xie, B. Lian, B. Jäck, X. Liu, C.-L. Chiu, K. Watanabe, T. Taniguchi, B. A. Bernevig, and A. Yazdani, Spectroscopic signatures of many-body correlations in magic-angle twisted bilayer graphene, Nature (London) **572**, 101 (2019).

[15] Y. Choi, J. Kemmer, Y. Peng, A. Thomson, H. Arora, R. Polski, Y. Zhang, H. Ren, J. Alicea, G. Refael *et al.*, Electronic correlations in twisted bilayer graphene near the magic angle, Nat. Phys. **15**, 1174 (2019).

[16] A. Kerelsky, L. J. McGilly, D. M. Kennes, L. Xian, M. Yankowitz, S. Chen, K. Watanabe, T. Taniguchi, J. Hone, C. Dean *et al.*, Maximized electron interactions at the magic angle in twisted bilayer graphene, Nature (London) **572**, 95 (2019).

[17] Y. Jiang, X. Lai, K. Watanabe, T. Taniguchi, K. Haule, J. Mao, and E. Y. Andrei, Charge order and broken rotational symmetry in magic-angle twisted bilayer graphene, Nature (London) **573**, 91 (2019).

[18] D. Wong, K. P. Nuckolls, M. Oh, B. Lian, Y. Xie, S. Jeon, K. Watanabe, T. Taniguchi, B. A. Bernevig, and A. Yazdani, Cascade of electronic transitions in magic-angle twisted bilayer graphene, Nature (London) **582**, 198 (2020).

[19] U. Zondiner, A. Rozen, D. Rodan-Legrain, Y. Cao, R. Queiroz, T. Taniguchi, K. Watanabe, Y. Oreg, F. von Oppen, A. Stern *et al.*, Cascade of phase transitions and dirac revivals in magic-angle graphene, Nature (London) **582**, 203 (2020).

[20] K. P. Nuckolls, M. Oh, D. Wong, B. Lian, K. Watanabe, T. Taniguchi, B. A. Bernevig, and A. Yazdani, Strongly correlated chern insulators in magic-angle twisted bilayer graphene, Nature (London) **588**, 610 (2020).

[21] Y. Choi, H. Kim, Y. Peng, A. Thomson, C. Lewandowski, R. Polski, Y. Zhang, H. S. Arora, K. Watanabe, T. Taniguchi, J. Alicea, and S. Nadj-Perge, Tracing out correlated chern insulators in magic angle twisted bilayer graphene, arXiv:2008.11746.

[22] Y. Saito, J. Ge, L. Rademaker, K. Watanabe, T. Taniguchi, D. A. Abanin, and A. F. Young, Hofstadter subband ferromagnetism and symmetry-broken chern insulators in twisted bilayer graphene, Nat. Phys. **17**, 478 (2021).

[23] I. Das, X. Lu, J. Herzog-Arbeitman, Z.-D. Song, K. Watanabe, T. Taniguchi, B. A. Bernevig, and D. K Efetov, Symmetry broken chern insulators and magic series of rashba-like landau level crossings in magic angle bilayer graphene, Nat. Phys. (2021), doi: 10.1038/s41567-021-01186-3.

[24] S. Wu, Z. Zhang, K. Watanabe, T. Taniguchi, and E. Y. Andrei, Chern insulators, van hove singularities and topological flat bands in magic-angle twisted bilayer graphene, Nat. Mater. **20**, 488 (2021).

[25] J. M. Park, Y. Cao, K. Watanabe, T. Taniguchi, and P. Jarillo-Herrero, Flavour hund's coupling, correlated chern gaps, and diffusivity in moiré flat bands, Nature **592**, 43 (2021).

[26] Y. Saito, J. Ge, K. Watanabe, T. Taniguchi, E. Berg, and A. F. Young, Isospin pomeranchuk effect and the entropy of collective excitations in twisted bilayer graphene, Nature **592**, 220 (2021).

[27] A. Rozen, J. M. Park, U. Zondiner, Y. Cao, D. Rodan-Legrain, T. Taniguchi, K. Watanabe, Y. Oreg, A. Stern, E. Berg, P. Jarillo-Herrero, and S. Ilani, Entropic evidence for a pomeranchuk effect in magic angle graphene, Nature **592**, 214 (2021).

[28] X. Lu, B. Lian, G. Chaudhary, B. A. Piot, G. Romagnoli, K. Watanabe, T. Taniguchi, M. Poggio, A. H. MacDonald, B. A. Bernevig, and D. K. Efetov, Fingerprints of fragile topology in the hofstadter spectrum of twisted bilayer graphene close to the second magic angle, arXiv:2006.13963.

[29] G. W. Burg, J. Zhu, T. Taniguchi, K. Watanabe, A. H. MacDonald, and E. Tutuc, Correlated Insulating States in Twisted Double Bilayer Graphene, Phys. Rev. Lett. **123**, 197702 (2019).

[30] C. Shen, Y. Chu, Q. Wu, N. Li, S. Wang, Y. Zhao, J. Tang, J. Liu, J. Tian, K. Watanabe, T. Taniguchi, R. Yang, Z. Y. Meng, D. Shi, O. V. Yazyev, and G. Zhang, Correlated states in twisted double bilayer graphene, Nat. Phys. **16**, 520 (2020).

[31] Y. Cao, D. Rodan-Legrain, O. Rubies-Bigorda, J. M. Park, K. Watanabe, T. Taniguchi, and P. Jarillo-Herrero, Tunable correlated states and spin-polarized phases in twisted bilayer-bilayer graphene, Nature (London) **583**, 215 (2020).

[32] X. Liu, Z. Hao, E. Khalaf, J. Y. Lee, K. Watanabe, T. Taniguchi, A. Vishwanath, and P. Kim, Spin-polarized Correlated Insulator and Superconductor in Twisted Double Bilayer Graphene, Nature (London) **583**, 221 (2020).

[33] G. Chen, L. Jiang, S. Wu, B. Lyu, H. Li, B. L. Chittari, K. Watanabe, T. Taniguchi, Z. Shi, J. Jung, Y. Zhang, and F. Wang, Evidence of a gate-tunable Mott insulator in a trilayer graphene moiré superlattice, Nat. Phys. **15**, 237 (2019).

[34] G. Chen, A. L. Sharpe, P. Gallagher, I. T. Rosen, E. J. Fox, L. Jiang, B. Lyu, H. Li, K. Watanabe, T. Taniguchi, J. Jung, Z. Shi, D. Goldhaber-Gordon, Y. Zhang, and F. Wang, Signatures of tunable superconductivity in a trilayer graphene moiré superlattice, Nature (London) **572**, 215 (2019).

[35] G. Chen, A. L. Sharpe, E. J. Fox, Y.-H. Zhang, S. Wang, L. Jiang, B. Lyu, H. Li, K. Watanabe, T. Taniguchi, Z. Shi, T. Senthil, D. Goldhaber-Gordon, Y. Zhang, and F. Wang, Tunable correlated Chern insulator and ferromagnetism in a moiré superlattice, Nature (London) **579**, 56 (2020).

[36] G. W. Burg, B. Lian, T. Taniguchi, K. Watanabe, B. A. Bernevig, and E. Tutuc, Evidence of emergent symmetry and valley chern number in twisted double-bilayer graphene, arXiv:2006.14000.

[37] G. Tarnopolsky, A. J. Kruchkov, and A. Vishwanath, Origin of Magic Angles in Twisted Bilayer Graphene, Phys. Rev. Lett. **122**, 106405 (2019).

[38] L. Zou, H. C. Po, A. Vishwanath, and T. Senthil, Band structure of twisted bilayer graphene: Emergent symmetries, commensurate approximants, and wannier obstructions, Phys. Rev. B **98**, 085435 (2018).

[39] Y. Fu, E. J. König, J. H. Wilson, Y.-Z. Chou, and J. H. Pixley, Magic-angle semimetals, Quantum Mater. **5**, 71 (2020).

[40] J. Liu, J. Liu, and X. Dai, Pseudo landau level representation of twisted bilayer graphene: Band topology and implications on the correlated insulating phase, Phys. Rev. B **99**, 155415 (2019).

[41] D. K. Efimkin and A. H. MacDonald, Helical network model for twisted bilayer graphene, Phys. Rev. B **98**, 035404 (2018).

[42] J. Kang and O. Vafek, Symmetry, Maximally Localized Wannier States, and a Low-Energy Model for Twisted Bilayer Graphene Narrow Bands, Phys. Rev. X **8**, 031088 (2018).

[43] Z. Song, Z. Wang, W. Shi, G. Li, C. Fang, and B. A. Bernevig, All Magic Angles in Twisted Bilayer Graphene are Topological, Phys. Rev. Lett. **123**, 036401 (2019).

[44] H. C. Po, L. Zou, T. Senthil, and A. Vishwanath, Faithful tight-binding models and fragile topology of magic-angle bilayer graphene, Phys. Rev. B **99**, 195455 (2019).

[45] J. Ahn, S. Park, and B.-J. Yang, Failure of Nielsen-Ninomiya Theorem and Fragile Topology in Two-Dimensional Systems with Space-Time Inversion Symmetry: Application to Twisted Bilayer Graphene at Magic Angle, Phys. Rev. X **9**, 021013 (2019).

[46] A. Bouhon, A. M. Black-Schaffer, and R.-J. Slager, Wilson loop approach to fragile topology of split elementary band representations and topological crystalline insulators with time-reversal symmetry, Phys. Rev. B **100**, 195135 (2019).

[47] K. Hejazi, C. Liu, H. Shapourian, X. Chen, and L. Balents, Multiple topological transitions in twisted bilayer graphene near the first magic angle, Phys. Rev. B **99**, 035111 (2019).

[48] B. Lian, F. Xie, and B. A. Bernevig, Landau level of fragile topology, Phys. Rev. B **102**, 041402(R) (2020).

[49] K. Hejazi, C. Liu, and L. Balents, Landau levels in twisted bilayer graphene and semiclassical orbits, Phys. Rev. B **100**, 035115 (2019).

[50] B. Padhi, A. Tiwari, T. Neupert, and S. Ryu, Transport across twist angle domains in moiré graphene, Phys. Rev. Research **2**, 033458 (2020).

[51] C. Xu and L. Balents, Topological Superconductivity in Twisted Multilayer Graphene, Phys. Rev. Lett. **121**, 087001 (2018).

[52] M. Koshino, N. F. Q. Yuan, T. Koretsune, M. Ochi, K. Kuroki, and L. Fu, Maximally Localized Wannier Orbitals and the Extended Hubbard Model for Twisted Bilayer Graphene, Phys. Rev. X **8**, 031087 (2018).

[53] M. Ochi, M. Koshino, and K. Kuroki, Possible correlated insulating states in magic-angle twisted bilayer graphene under strongly competing interactions, Phys. Rev. B **98**, 081102(R) (2018).

[54] X. Y. Xu, K. T. Law, and P. A. Lee, Kekulé valence bond order in an extended hubbard model on the honeycomb lattice with possible applications to twisted bilayer graphene, Phys. Rev. B **98**, 121406(R) (2018).

[55] F. Guinea and N. R. Walet, Electrostatic effects, band distortions, and superconductivity in twisted graphene bilayers, Proc. Natl. Acad. Sci. USA **115**, 13174 (2018).

[56] J. W. F. Venderbos and R. M. Fernandes, Correlations and electronic order in a two-orbital honeycomb lattice model for twisted bilayer graphene, Phys. Rev. B **98**, 245103 (2018).

[57] Y.-Z. You and A. Vishwanath, Superconductivity from Valley Fluctuations and Approximate SO(4) Symmetry in a Weak Coupling Theory of Twisted Bilayer Graphene, npj Quantum Mater. **4**, 16 (2019).

[58] F. Wu and S. Das Sarma, Collective Excitations of Quantum Anomalous Hall Ferromagnets in Twisted Bilayer Graphene, Phys. Rev. Lett. **124**, 046403 (2020).
[59] B. Lian, Z. Wang, and B. A. Bernevig, Twisted Bilayer Graphene: A Phonon-Driven Superconductor, Phys. Rev. Lett. **122**, 257002 (2019).
[60] F. Wu, A. H. MacDonald, and I. Martin, Theory of Phonon-Mediated Superconductivity in Twisted Bilayer Graphene, Phys. Rev. Lett. **121**, 257001 (2018).
[61] H. Isobe, N. F. Q. Yuan, and L. Fu, Unconventional Superconductivity and Density Waves in Twisted Bilayer Graphene, Phys. Rev. X **8**, 041041 (2018).
[62] C.-C. Liu, L.-D. Zhang, W.-Q. Chen, and F. Yang, Chiral Spin Density Wave and $d + id$ Superconductivity in the Magic-Angle-Twisted Bilayer Graphene, Phys. Rev. Lett. **121**, 217001 (2018).
[63] N. Bultinck, S. Chatterjee, and M. P. Zaletel, Mechanism for Anomalous Hall Ferromagnetism in Twisted Bilayer Graphene, Phys. Rev. Lett. **124**, 166601 (2020).
[64] Y.-H. Zhang, D. Mao, Y. Cao, P. Jarillo-Herrero, and T. Senthil, Nearly flat chern bands in moiré superlattices, Phys. Rev. B **99**, 075127 (2019).
[65] J. Liu, Z. Ma, J. Gao, and X. Dai, Quantum Valley Hall Effect, Orbital Magnetism, and Anomalous Hall Effect in Twisted Multilayer Graphene Systems, Phys. Rev. X **9**, 031021 (2019).
[66] X.-C. Wu, C.-M. Jian, and C. Xu, Coupled-wire description of the correlated physics in twisted bilayer graphene, Phys. Rev. B **99**, 161405(R) (2019).
[67] A. Thomson, S. Chatterjee, S. Sachdev, and M. S. Scheurer, Triangular antiferromagnetism on the honeycomb lattice of twisted bilayer graphene, Phys. Rev. B **98**, 075109 (2018).
[68] J. F. Dodaro, S. A. Kivelson, Y. Schattner, X.-Q. Sun, and C. Wang, Phases of a phenomenological model of twisted bilayer graphene, Phys. Rev. B **98**, 075154 (2018).
[69] J. Gonzalez and T. Stauber, Kohn-Luttinger Superconductivity in Twisted Bilayer Graphene, Phys. Rev. Lett. **122**, 026801 (2019).
[70] N. F. Q. Yuan and L. Fu, Model for the metal-insulator transition in graphene superlattices and beyond, Phys. Rev. B **98**, 045103 (2018).
[71] J. Kang and O. Vafek, Strong Coupling Phases of Partially Filled Twisted Bilayer Graphene Narrow Bands, Phys. Rev. Lett. **122**, 246401 (2019).
[72] N. Bultinck, E. Khalaf, S. Liu, S. Chatterjee, A. Vishwanath, and M. P. Zaletel, Ground State and Hidden Symmetry of Magic-Angle Graphene at Even Integer Filling, Phys. Rev. X **10**, 031034 (2020).
[73] K. Seo, V. N. Kotov, and B. Uchoa, Ferromagnetic Mott State in Twisted Graphene Bilayers at the Magic Angle, Phys. Rev. Lett. **122**, 246402 (2019).
[74] K. Hejazi, X. Chen, and L. Balents, Hybrid wannier chern bands in magic angle twisted bilayer graphene and the quantized anomalous hall effect, Phys. Rev. Research **3**, 013242 (2021).
[75] E. Khalaf, S. Chatterjee, N. Bultinck, M. P. Zaletel, and A. Vishwanath, Charged skyrmions and topological origin of superconductivity in magic angle graphene, arXiv:2004.00638 [cond-mat.str-el].
[76] H. C. Po, L. Zou, A. Vishwanath, and T. Senthil, Origin of Mott Insulating Behavior and Superconductivity in Twisted Bilayer Graphene, Phys. Rev. X **8**, 031089 (2018).
[77] F. Xie, Z. Song, B. Lian, and B. A. Bernevig, Topology-Bounded Superfluid Weight in Twisted Bilayer Graphene, Phys. Rev. Lett. **124**, 167002 (2020).
[78] A. Julku, T. J. Peltonen, L. Liang, T. T. Heikkilä, and P. Törmä, Superfluid weight and berezinskii-kosterlitz-thouless transition temperature of twisted bilayer graphene, Phys. Rev. B **101**, 060505 (2020).
[79] X. Hu, T. Hyart, D. I. Pikulin, and E. Rossi, Geometric and Conventional Contribution to the Superfluid Weight in Twisted Bilayer Graphene, Phys. Rev. Lett. **123**, 237002 (2019).
[80] J. Kang and O. Vafek, Non-abelian dirac node braiding and near-degeneracy of correlated phases at odd integer filling in magic-angle twisted bilayer graphene, Phys. Rev. B **102**, 035161 (2020).
[81] T. Soejima, D. E. Parker, N. Bultinck, J. Hauschild, and M. P. Zaletel, Efficient simulation of moire materials using the density matrix renormalization group, Phys. Rev. B **102**, 205111 (2020).
[82] J. H. Pixley and E. Y. Andrei, Ferromagnetism in magic-angle graphene, Science **365**, 543 (2019).
[83] E. J. König, P. Coleman, and A. M. Tsvelik, Spin magnetometry as a probe of stripe superconductivity in twisted bilayer graphene, Phys. Rev. B **102**, 104514 (2020).
[84] M. Christos, S. Sachdev, and M. Scheurer, Superconductivity, correlated insulators, and wess-zumino-witten terms in twisted bilayer graphene, Proc. Natl. Acad. Sci. USA **117**, 29543 (2020).
[85] C. Lewandowski, D. Chowdhury, and J. Ruhman, Pairing in magic-angle twisted bilayer graphene: role of phonon and plasmon umklapp, arXiv:2007.15002.
[86] M. Xie and A. H. MacDonald, Nature of the Correlated Insulator States in Twisted Bilayer Graphene, Phys. Rev. Lett. **124**, 097601 (2020).
[87] J. Liu and X. Dai, Theories for the correlated insulating states and quantum anomalous hall phenomena in twisted bilayer graphene, Phys. Rev. B **103**, 035427 (2021).
[88] T. Cea and F. Guinea, Band structure and insulating states driven by coulomb interaction in twisted bilayer graphene, Phys. Rev. B **102**, 045107 (2020).
[89] Y. Zhang, K. Jiang, Z. Wang, and F. Zhang, Correlated insulating phases of twisted bilayer graphene at commensurate filling fractions: A hartree-fock study, Phys. Rev. B **102**, 035136 (2020).
[90] S. Liu, E. Khalaf, J. Y. Lee, and A. Vishwanath, Nematic topological semimetal and insulator in magic angle bilayer graphene at charge neutrality, Phys. Rev. Research **3**, 013033 (2021).
[91] Y. Da Liao, Z. Y. Meng, and X. Y. Xu, Valence Bond Orders at Charge Neutrality in a Possible Two-Orbital Extended Hubbard Model for Twisted Bilayer Graphene, Phys. Rev. Lett. **123**, 157601 (2019).
[92] Y. D. Liao, J. Kang, C. N. Breiø, X. Y. Xu, H.-Q. Wu, B. M. Andersen, R. M. Fernandes, and Z. Y. Meng, Correlation-Induced Insulating Topological Phases at Charge Neutrality in Twisted Bilayer Graphene, Phys. Rev. X **11**, 011014 (2021).

[93] L. Classen, C. Honerkamp, and M. M. Scherer, Competing phases of interacting electrons on triangular lattices in moiré heterostructures, Phys. Rev. B **99**, 195120 (2019).

[94] D. M. Kennes, J. Lischner, and C. Karrasch, Strong correlations and d+ id superconductivity in twisted bilayer graphene, Phys. Rev. B **98**, 241407(R) (2018).

[95] P. M. Eugenio and C. B. Dağ, Dmrg study of strongly interacting z_2 flatbands: a toy model inspired by twisted bilayer graphene, SciPost Phys. Core **3**, 015 (2020).

[96] Y. Huang, P. Hosur, and H. K. Pal, Deconstructing magic-angle physics in twisted bilayer graphene with a two-leg ladder model, Phys. Rev. B **102**, 155429 (2020).

[97] T. Huang, L. Zhang, and T. Ma, Antiferromagnetically ordered mott insulator and d+ id superconductivity in twisted bilayer graphene: A quantum monte carlo study, Sci. Bull. **64**, 310 (2019).

[98] H. Guo, X. Zhu, S. Feng, and R. T. Scalettar, Pairing symmetry of interacting fermions on a twisted bilayer graphene superlattice, Phys. Rev. B **97**, 235453 (2018).

[99] P. J. Ledwith, G. Tarnopolsky, E. Khalaf, and A. Vishwanath, Fractional chern insulator states in twisted bilayer graphene: An analytical approach, Phys. Rev. Research **2**, 023237 (2020).

[100] C. Repellin, Z. Dong, Y.-H. Zhang, and T. Senthil, Ferromagnetism in Narrow Bands of Moiré Superlattices, Phys. Rev. Lett. **124**, 187601 (2020).

[101] A. Abouelkomsan, Z. Liu, and E. J. Bergholtz, Particle-Hole Duality, Emergent Fermi Liquids, and Fractional Chern Insulators in Moiré Flatbands, Phys. Rev. Lett. **124**, 106803 (2020).

[102] C. Repellin and T. Senthil, Chern bands of twisted bilayer graphene: Fractional chern insulators and spin phase transition, Phys. Rev. Research **2**, 023238 (2020).

[103] O. Vafek and J. Kang, Towards the hidden symmetry in coulomb interacting twisted bilayer graphene: renormalization group approach, Phys. Rev. Lett. **125**, 257602 (2020).

[104] R. M. Fernandes and J. W. F. Venderbos, Nematicity with a twist: Rotational symmetry breaking in a moiré superlattice, Sci. Adv. **6**, eaba8834 (2020).

[105] J. H. Wilson, Y. Fu, S. Das Sarma, and J. H. Pixley, Disorder in twisted bilayer graphene, Phys. Rev. Research **2**, 023325 (2020).

[106] J. Wang, Y. Zheng, A. J. Millis, and J. Cano, Chiral approximation to twisted bilayer graphene: Exact intra-valley inversion symmetry, nodal structure and implications for higher magic angles, arXiv:2010.03589.

[107] B. A. Bernevig, Z.-D. Song, N. Regnault, and B. Lian, Twisted bilayer graphene. I. Matrix elements, approximations, perturbation theory, and a $k \cdot p$ two-band model, Phys. Rev. B **103**, 205411 (2021).

[108] Z.-D. Song, B. Lian, N. Regnault, and B. A. Bernevig, Twisted bilayer graphene. II. Stable symmetry anomaly, Phys. Rev. B **103**, 205412 (2021).

[109] B. A. Bernevig, Z.-D. Song, N. Regnault, and B. Lian, Twisted bilayer graphene. III. Interacting Hamiltonian and exact symmetries, Phys. Rev. B **103**, 205413 (2021).

[110] B. Lian, Z.-D. Song, N. Regnault, D. K. Efetov, A. Yazdani, and B. A. Bernevig, Twisted bilayer graphene. IV. Exact insulator ground states and phase diagram, Phys. Rev. B **103**, 205414 (2021).

[111] F. Xie, A. Cowsik, Z.-D. Song, B. Lian, B. A. Bernevig, and N. Regnault, Twisted bilayer graphene. VI. An exact diagonalization study at nonzero integer filling, Phys. Rev. B **103**, 205416 (2021).

[112] R. W. Richardson, A restricted class of exact eigenstates of the pairing-force hamiltonian, Phys. Lett. **3**, 277 (1963).

[113] R. W. Richardson and N. Sherman, Exact eigenstates of the pairing-force hamiltonian, Nucl. Phys. **52**, 221 (1964).

[114] R. W. Richardson, Numerical study of the 8-32-particle eigenstates of the pairing hamiltonian, Phys. Rev. **141**, 949 (1966).

[115] R. W. Richardson, Pairing in the limit of a large number of particles, J. Math. Phys. **18**, 1802 (1977).

[116] T. Neupert, C. Chamon, and C. Mudry, Measuring the quantum geometry of bloch bands with current noise, Phys. Rev. B **87**, 245103 (2013).

[117] H. B. Nielsen and S. Chadha, On how to count goldstone bosons, Nucl. Phys. B **105**, 445 (1976).

[118] R. E. Throckmorton and O. Vafek, Fermions on bilayer graphene: Symmetry breaking for $B = 0$ and $\nu = 0$, Phys. Rev. B **86**, 115447 (2012).